KU LEUVEN

FACULTY OF SCIENCE

The contribution of hippocampal memory-trace reactivation to recent-event working memory

The effect of closed-loop perturbation of hippocampal replay

Lies DECEUNINCK

Promotor: Prof. F. Kloosterman
NERF, imec

Co-promotor: Prof. C. Bartic
KU Leuven

Supervisors: D. Cilliberti, J.J. Sun, C.Y. Kim, F. Michon
NERF, imec

Thesis presented in
fulfillment of the requirements
for the degree of Master of Science
in Biophysics, Biochemistry and Biotechnology

Academic year 2017-2018

Preface

Ever since I started university, neurology has been my main field of interest. After I graduated high school I did an internship at NERF, which triggered my specific interest. I worked for two weeks with the team of Fabian Kloosterman.

I chose a bachelor degree in physics because I wanted to have the broadest and most general science education. Physics taught me the fundamental principles of nature and it has always been my intent to use this knowledge for a biological/human purpose, which explains my master choice for Biophysics.

Over the years I stayed in touch with Davide Cilliberti, one of the PhD students of Fabian Kloosterman, who explained to me the progress of their research. I am fascinated by their work. Fundamental neuroscience is one of the research fields that combines research techniques of all different sciences; biology, physics, chemistry, statistics,... And this is what the master program of biophysics is all about.

My special thanks go to my promotor, Fabian Kloosterman. With this master thesis project he gave me the opportunity to develop my skills in the area of neuroscience, both practical and theoretical, and to become a biophysicist in this field, my goal from the start. The project completes a full experimental life cycle including the construction of brain implants, behavioural assessment of memory function, neural recordings in behaving animals and analysis of the data. I was able to execute all parts largely independently, except for the drive implantation surgery. This would not have been possible without the unlimited guidance and trust from all lab members. Specifically I want to thank Davide Cilliberti for the project proposal and his scientific creativity throughout the year, Jyh-Jang Sun for introducing me to the electrophysiological measurement techniques, Chae-Young Kim for performing flawless drive implantations and Frédéric Michon for his patience while teaching my how to make a hyperdrive. Finally I thank professor Carmen Bartic for accepting! to be my co-promotor on this collaborative master project with the Kloosterman lab of the neuroscience laboratory NERF, Neuro-Electronic Research Flanders.

Summary

Recent-event working memory (RE-WM) is defined as that part of the brain that is responsible for making decisions based on recent events. It thus represents a combination of short-term memory and decision making. The hippocampus (HC), localised deep in the temporal lobe of the human cortex, is a highly specialised brain structure that has been associated with learning and memory since the early 50s. Previous hippocampal research in rodents revealed that during short pauses in locomotion the overall activity of hippocampal cells slows down significantly. However, during short approximately 50 ms long episodes in the break, the HC again strongly increases its activity when high amplitude, high frequency oscillations called sharp-wave ripples (SWRs) occur. The cells that become predominantly active are the same cells that also fire during previous experiences, even in the same temporal order. The re-expression of neural activity patterns strongly suggests a role for learning and memory and for that reason the reactivations are also referred to as memory-trace reactivations or replay.
Awake replay has been suggested to be important for short-term memory and decision making. In addition to this Jadhav et al. demonstrated a drop in learning speed of a short-term spatial memory based rule when awake SWRs are disrupted in rodents, strongly suggesting a causal link between awake replay and decision making based on short-term spatial memories. This project wants to test the specific hypothesis that awake hippocampal replay has a decisive role in short-term memory and decision making (RE-WM) without any involvement of learning. For this we use extra-cellular recordings and closed-loop electrical disruption of hippocampal SWRs in freely-moving rats. The rats perform a RE-WM task (win-shift paradigm) on the 8-arm radial maze. The data presented come from one rat that had a functional stimulation wire and good quality signals.

To optimise the protocol, unequal angles between the 8 arms of the radial maze were introduced which postponed the development of complete stereotypical arm choice behaviour (e.g. clockwise strategies) but did not prevent it. Throughout the whole experiment the rat showed a high arm-pick bias for one or two arms. In the beginning of the experiment, arms changed every trial but since this appeared to be to difficult to learn for the animals eventually the arms were changed only every daily session.
Behavioural analysis with this protocol showed that the rat had a higher average performance than a simulated random-choice rat showing that it did not pick arms randomly. The rat was also observed to spend more time on the reward and platforms site with increasing arm visits but not across performance levels.
Electrophysiological analysis did not reveal any significant link between behaviour and ripple rate, possibly due to a lack of engagement in the task. However, the number of

ripples did increase with increasing visits, mirroring the similar increase in time spent on the reward site. The number of ripples did not vary across performance levels. Based on these observations we propose two different roles for replay in RE-WM. It is possible that replays during reward site and platform visits represent the consolidation and retrieval of previous arm visits. On the other hand our data also suggests that replays might represent the possible future choices. Further analysis should provide more clarity. In both models, SWR disruption should effect RE-WM and thus the trial performance.

In the last part of the experiment closed-loop disruption of hippocampal SWRs was performed using an electrical stimulation of the ventral hippocampal commisurre. After long training on the previous configuration, the rat used a counterclockwise strategy to solve the task, a strategy that does not rely on RE-WM. A different maze configuration (equal angles between the arms) was recognised by the rat as a different environment. On this maze the rat did not use the counterclockwise strategy anymore to solve the task which allowed us to continue the experiments.
No performance deficit nor running speed difference was observed between trials with ripple disruption and stimulated control trials. In stimulated control trials stimulation occurred 100-250 ms after ripple detection to control for the effect of electrical stimulation alone. It is currently unclear why no performance deficit was observed. Possibly the arm-pick preference decreased the RE-WM load and therefor also the need for SWRs and co-occurring replay to solve the task. However, the time spent at reward and platform showed a negative correlation with increasing visits only when ripples were disrupted. More time at the rewards site implies more ripples. If ripples represent possible future choices, the additional time spent at the reward site due to ripple disruption might represent an increased level of uncertainty of the rat concerning its next arm choice.

Awake hippocampal replay during SWRs, has been causally linked to the learning of a short-term memory based rule. In addition to this our results suggest a role for awake replay to execute the rule, i.e. RE-WM, either by consolidating and retrieving recent events or by evaluating possible future choices. Closed-loop disruption of awake hippocampal SWRs did not impair RE-WM performance, likely because the rat could use stereotyped solving strategies that decreased the RE-WM load, but did seem to increase the rats uncertainty concerning its next arm choice. This hints for a causal link between awake hippocampal replay and RE-WM. In the future a version of the win-shift paradigm where performance is not influenced by stereotyped behaviour might provide more clarity on the role of awake hippocampal replay in RE-WM.

List of Figures

List of abbreviations and symbols

The next list describes several abbreviations and symbols that will be later used within the body of the document

AH	ammon's horn
AP	action potential
CSD	current-source density
dB	decibel
DG	dentate gyrus
EC	entorhinal corex
EIB	electrode interface board
EPSP	excitatory post-synaptic potential
ETR	entries until repeat
HC	hippocampus
Hz	hertz
IIR	infinite impulse response
IQR	interquartile range
kOhm	kilo ohm
KW	kruskal-wallis
LED	light-emitting diode
LFP	local field potential
LIA	large irregular amplitude
ms	milliseconds
PaS	parasubiculum
PrS	presubiculum

RE-WM	recent-event working memory
REM	rapid-eye movement
RMS	root mean square
RP	ripple power
S	subiculum
s	seconds
s.e.m	standard error of the mean
SI	stereotypy index
SIA	small irregular amplitude
SW	sharp-wave
SWR	sharp-wave ripple
TTL	transistortransistor logic
VHC	ventral hippocampal commissure
VTE	vicarious trial and error
WM	working memory

Contents

Chapter 1

Introduction

The brain consists of about 86 billion cells and can be considered to be one of the most complex organs of the human body [4]. The first scientists that spent their careers exploring its anatomy and function had very different backgrounds: medicine, physics, biology, chemistry or mathematics. Soon it became clear that collaborative research amongst these would be necessary to unravel the mysteries of the brain and for that reason a new interdisciplinary scientific field emerged: neuroscience. The name became official after the foundation of the Society of Neuroscience in 1970.
The experiments reported here are performed in the laboratory NERF, Neuro-Electronic Research Flanders. This neuroscience laboratory, empowered by imec, KULeuven en VIB, promotes collaborative, interdisciplinary brain research. It develops innovative neurotechnologies and novel experimental assays that can link activity in neuronal circuits with mental function. Neuronal circuits that establish spatial memory are the focus of this project.

Fascination for the brain is not as new as the name for the corresponding science. Already 7000 years ago people drilled holes in the skull and judging from the precision, clearly with the intention to cure and not to kill. A remarkable observation people made back then was that depending on where the hole was drilled, different things happened to the patient. For example, blindness emerged after damage to the back of the skull or motor function impairments were observed when there was damage to the top of the head. Now it is understood that the brain can be divided in different areas, each responsible for a separate function of the human body.
Another remarkable feature of the brain is that it never stops changing. In addition to growing like the rest of our body, the connections between brain cells are constantly modified depending on encountered events. In other words, the brain changes based on experience. The past 70 years of neuroscience research have indicated that this constant modification is the key to remembering and learning new information or skills [51]. Re-experiencing a certain event enough times causes the neurons in the brain to form corresponding new connections and this allows the brain to reproduce or recall that experience in the future. Repetition thus seems to be the key to memory.

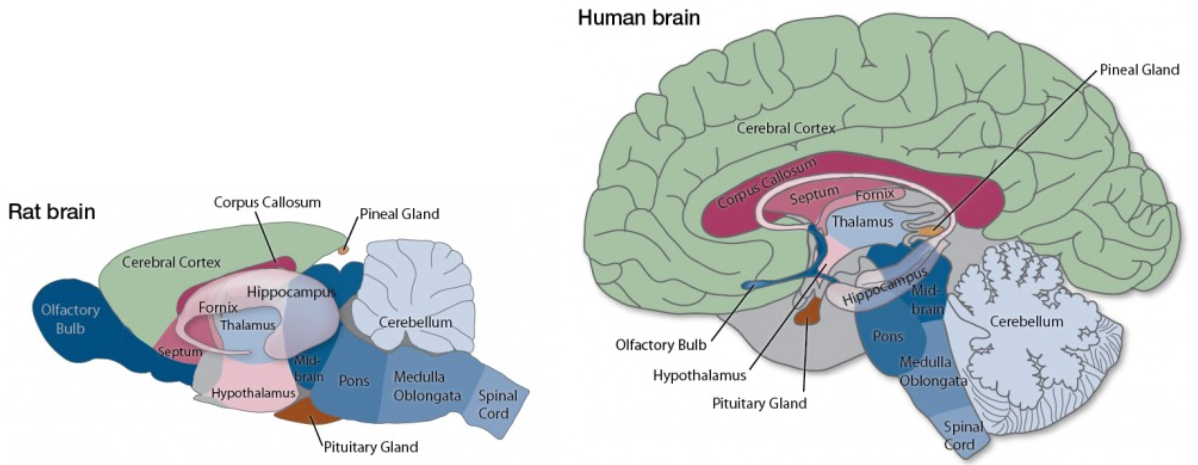

Figure 1.1: Similar organisational principle of a rat (left) and human (right) brain [114].

There are many different things that can or have to be remembered by our brain. Unfortunately, the memory space is not infinite and new information that comes in to the brain has to be processed and filtered so that only the necessary information gets stored. A healthy brain does this very efficiently and makes sure that all stored information can be accessed when a particular function requires it.
Navigation is one of those functions. Remembering where to go, recognising where you are, estimating how far you still have to go, etc., all rely on memory, or more specifically, spatial memory. Spatial memory is often used to guide you through an environment. Memories that are used to execute daily tasks are referred to as working memory (WM). There are several types of WM categorised based on the type of memory used and the task to be executed. When the brain uses a very recent spatial experience to make navigational decisions, the working memory is named recent-event working memory (RE-WM) [25]. Think about all those times that you searched something that you had lost. Spontaneously, your brain helps you to remember the places that you already searched to prevent you from going there again. The results of this project help to understand the neural activity and circuits behind RE-WM.

Most of what we know from the brain comes from animal research. This is because the techniques that provide direct access to neural activity are still too invasive for use in healthy humans. Rodents are used very often in memory research and the brain region mostly focussed on is the hippocampus (HC). Localised deep in the temporal lobe of the human cortex, the HC is a highly specialised structure that has been associated with learning and memory since the early 50's. Its internal structure is very similar across almost all mammalian brains, which explains why so much memory research is conducted using rodents. The location of the HC in a rat and human brain is shown in figure 1.1. Understanding its precise function is still one of the important challenges for the future. Important because failure of the hippocampal circuits is associated with pathological conditions such as Alzheimer's disease [121] [50] [87], sleep disorders [7] [110] and epilepsy [5] [55].

Very interesting observations were made when arrays of wires, capable of recording neuronal activity, were inserted in the HC of a rat when it freely explored an environment. Short pauses in locomotion caused the overall activity of the hippocampal cells to slow down significantly. However, during short approximately 50 ms long episodes in the break, the HC again strongly increased its activity in high amplitude, high frequency oscillations called ripples occurred (see figure 1.2). Deeper analysis revealed that the hippocampal cells are not activated randomly during ripple events. The cells that become predominantly active are the same cells that also showed high activity during the preceding exploration [90]. Furthermore, cells active in both exploration and resting periods are activated in the same relative temporal order [106]. The hippocampus thus shows the same activity pattern of a certain event during a subsequent resting period as if it uses that time to re-experience that previous event again. The re-expression of neural activity patterns strongly suggests a role for learning and memory and for that reason the reactivations are also referred to as memory-trace reactivations or replay [67] [43]. A direct causal link with learning was recently established in a project from Jadhav et al. in which rats exhibited an impaired spatial learning when memory-trace reactivations were artificially blocked [58]. The real-time detection and disruption of memory-trace reactivations is referred to as closed-loop perturbation of hippocampal replay.

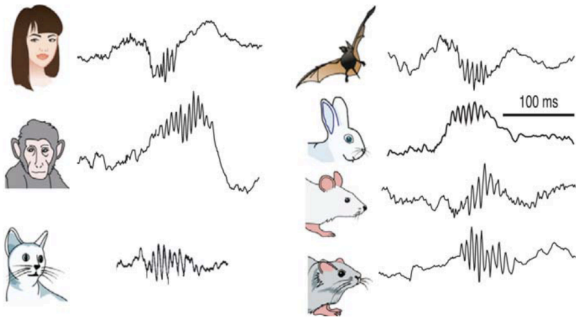

Figure 1.2: Hippocampal ripples conserved across mammals. Illustrative ripples recorded from different species [19].

Apart from contributing to a learning process, memory-trace reactivations during short breaks could also be used by the hippocampus to make a recent-experience motivated decision. This is exactly what a RE-WM function of the hippocampus would entail.

In this thesis closed loop perturbation of awake hippocampal SWRs is used to investigate a causal link between replay and RE-WM in rats. The experimental setup is similar to the experiment from Jadhav et al. ([58]) except that perturbation occurs after the rats have learned a spatial task. In this way we solely investigate the role of replay in RE-WM and not in learning.

The next chapter introduces the field of rodent hippocampal memory research. It discusses briefly the techniques used for extracellular recordings in freely moving animals and basic anatomical and electrophysiological features of the rodent hippocampus. The last part focusses in more detail on the recent research concerning the function of awake hippocampal replay. Chapter 3 provides a detailed overview of the experimental approaches and techniques that are used. Chapter 4 and 5 present and discuss the results. The first part of these chapters characterise the behaviour of the rat in a RE-WM task and the link with its hippocampal activity. The last parts present and discuss the behavioural effect of closed-loop perturbation of hippocampal replay. A last we propose new ideas for future research and conclude our findings.

Chapter 2

Background information

2.1 Recording from the brain

2.1.1 Historical introduction

Like many revolutionary discoveries, the legend goes that the electrical nature of our nervous system was discovered by accident. The assistant of the Italian physician Luigi Galvani (1737-1798) unintentionally touched an exposed nerve in a dead frog (the sciatic nerve) which triggered, to the highest surprise of both, a movement of the frog's leg as if it were back alive. Galvani presumed that the movement of the muscle was caused by electrical interactions and he named this intrinsic property *animal electricity* [20]. In 1791, he published *De Viribus Electricitatis in Motu Musculari Commentarius* and together with the work of other revolutionary people like Emil de Bois-Reymond, the nervous system became understood as a complex network of neural wires conducting electricity from and towards the brain [1].
However, science had to wait for the work of the German neurologist Franz Nissl and the Italian histologist Camillo Golgi in the late nineteenth century to finally 'literally' see the real nature of those neural wires [8]. They developed independently from each other two techniques that enabled the visualisation of individual brain cells (see figure 2.1b and 2.1c). Thanks to the work of the Spanish anatomist Santiago Ramón y Cajal, who spent 25 years of his life unravelling these beautiful stainings of brain tissues, we now know that cell theory [2] also applies to the nervous system and this became known as *the neuron doctrine*. More precisely, Cajal suggested that the nervous system is a complex network made up of individual, discrete electrically active cells (neurons) together with several different supporting glial cells (e.g. astrocytes and microglia), that all communicate with each other via specialised contact points (synapses) and thereby transfer information throughout the whole body. Figure 2.1d shows one of Cajal's famous drawings.
The understanding of how neurons produce and conduct electrical signals was rewarded with the Nobel price for physiology in 1963 awarded to Andrew Fielding Huxley

[1] Previously, famous scientists like the anatomist Andreas Vesalius and the French philosopher and mathematician Réné Descartes believed that the nervous system formed a continuous reticulum with the brain pumping an electrically active fluid around the body, similar to the circulatory system, where blood circulates through the body by the pumping of the heart.

[2] for review on cell theory see [71].

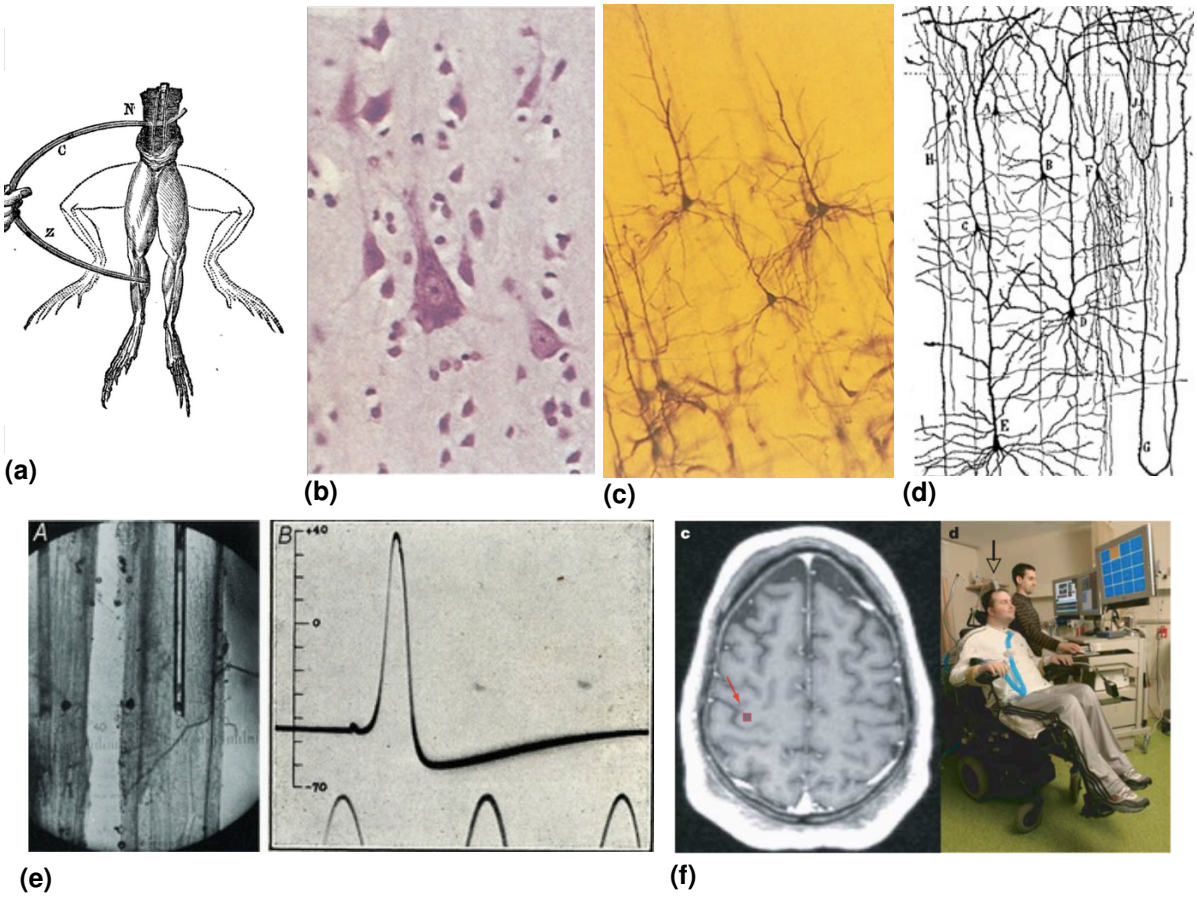

Figure 2.1: Overview of major steps in neuroscience a) Schematic representation of the experiment of Luigi Galvani showing legs of a frog with the upper part dissected, C and Z represent copper and zinc wires respectively. When C and Z are connected the legs move as if the frog were alive. b) Example of a Nissl stain from a brain slice. The dark spots represent the cell bodies of the neurons. c) Example of a golgi stain from a brain slice. This stain allows the visualisation of neurons as a whole; cell body and neurites. d) Famous drawing of Santiago Ramón y Cajal where he identified the different cell types and cell layers in the human cortex. e) Results of the experiments of Hodgkin and Huxley from 1939-1945. On the left a photomicrograph of an electrode inside a squid giant axon (diameter $500\mu m$). Two views of the same axon are visible from an ingenious system of mirrors devised by Huxley. This allowed simultaneous viewing of the electrode from both front and side and was essential to avoid the electrode damaging the nerve membrane as it was threaded down the axon. On the right the first intracellular recording of an action potential (=neural signal). The sine wave time marker has a frequency of 500 Hz. f) Tetraplegia patient implanted with a 96-microelectrode array (4 x4 mm) in the primary motor cortex. This allowed the patient to perform basic tasks such as opening an email and operate devices such as a television or radio. On the left an MRI of the brain of the participant indicating the location of the implant (image taken before the implantation). (Figures a) to f) reproduced from [116], [49] [56] [102] [53])

and Alan Lloyd Hodgkin *for their discoveries concerning the ionic mechanisms involved in excitation and inhibition in the peripheral and central portions of the nerve cell membrane* [102]. Hodgkin and Huxley isolated the giant axon of a long-finned squid (Loligo forbesi) and by recording (and controlling) its electrical activity they came up with a first mathematical model for neural activity [54]. These series of experiments clearly showed that direct recordings of neural activity provide fundamental information about the physiology of the brain.
Modern technology has now evolved to allow electrical recordings of individual neurons in unrestrained animals and even humans. These kind of in-vivo experiments allow to correlate electrical patterns directly with behaviour and even allow to interfere with the neural activity to establish a direct causal link or even have clinical applications (see figure 2.1f). In the remainder of this section we will shortly introduce the in-vivo techniques after providing a bird's-eye view of the fundaments of our beautiful nervous system.

2.1.2 Neurons and electricity

Golgi stains of brain slices reveal that neurons have two clearly distinguishable parts: a central part containing the cell nucleus (cell body, soma or perikaryon) and thin tubes extending radially from the cell body (neurites), see figure 2.2a. These neurites can be divided in two groups: dendrites and axons. Dendrites branch heavily when they originate from the soma and together form a large dendritic tree. They are covered with many synapses, highly specialised membrane structures that enable signals to transfer from one neuron to another. As a result the dendritic tree receives many signals from other cells and thus serves as the antenna of the neuron. The axon serves as a wire to conduct signals from the soma all the way to the presynaptic site to transfer information from one neuron to the next. The axon size in humans varies a lot, from $<$ 1 mm to $>$1 m in length and from 1 μm to 25 μm in diameter. Dendrites are generally much shorter, up to 2 mm, suggesting different conduction mechanisms for neural signals in dendrites and axons [9].
When an excitatory input is given at the synapse on a dendritic branch, this is generally a neurotransmitter released from the presynaptic cell (e.g. glutamate or acetylcholine) that binds to its receptor on the postsynaptic cell, the postsynaptic cell membrane depolarises due to an influx of sodium ions (Na^+) through dedicated channels. This excitatory post-synaptic current generates an excitatory post-synaptic potential (EPSP) across the cell membrane that passively travels all the way down to the soma. There it gets summed (spatially and temporally) with EPSPs from other synapses and branches, eventually leading to a depolarisation of the initial segment of the axon, the axon hillock. When this depolarisation passes a threshold, the sodium channels from the axon hillock open and due to the specific membrane properties of the axon this initiates an action potential (AP). Figure 2.2b shows this process schematically.
An AP is a short characteristic ($\sim$ 2 ms) depolarisation/repolarisation of the axon membrane that actively travels (constantly reinforced) down the axon length and the rate at which these action potentials are fired (i.e. initiated from the axon hillock) represents the response of the neuron to the input signals. Because both the EPSP and AP are depolarisations/repolarisations of the membrane caused by influx and efflux of ions between the extracellular and intracellular medium, the activity of a cell can be mea-

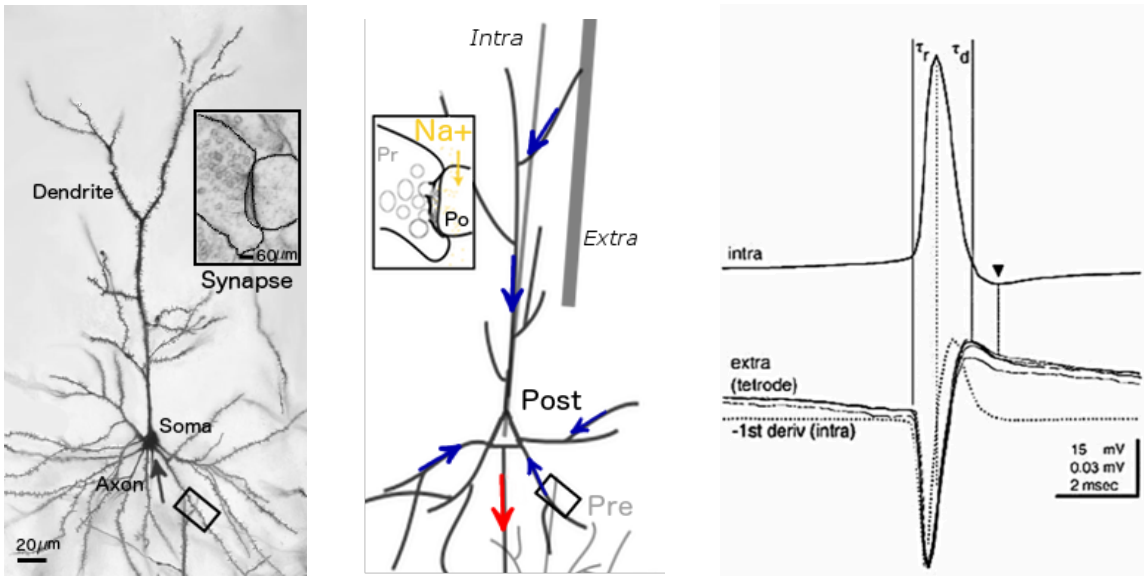

Figure 2.2: Basic anatomy and physiology of a pyramidal neuron a) Golgi stain of a pyramidal neuron in the parietal cortex of a rat brain, the arrow indicates the axon which disappears out of the image plain. The inset is an enlargement of the boxed region showing an electron-microscopic image of an individual axodendritic synaps (osmium stained). Both pre - and post-synaptic neuron are visible, the former filled with synaptic vesicles containing neurotransmitters. b) a schematic representation of a pyramidal neuron. Activation at the dendritic synapses create EPSPs (blue arrows) that travel all the way down to the soma where they get both spatially and temporally summed. Above threshold depolarisation of the intial segment of the axon creates an AP (red arrow) that travels down the axon membrane actively towards other neurons. In the inset a schematic representation of an activated synapse triggering the influx of sodium ions (Na^+) into the post-synaptic cell. c) Comparison of an AP recorded from both an intra- and extra-cellular measurement (see b)). The extra-cellular recording approximates the first derivative of the intracellular AP. (source: In a. neuron [62], synaps [1], in b. recordings [52])

sured both intracellularly and extracellularly using recording electrodes. Figure 2.2c shows both intracellular and extracellular measurements of an AP. Important to notice is that the extracellular potential varies only within the range of 100 μV whereas the intracellular potential varies with several tens of mV. However, intracellular recordings cannot provide high throughput brain recordings as a single electrode only records the activity of a single cell. High throughput brain recordings are necessary to analyse the cooperation of neurons that establish functional neural circuits. Additionally, intracellular recordings are very challenging since puncturing the cell membrane increases the chance for cell death. Notably, scientists recently succeeded to perform intracellular measurements in a freely moving animal for about 20-60 min [66]. On the other hand extracellular recording electrodes pick up signals from multiple surrounding cells and have a lower risk to damage the cell. This increases the likelihood for more stable and long term recordings of a large population of neurons. These advantages motivate the usage of extracellular recordings for in-vivo applications.

2.1.3 Measurements in freely moving animals

Electrophysiological brain recording generally requires 3 connections to the animal [111], see figure 2.3. The first is the ground lead. Usually this is a connection from

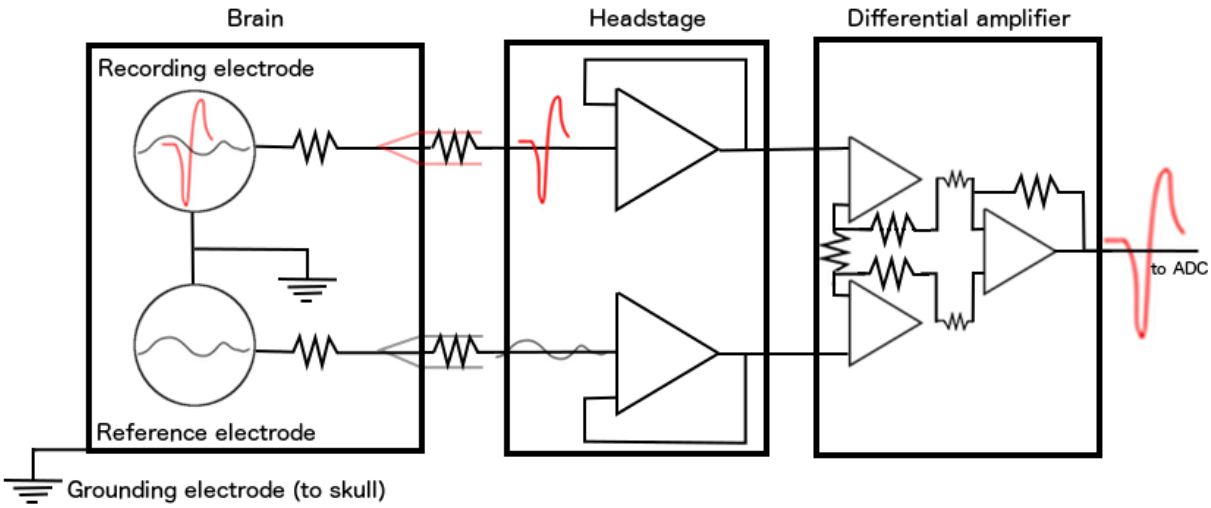

Figure 2.3: Schematic representation of setup for extracellular recordings. There are three contacts with the animal, the grounding electrode fixed to the skull, and the recording and reference electrodes in the brain. To buffer and protect the signals they are sent to a nearby headstage where the current is amplified but voltage held constant. Using a differential amplifier the common mode of the reference and recording electrode is removed and the signal of interest can be sent to an analog-digital converter. Between the brain an the headstage the signal must interface with the electrode tip through its impedance and some of the charge that passed the tip is lost due to the dissipation across the electrode insulation (not indicated in this scheme for simplicity). (Scheme modified from [111])

the skull to a Faraday cage and it minimises the interference from outside signals, mainly the 50 Hz power-line. The remaining two are the recording electrode, inserted in the soma of a cell for intra-cellular recordings or inserted in the region of interest to pick up the desired extra-cellular signals, and a reference electrode. The reference electrode is placed in such a way that it ideally picks up the same 'far field' noise (e.g. internal signals like chewing artefacts, heartbeat,...) as the recording electrode but not the signal of interest. Using a differential amplifier the common mode of the reference and recording signal is subtracted from the latter to increase the signal to noise ratio significantly. In behaving animals both signals are first sent to an amplifier on a nearby headstage which increases the current (but keeps constant voltage) in order to prevent interference from the environment during conduction over the long tethers. The resulting combined signal can then be sent to an analogue-digital converter and computer for recording and further analysis.

A single tungsten wire was one of the first metal micro-electrodes used in mammals (before glass micro-electrodes were used) [57]. It was mainly chosen for its durability and strength which allowed easy penetration of the protective brain membranes (=meninges [3]), especially the dura mater. Later tungsten was replaced by stainless steel which showed less noise [46]. Using 80 μm stainless steel micro-electrodes the first recordings in unrestrained mammals (California ground squirrel) got published. These groundbreaking experiments by F. Strumwasser served as a proof of concept and started a new era where scientists continuously search for new and better methods for in vivo experiments of unrestrained animals [107].

[3]There are three protective membranes surrounding the mammalian brain. From brain to outside: pia mater, arachnoid membrane and dura mater.

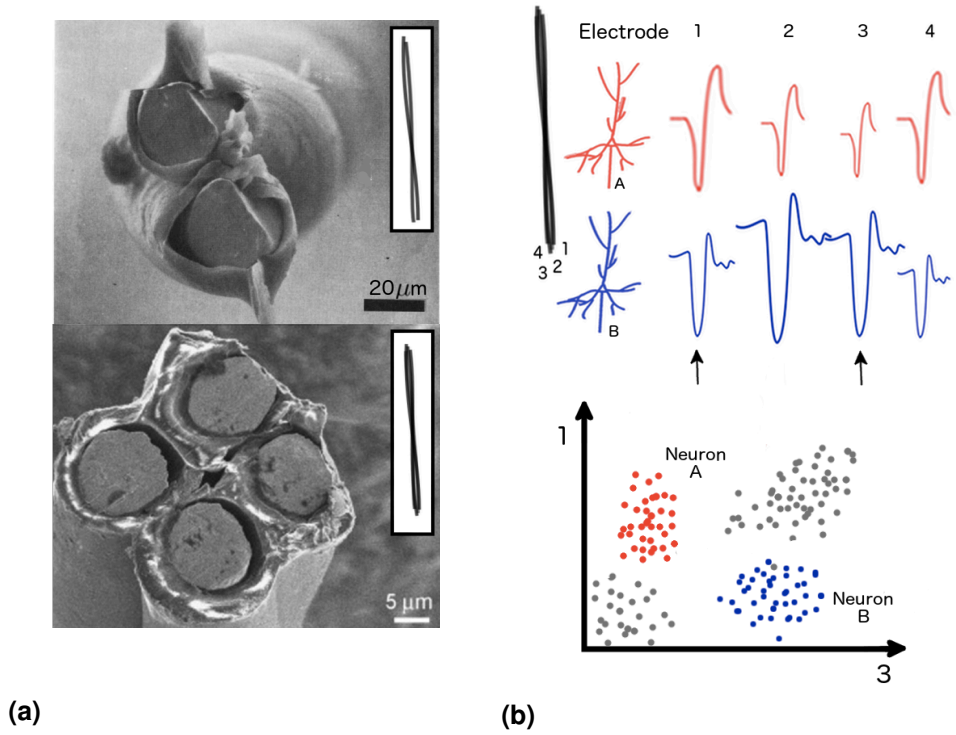

Figure 2.4: Method for initial spike sorting. a) EM pictures of the crosssection of a stereotrode (top) and tetrode (bottom). Insets provide the side view schematically, showing the twisting of the wires. To make one stiff wire the insulation of the electrodes is heated. b) Cartoon showing the advantage of multiple-electrode wires for spike sorting. The AP of one neuron has a different amplitude at different electrodes as a consequence of diffusion through the extracellular space. This difference is characteristic for each neuron as it depends on the origin of the signal (=position of the cell). Plotting the amplitude of detected spikes from one electrode against another creates statistical clusters representing spikes from a single neuron. (source: The stereotrode form [73] and tetrode from [94])

Nowadays the micro-electrodes used often consist of two (stereotrode) or four (tetrode) isolated micro-electrode wires, twisted together and cut at a blunt angle at the bottom, see figure 2.4a (initial designs for stereotrode and tetrode by [73] and [94] respectively). The material used can vary amongst different labs with nichrome (nickel and chrome) or polyamide coated iridium as the most popular choices. The main advantage of this stereotrode/tetrode configuration is that the wires will pick up spikes from the same neurons, as they are in very close proximity to each other, but all with a different amplitude (see figure 2.4b). Plotting the signal amplitudes picked up by the four wires against each other results in the formation of statistical clusters of the neural data, where each cluster can be interpreted as a group of spikes originating from the same neuron.

Recording activity of individual cells is very informative. This also immediately raises the question amongst scientists studying neural circuits how we can increase the number of recorded cells. Recording the activity of over a hundred units can provide very direct evidence of communication and firing patterns in the neural network. For this purpose several designs of *hyperdrives* have been developed. In short, a hyperdrive consists of a (plastic) holder with multiple micro-drives that carry the tetrodes

and allow for lowering them into the correct spot in the brain. The hyperdrive with all the micro-drives loaded is also referred to as a micro-drive array [111]. The lowering of the electrodes starts after the implantation of the drive on the head of the animal and is spread over several days or weeks to minimise the inflammatory reaction of the brain. For an excellent review of the measures taken to minimise the tissue reaction see [93]. Hyperdrives with both manual and automatic micro-drives have been designed in which lowering of the tetrodes happens manually with a screw driver or is steered by a rotary motor respectively. The advantage of the automated version is that the animal does not have to be restrained to move the tetrodes. The downside is that the drives are heavier, which can limit the animal in its free movements, and are also quite costly. In this project the manual Kloosterman hyperdrive is used with polyamide coated iridium tetrodes [61]. A more detailed description is provided in methods.

2.2 Rat hippocampus

The human brain contains roughly 86 billion neurons and weighs about 1300-1400 g. The rat brain on the other hand contains only 200 million cells and weighs only 2 g [4]. Still, the two brains have many similarities in structure and function as do most other mammalian brains and this allows for projection of the results to some extent. Rodents are often used in experiments with invasive recordings because of ethical considerations. We use rats instead of mice as their brain is larger and thus allows easier access with electrodes. Furthermore spatial learning and memory of rats is believed to be a close equivalent of human declarative memory, a topic we will return to in more detail later (see section 2.3.1). All this together motivates the use of rats in this kind of research.
This section will focus on the specific anatomy and neural activity of the highly specialised region of the rat midbrain from which recordings in this experiment have been done; the hippocampus (HC), present in all mammalian brains. The anatomy and function of the HC is of high interest for scientist all over the world ever since the first report in 1957 suggesting a role for the HC to memory [103]. In this report a patient H.M. suffered from severe memory deficits after undergoing psychosurgery. Further investigation showed that the HC was severely damaged on both sides and that the patient had mostly troubles with remembering new (recent) information. Nowadays a healthy HC can be seen (to a first order) as a relay station for transforming short term to long term memory and as a spatial navigator.

2.2.1 Hippocampus anatomy

The HC is part of the hippocampus formation group. This group consist of five different anatomical midbrain regions surrounding the thalamus; the HC, entorhinal cortex (EC), subiculum (S), presubiculum (PrS) and the parasubiculum (PaS). They are all heavily connected and are therefore considered to be one big functional unit (see figure 2.5a).The HC itself is sometimes also referred to as the HC proper to avoid confusion with the hippocampus formation group [2].
The hippocampus proper consists of two major parts: the dentate gyrus (DG) with granule neurons and ammon's horn (AH) with pyramidal neurons (layers CA3, CA2,

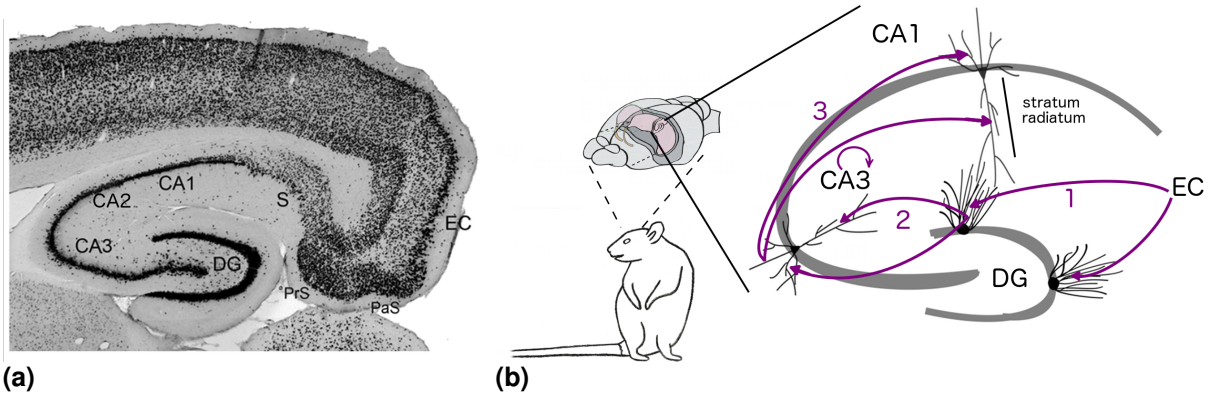

Figure 2.5: Tri-synaptic pathway in rodent hippocampus. a) Horizontal section of a rat brain (Nissl-stained) showing the HC (DG, CA3, CA2, CA1) and surrounding cortex. EC entorhinal cortex, S subiculum, PrS presubicu- lum, PaS parasubiculum. b) Cartoon of the tri-synaptic pathway in the rodent HC. Major input comes from the EC innervating the granule cells of the DG. Next both the apical and basal dendrites of CA3 are activated by axons of the DG (mossy fibers). The third step is the projection from CA3 to CA1. The axons of CA3 (schaffer collaterals) synapse mainly on the apical dendrites of CA1 neurons in the stratum radiatum. (source: Nissl stain from [111]

CA1). The connection between these different regions is very specific and is referred to as a *unidirectional, tri-synaptic excitatory pathway* [111]. The first stage is the major input from the EC, which gets its input from the neocortex (mainly the cortical association areas), to the granule cells of the DG. The mossy fibers (axons of the DG neurons) that synaps on the dendrites of CA3 pyramidal neurons form the second stage. CA1 pyramidal neurons get their input from the CA3 neurons (axons = Schaffer colatterals) that synapse mainly on their dendrites located in the stratium radiatum, apical dendrites. This completes the tri-synaptic excitatory pathway and as the name already reveals all connections are excitatory. This kind of network connectivity is referred to as a feed-forward loop. This feed-forward loop is further regulated by CA3 neurons that not only project to CA1 but also to other CA3 neurons. This recurrent projection is in part responsible for the characteristic activity observed in the local field potential of the CA1 region. Figure 2.5b summarises the neural connections forming the tri-synaptic pathway.

On top of these principal neurons in the HC, there are also at least five different interneurons [4] (good for 11% of the hippocampal cells) that also modify the cell firing patters of the hippocampal neurons [64]. Because CA2 neurons are not part of the tri-synaptic excitatory pathway, memory research has mainly focussed on CA3 and CA1 neurons although the CA2 activity has been shown to be essential for proper cognitive function (for a review see [96]).

The highly structured arrangement of cell types in thin layers makes the HC a very interesting region for micro-electrode recordings. Moving the electrodes from dorsal to ventral in the rat HC changes the polarisation of the overall activity (summed electrical currents flowing from surrounding neurons) and this gives relatively precise feedback on the position of the electrode [18] [108]. This extracellularly recorded summed neural activity is called the local field potential and is very specific in the HC.

[4] classification based on the principal cell compartment that they target [44].

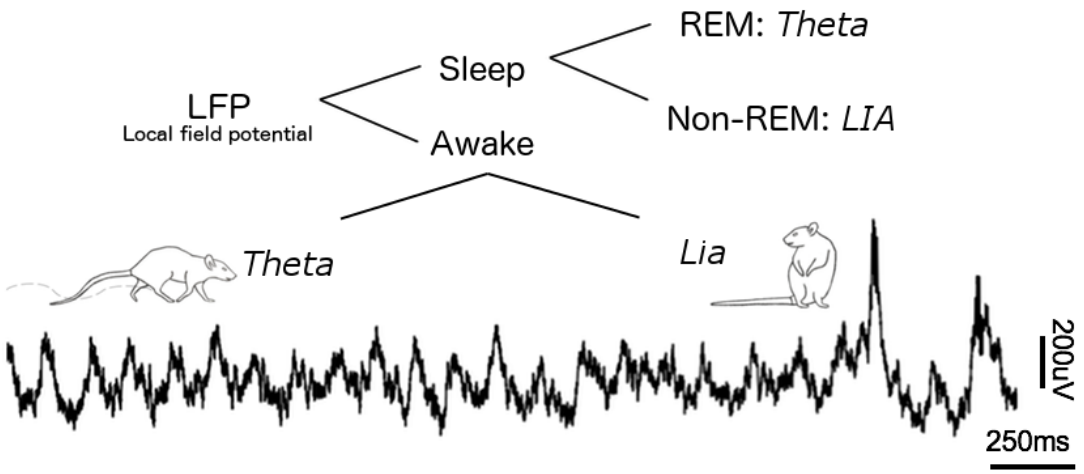

Figure 2.6: Overview of the hippocampal LFP states in rodents in relation to behaviour. The local-field potential in the HC changes depending on the behavioural state of the animal. Theta and LIA occur both during sleep and awake states. Signal trace is an example of LFP recorded from the HC during awake behaviour, showing the transition from theta to LIA when the animal stops running. A third LFP state, SIA, is not indicated in this schema but occurs mostly during transitions between LIA and theta.

2.2.2 Hippocampal local field potential forms: Theta and LIA

The local field potential (LFP) observed in the rat HC is divided into three types; theta, large irregular amplitude (LIA) and small irregular amplitude (SIA) , each associated with a specific behaviour [15]. Theta is a regular LFP characterised by small regular 6-10 Hz oscillations. The other two, LIA and SIA, are both irregular LFP signals with irregularly occurring large and small high frequency oscillations respectively. The regular oscillations observed during theta are called theta waves, simply as a result of the sequence in which LFP oscillations were identified. (Other LFP frequencies are designated with other Greek letters like α, β,. . . [2]).
Both theta and LIA are observed during the awake and sleep state but characterise different behaviours. In sleep it is accepted that theta characterises the rapid-eye movement (REM) sleep while LIA occurs during the non-REM sleep. Figure 2.6 indicates what happens during the awake state. When the animal displays preparatory behaviour, such as exploring, rearing, sniffing and ambulation, the LFP shows stable theta oscillations. Once the animal is immobile, during grooming for example or for consumption of food and water, the characteristic irregularly occurring high amplitude oscillations of LIA are measured. The next paragraph focusses in more detail on the neural activity in this brain state as this is the neural activity of interest for this project. SIA is sometimes observed during transitions between brain states [59], but its function and precise association with behaviour is not yet well understood. In the remainder of this report we will follow the nomenclature introduced by Buzsáki Gyorgy namely, behaviours associated with theta state are *preparatory behaviours* and those associated with LIA state are *consummatory behaviours* [15].

During LIA the overall cell activity slows down which creates a slow low amplitude LFP oscillation of 1-4 Hz. However the signature of LIA are the irregularly occurring transient large amplitude deflections. These deflections, called sharp-waves

(SW), last 40-100 ms and originate in the stratum radiatum where the CA3 axons excite the CA1 apical dendrites [27] [123]. The excitation creates EPSPs in the apical dendrites of a CA1 neuron and can be observed as a negative polarisation in extracellular potential [15]. The recurrent excitation network organisation in CA3 almost always causes a population burst [5] in response to the input from the DG (=epsilon bursts [120] [11]) and it is this synchronous excitation of almost all CA1 apical dendrites that explains the observed very large negative polarisation in stratum radiatum, the sharp wave (see figure 2.7). Mostly the bursting of CA3 neurons, resulting in the sharp wave, induces a bursting of the CA1 neurons [123]. In most cases, an increase in LFP frequency comes together with a decrease in LFP amplitude for the reason that the high negative-positive amplitudes induced by the spikes cancel each other [17]. Due to the network properties of the CA3-CA1 connection, the bursting of CA1 neurons is highly synchronised and instead of cancelling each other out they create very characteristic high amplitude oscillations (150-200 Hz) which are called 'ripples', with the highest amplitude in the center of the CA1 cellular layer [74]. The rhythm generation of this burst is due to the interference of many different interneurons with the spiking activity of CA1/CA3 neurons [64]. The ripple with the co-occuring (SW) is referred to as *sharp-wave ripple (SWR)* and is one of the most synchronous, self-organized population events in the mammelian brain [13] [23] [26]. The precise neural mechanism behind the SWR is still under a lot of debate but some basic models start to emerge showing the importance of cell-type specific connections [15].

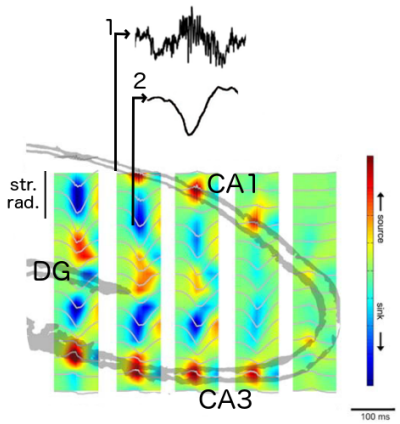

Figure 2.7: Vertical change in recorded LFP signal. Current-source density (CSD) maps (1 Hz to 10 kHz) showing the regional distribution of SW currents (superimposed in gray traces), originating from the stratum radiatum. During LIA the SW initiates synchronous firing of CA1 neurons, measured in the LFP as high amplitude high frequency oscillation (=ripples) and best observed with an electrode in the cellular layer (1). The high synaptic activation at the apical dendrites of CA1 neurons is reflected by the negative region (sink) in the stratum radiatum (2). (CSD map modified from [108])

Analysing the LFP signals and trying to understand their correlation with behaviour is very informative and is what we will do in this project. In order to clearly understand why looking at hippocampal LFP helps to understand spatial memory we have to zoom in and look at single cell activity, also referred to as unit activity.

[5] many cells firing at the same time.

2.2.3 Unit activity: Place cells and replay

In 1971 O'Keefe and Dostrovsky recorded the activity of single neurons in rodents from the CA1 region (with tetrodes lowered in CA1, see section 2.1.3) and observed that the pyramidal cells showed an overall low firing activity. However when the animal entered a specific location in the environment, some ensemble of cells increased their firing rate dramatically, a burst firing [80]. Later Lee and Wilson demonstrated beautiful sequences of cell ensemble firing when a rat moved back and forth on a linear track [67], see figure 2.8a and 2.8b. These cells and their corresponding spatial region in the environment are called place cells and place fields respectively. Place cells are also found in monkey HC and human HC, the last one recorded in epileptic patients (for monkey see [85], [97] and [68] and for human see [42]).
The discovery of place cells served as first electrophysiological evidence for the cognitive map theory proposed by Tolman and thus also the role of HC for spatial memory (see next session) [112]. A second insight resulting from the discovery of place cells is that, if the activity of enough units can be recorded, thereby showing clear sequences when moving through an environment, the position of the animal can be reconstructed using proper decoding techniques. This was first demonstrated by Wilson and McNaughton [119] and later by many others, each contributing to the improvement of the decoding algorithms [6] [12] [124] [29] (for an example see figure 2.9a). The decoding of the animal's position was a great success and lead to the discovery of what is now referred to as memory-trace reactivations or just replay.

Replay is the reactivation of a place-cell sequence from active behaviour during immobility and non-REM sleep, in the same temporal ordering but on a compressed time scale. First it was shown by Pavlides and Winson that the firing of place cells during consummatory behaviours is influenced by their activity during preparatory behaviours [90]. The firing rate (spikes per second) of a place cell during sleep significantly increased when the rat had frequently entered the corresponding place field in the preceding awake session. Thus, when a cell fires a lot during the exploration of an environment, it will fire a lot during sleep.

But what about ensembles of cells, for example a pair of cells with overlapping place fields? Their activity is highly correlated during exploring, and Wilson and McNaughton [119] showed that this correlation persists during sleep. Finally in 1996 it was shown that the temporal ordering of neuronal cell firing during sleep reflects their firing ordering during awake behaviour [106]. Skaggs and McNaughton also showed that this relation, cell firing correlation, was stronger after the task compared to before, showing that these reactivations are strengthened by experience.
The real replay of sequences during LIA was shown in the experiment of Lee et al. [67] and their experiments also clearly showed the sequence time compression (see figure 2.8c). An important observation in these experiments is that replay is observed during cell activity burst and that these bursts generally co-occur with SWRs, the signature of LIA state. We know that LIA occurs during non-REM sleep, but also during immobility periods in the awake state. And indeed, a few years later replay was also observed in the awake state [43].
To summarise, experiences from preparatory states, such as exploration, are replayed during consummatory behaviours, such as non REM sleep and immobility periods during the awake state. This reactivation of place cell sequences or *replay* is also referred

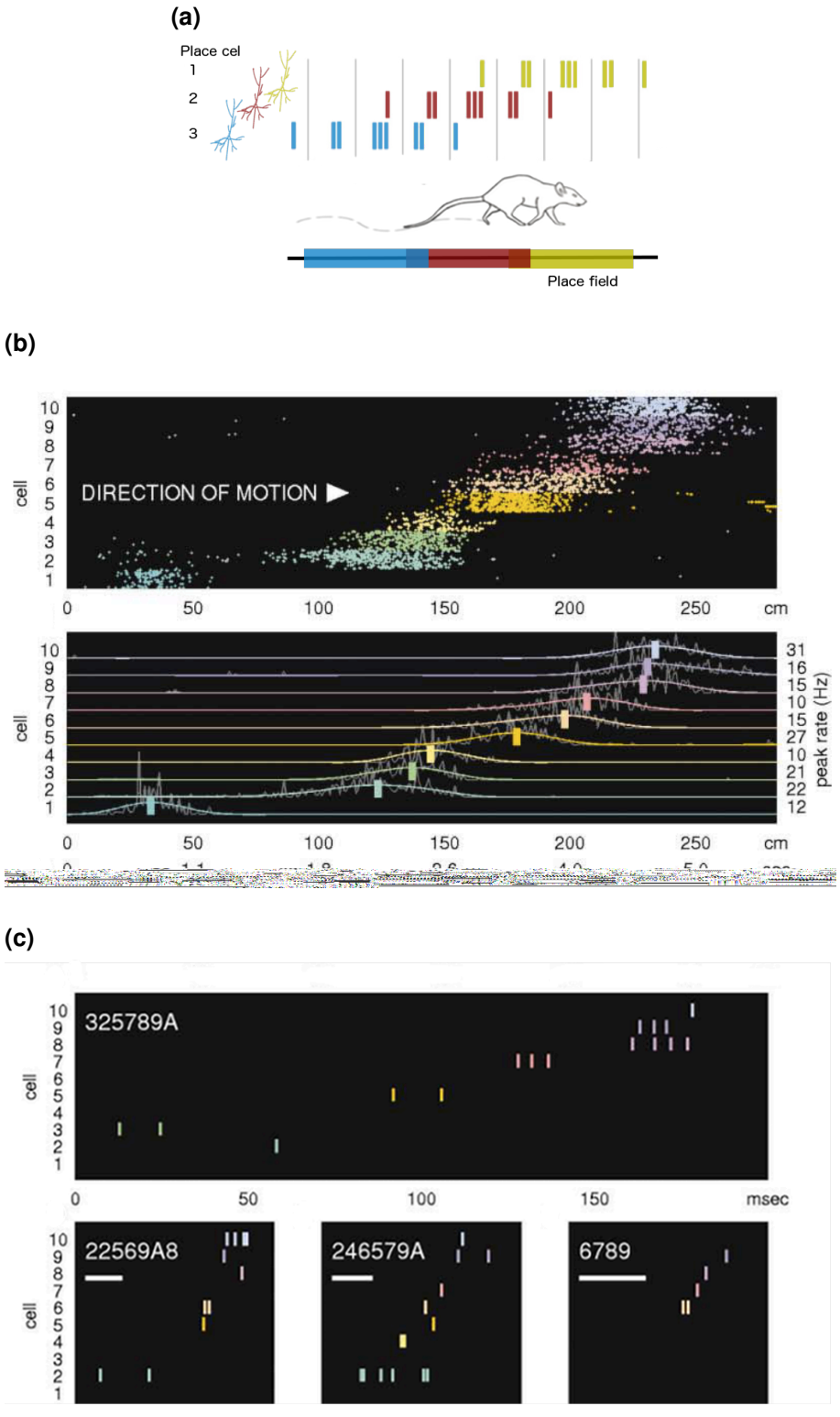

Figure 2.8: Hippocampal place cells, place fields and replay during sleep. a) Cartoon showing the sequential firing of place cells (vertical bars) when the animal crosses the corresponding place field (horizontal bars). b) On top a lap-by-lap raster of the activity of ten place cells (different colours). For each cell, 30 laps are stacked from bottom to top. In each lap the same cells are active at the same point in space creating a place-cell sequence. Bottom graph shows smoothed place fields (coloured lines) of the same ten cells. Vertical bars mark the positions of the peaks of the smoothed fields. Smoothed firing rate (Hz) at these peaks shown to the right. Nonuniform time axis below shows time within average lap when above positions were passed, the animal was thus moving (although not at a constant speed). c) Same experiment as in b) but now recordings from a subsequent sleep session. The same place cells fire in the same sequential order but now on a much smaller time scale. Bottom three graphs show other examples of replay post-experience sleep. (source: data in b) and c) from [67])

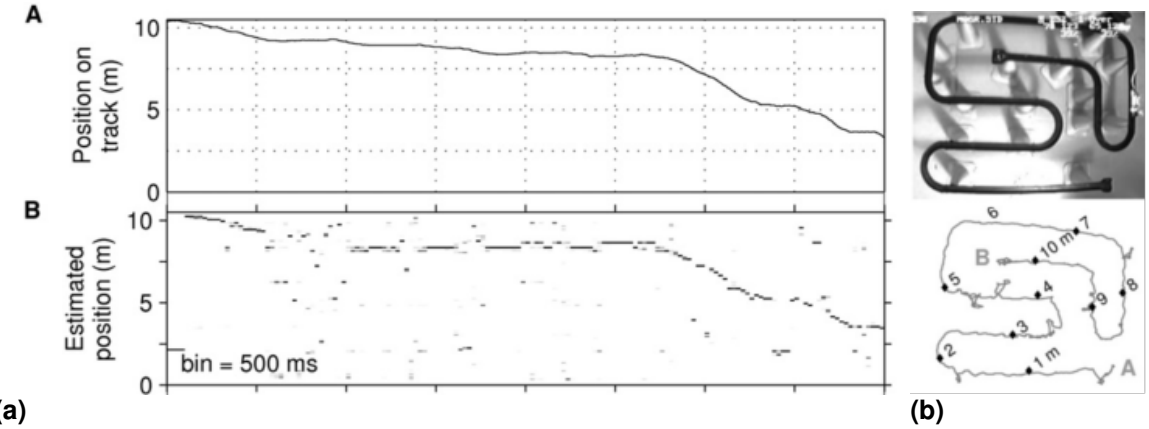

Figure 2.9: Decoding the position of an animal using place-cell activity. Graphs in a) show the real (top) and decoded (bottom) position of a rat running 80 seconds on a 10 m long track (see b)). Each column in the bottom graph is a probability density function estimated from unit activity in a 500 ms window. White, p = 0; black, p = 1. (source: [29])

to as memory-trace reactivation as the properties of this replay strongly suggests their role in memory, in the form of what is called memory consolidation.

2.3 Short term memory and awake replay

There exist many different forms of memory and research of the past century has shown the involvement of many different brain regions to each of these [113]. The categorisation of memory systems into distinct groups can happen in different ways. One way is to distinguish declarative and non-declarative memory [89]. Declarative memory constitutes memories that are easy to verbalise. The category can be subdivided into episodic memory, a recollection of experiences and semantic memory, facts and knowledge of the environment without a specific timestamp. Habits, reflexes and skills on the other hand are examples of non-declarative memory [113]. Another frequently used way to distinguish different memories is between short-term and long-term memory [75]. Spatial memory cannot be categorised in any of these because it is a combination of declarative, non-declarative, short-term and long-term memory [89].

2.3.1 Spatial memory: Two stage model

Spatial memory thus forms a category by itself and was defined by Paul et al. as: *That brain function responsible for recognizing, codifying, storing and recovering spatial information about the arrangement of objects or specific routes* [89]. This spatial information can be processed using two different strategies: egocentric and allocentric. The first strategy ignores completely the spatial cues and only relies on proprioception of the body. It can lead to stereotyped behaviour, for example always turning to your right at choice points. With the allocentric strategy not your body but external cues serve as the point of reference to localise target locations and reward sites. In 1948

Tolman observed that rats, after some learning period, solved maze tasks using strategies and shortcuts instead of simply using the association between external stimuli and behavioural responses (as they do in the beginning) [112]. To understand this behaviour Tolman hypothesised that rats are capable of creating an internal representation of an external environment; the cognitive map. Humans are also able to navigate strategically through an environment and are in addition to this able to recall and verbalise their experience afterwards. This suggest that spatial memory, or at least a big part of it, is a form of declarative memory. Even though rodents cannot verbalise their actions, their spatial memory is believed to be very similar to that of humans. For that reason spatial memory of rodents is used nowadays as a model for the human declarative memory [92].
The existence of a cognitive map was later confirmed by other behavioural experiments but especially the discovery of place cells in rodents by O'Keefe and Dostrovsky confirmed this hypothesis [80]. The allocentric strategy is thus all about using external stimuli to create an internal representation of the external world and use this cognitive map to better navigate towards a goal location.

The two-stage model of memory, proposed by Buzaki in 1989, is one of theories trying to explain how the HC is involved in spatial memory [14]. The basic idea is that there exist two forms of memory-traces in the HC: a labile and strong form of which the last one, if strong enough, is transported to the neocortex for long term storage. The labile trace originates during learning when the brain is in the theta state (preparatory behaviour). Its content is the temporal firing order of place cells in CA1 (and CA3) and is temporarily stored in the CA3 network. It's assumed that temporary storage occurs in CA3 and not in CA1 because the CA3 network provides the major activating input for CA1 place cell firing and has a complex architecture with recurrent activations (almost not present in CA1) that could account for the temporal aspect of the place cell firing of CA1 (and CA3).
Transforming the labile trace into a strong memory-trace for long term storage requires memory consolidation. Memory consolidation is a concept based on Hebb's postulate: *cells that fire together wire together* [51]. The more a certain trace is reactivated, the stronger the firing correlation (synaptic connection) between the cells forming the memory-trace (via a process called long term potentiation LTP) and the stronger the memory-trace can become [21]. The memory-trace reactivation is exactly what replay does and the fact that it co-occurs with SWRs strengthens this hypothesis. The high amplitude oscillations of the ripple have some properties that are thought to be important to induce synaptic changes (synaptic plasticity). Nevertheless, the precise circumstances necessary for synaptic plasticity still have to be established, an important task for the future [15]. Other theories have also been proposed, all showing a determining role for replay in memory consolidation in rodents; standard memory consolidation theory, multiple trace theory, multiple storage site (for a review see [109]).

2.3.2 Awake replay

Most of the direct evidence for the memory role of replay in the HC comes from rodent research, although there exist a few reports where SWRs were recorded in humans

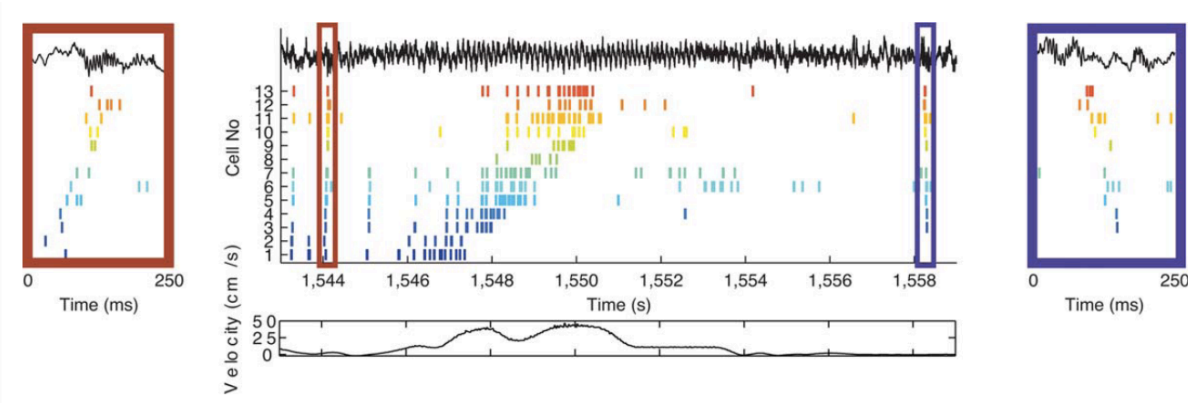

Figure 2.10: Forward and reverse replay during the awake state. This figure presents the first results showing the reactivation of place cell sequences (replay), both in forward (left inset, red box) and reverse order (right inset, blue box) before and after the experience respectively, while an animal is awake on the maze. Activity for place fields of 13 CA3 pyramidal cells on the track are shown before, during and after a single trial. The CA1 local field potential is shown on top and the animals velocity is shown below. Both forward and reverse replay occur while the animal is immobile. (source: data from [32] and modified by [15])

(epileptic patients [70] [3]).
A lot of the rodent HC replay research of the past few decades has focussed on replay during sleep. Since the initial memory-trace in the HC network is labile, it can easily be influenced by novel information and sleep could be a protective state in which the strong memory-trace can be formed and transported to other cortical areas. In addition to this passive role, sleep can also play an active role as it has been shown to be more beneficial for learning processes than the same amount of waking time [34].
By focussing on the influence of waking behaviour on replay during sleep, several experiments suggest that sleep replay is the signature of consolidation of learned information and rules [90] [119] [106] [67]. The real causal link between sleep replay and spatial memory and learning was shown in several experiments where SWRs, and thus also replay since they co-occur, were disrupted during sleep either with electrical stimulation (e.g. [45] [41]) or using optogenetic techniques (e.g. [115] [63]). Taken all together we can conclude that sleep replay seems to be important for memory consolidation and learning.

As SWRs and replay are also observed during pauses in awake behaviour, the next question is of course whether the role of awake replay is the same as sleep replay, or whether it has additional functions?
As mentioned before, Foster and Wilson were the first to show memory-trace reactivation (replay) when the animal was awake on a linear track [43]. The replay occurred immediately after a spatial experience and identical to sleep replay it was compressed in time and co-occurred with high correlation with SWRs. The main difference was that this awake replay seemed to be in reversed order (reverse replay). Shortly after, awake replay in the correct order (forward replay) was also observed and seemed to occur predominantly before the spatial experience [32], see figure 2.10.

A model to account for both forward (pre-experience) and reverse replay (post-

experience) was put forward by Diba and Buzaki [33], see figure 2.11, and similar models were proposed by Foster et al. [43] and O'Neill et al. [84]. This first basic model starts from a spike threshold which is different in the theta and LIA state. The spiking probability of place cells can be interpreted in first-order as a gaussian-like distribution centred around the centre of the corresponding place field. During the run along the track the spiking threshold is theta modulated (6-12 Hz) and the place cell sequence is observed. During SWRs, occurring during LIA while the animal is immobile both before and after the track run, the threshold drops dramatically allowing the place cells to fire outside their place field. Adding the principle of *the most excitable cell (highest spiking probability) fires first* we can now understand why forward replay before and reverse replay after an experience occur (see figure 2.11).

Ever since its discovery many different functions for awake replay have been proposed and investigated. A first possibility is that awake replay serves as a consolidation mechanism for recent experiences, in the same way as sleep replay does for more distant experiences [60]. In that case the HC appears to use pauses in exploration to consolidate past experiences by replaying/reactivating them [22] [30]. Other possibilities are that awake replay is necessary for building a spatial map [122] and embedding new information in the map [40] [101] [98]. Finally, awake replay has also been proposed as a mechanism for planning or decision making [48] [91].

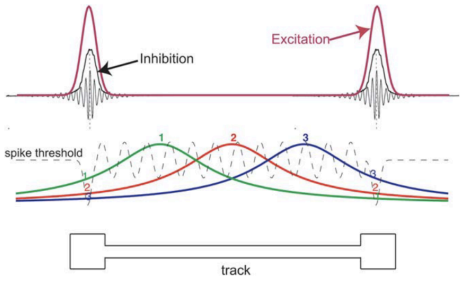

Figure 2.11: Model to account for forward and reverse replay. Coloured curves represent the firing probability of individual place cells. Dotted line represents a firing threshold which is theta modulated during run and drops dramatically when the animal is immobile both before and after the run. Due to this drop the place cells fire outside their place field despite their low firing probability. The principle of *most excitable cell fires first* accounts for the forward (1, 2, 3) and reverse (3, 2, 1) firing order before and after the experience respectively. (source: concept from [33], modified by [15])

Real causal relations between replay and behaviour can be shown in experiments where replays are disrupted. These closed-loop experiments target the more easily detectable SWRs to disrupt replays and experiments using rats [58] [98] and rabbits [78] have been reported. They show that awake replay disruption impairs learning [58] [78] and destabilises the spatial map when new information has to be imbedded [98]. Jadhav et al. [58] also tried to show that awake replay is necessary for decision making using short term memory, something that was later also suggested by Singer et al. [105]. The next paragraph describes in more detail the experiment from Jadhav et al. and their findings as the main research question of this project results from one of their unanswered questions.

Jadhav et al. used rodents performing a spatial alternation task (see figure 2.12a). The maze has a W-shape and the animals are supposed to alternate between left and right, always returning to the center arm in between. There are thus two types of choices: the inbound choice, where the animal exits arm left or right and has to enter the center arm. The only memory required here is to remember the rule and the knowledge of coming from a distal arm. The outbound choice on the other hand requires the

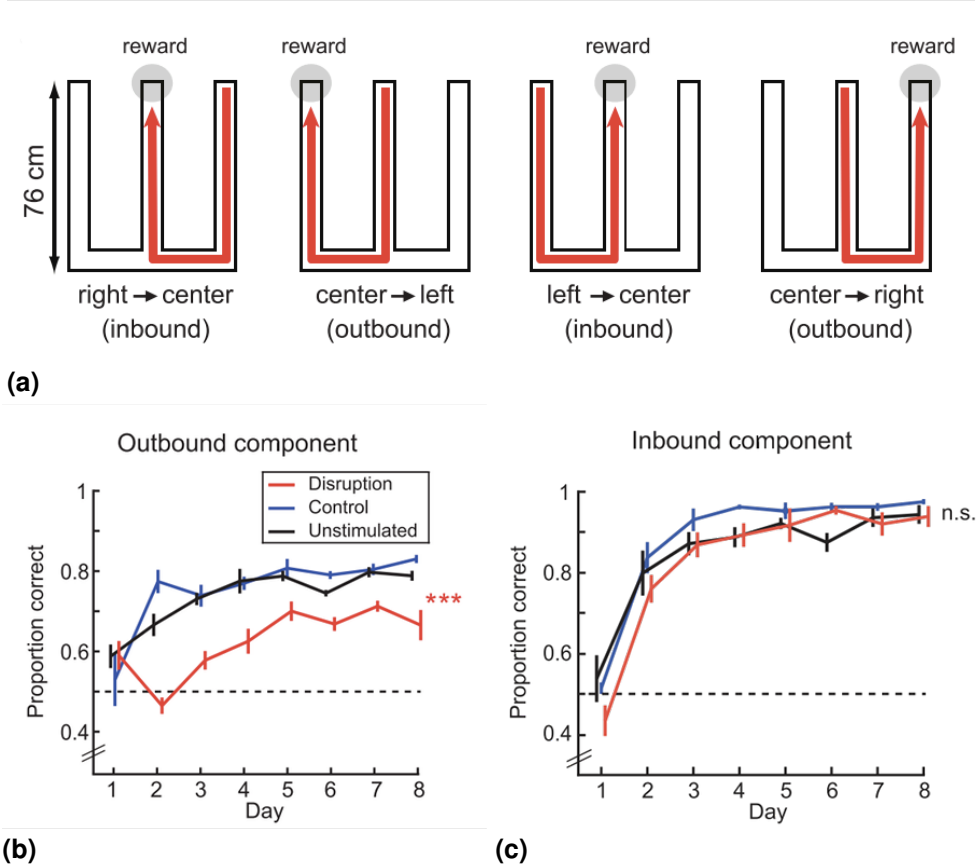

Figure 2.12: SWR disruption impairs learning of a short-term memory rule. a) Spatial alternation task used by Jadhav et al. The rat has to alternate between the left and right arms by visiting the center arm in between. Choice from center to left or right is called an outbound choice and a choice from left or right to the center is called an inbound choice. b) Learning curve for the outbound choice for the test group with ripple disruption (red) and control groups (black and blue). Test group has a significant lower performance ($p<0.001$). c) Learning curve for the inbound choice for the same groups as in b). This time no significant difference is observed amongst the groups.

memory of the rule, knowledge of coming from the center arm and the choice it made previously. It has to choose left if it chose right the previous time and the other way around.
The increase in correct choices over time (due to learning) was significantly lower on the outbound choice for the test group where awake SWRs were disrupted compared to rats from the control groups (see figure 2.12b). The fact that this difference was not observed on the inbound choice (see figure 2.12c) argues that rats were still able to learn the task. Or in other words, the disruption didn't seem to interfere with the memory consolidation of the rules but only seemed to interfere with the short-term spatial memory as this is necessary for correct outbound choices.
Nevertheless it is still possible that these results only indicate a role for learning and not short-term spatial memory for awake replay. The explanation of the results would then be that the outbound rule is more difficult to learn than the inbound rule and is therefore more dependent on replay (=memory consolidation of the rule), hence the stronger performance deficit compared to the inbound rule.
In literature the results from the experiment of Jadhav et al. are considered to be definite proof of the involvement of awake replay in short-term memory and decision making. However, as argued above, that claim can only be made with an experiment specifically designed to test this hypothesis. That is the idea for this project. We will disrupt SWRs after the rats have learned a short-term spatial memory task, thereby testing the involvement of replay in short-term memory and decision making, and not in learning.

2.3.3 Closed-loop experiment: 8-arm radial maze

As explained above, we want to disrupt hippocampal SWRs while the animal performs a spatial short-term memory task, a closed-loop experiment. Therefore it is important to find both the right technique for the disruption and the right short-term memory task. This section discusses both elements.

To conduct successful closed-loop experiments there are two main requirements. Firstly you need a mechanism by which the normal hippocampal activity can be deactivated bilaterally for only a very short period of time (50-100 ms, the duration of a ripple), called a transient inhibition. Secondly, the inhibition should be precisely timed with the onset of SWRs so you need a detection mechanism with very low latency.
The transient bilateral disruption of hippocampal activity can be achieved by stimulating the VHC. Experiments in anaesthetised animals have shown that with a single pulse stimulation to the VHC all pyramidal cells and interneurons are unnaturally synchronously activated, triggering a cascade of effects (GABA receptormediated inhibition, Ca^{2+}-mediated K^{+} conductance increase and disfacilitation) [125]. The eventual effect is that all pyramidal cells, granule cells and interneurons are silenced for 50-250 ms, depending on the strength of stimulation [16] [35] [125]. After this short silencing period the HC firing returns to normal almost immediately [125]. The general idea to detect the onset of SWRs online is by setting a threshold on the brain signal after filtering it in the ripple band. The time it takes for the real-time processor to filter the data, detect the threshold passing caused by a SWR and respond, has to be as small as possible. The total time from the start of the SWR to the response of the software

of course also depends on the data acquisition system that integrates the signals and converts the data from analog to digital. Many different closed-loop systems have been developed over the past years, most of them hardware specific (eg. [77]), application specific (eg. [31] [95] [86] [10]) or primarily designed for only data acquisition ([104] [76]). In this project we use a non-hardware specific software Falcon that is known for its very high flexibility and adaptability to each application [24]. Falcon consists of three interacting subsystems that provide easy live interaction with the user. The core subsystem of Falcon responsible for data processing consists of a flow graph that is constructed with nodes and node connections and can be self configured to meet the needs of each experiment.

As is evident from the vast literature, there exist many different behavioural paradigms to test (short term) spatial memory in rodents. Mostly used are the Morris water maze and the 8-arm radial maze [69] [117] [39]. In this project we use the 8-arm radial maze which is a prototypical example of a multiple-solution task [89]. The maze consists of a central platform with 8 arms extending radially at equal angles. Several variants can be used by variating the number of arms (N=4,6,8,...) and by using different paradigms (win shift, win-return,...[92]). Olton and Samuelso were the first to use the radial maze and they picked the variant with 8-arms and win-shift paradigm, similar to the paradigm used in this experiment [83]. In the 8-arm radial maze task with win-shift paradigm all arms initially contain a reward and after the rat is placed on the central platform it is allowed to freely explore the whole environment aiming at finding all the rewards in the most efficient way. This means entering each arm only once (=no re-entries). The nature of these rewards varies, ranging from a small amount of water to chocolate cornflakes. Rats are able to learn this paradigm within 10-20 training days (mostly depending on their motivation) [69] [117] [39] [89] [92].

The win-shift paradigm was originally designed to test the rat's ability to remember a certain amount of information. In a later experiment that ability was called the *working memory* of the rat [82]. This term is widely used in many different experiments and its precise meaning is usually very unclear. A recent review ([25]) tries to order all the different kinds of working memory and according to this author the working memory tested using the 8-arm radial maze is called: the *recent-event working memory (RE-WM): A part of the mind that can be used to keep track of recent actions and their consequences in order to allow sequences of behaviors to remain effective over time.* The most important properties that distinguishes RE-WM from other WMs is that there's no hierarchy in the goals nor any clear motivation for long term memory storage. All reward/goal sites in the 8-arm radial maze are indeed equal and unordered and it is not necessary for the rat to remember its actions of a previous attempt to solve the present task. Some authors go further to characterise the memory involved in the radial maze and divide the RE-WM in two subcategories: a retrospective memory that informs the animal about the arms that have already been visited, and a prospective memory that anticipates the action for the election of new options [89]. Or in other words, to solve the 8-arm radial maze with win-shift paradigm the rat needs a good short-term spatial memory that communicates well with his decision making centre. The involvement of the HC these memory processes was shown a few years later in lesion experiments (eg. [72]).

2.3.4 Summary

Previous hippocampal research suggests a determining role of awake replay for short-term memory [60] [22] and decision making [30] [48] [91]. In addition to this Jadhav et al. [58] demonstrated a drop in learning speed of a short-term spatial memory based rule when awake SWRs are disrupted in rodents, strongly suggesting a causal link between awake replay and decision making based on short term memories. This project wants to test the specific hypothesis that awake hippocampal replay has a decisive role in short-term memory and decision making without any involvement of learning. To investigate this we use closed-loop disruption of awake SWRs in rats performing the 8-arm radial maze with win-shift paradigm, after the learning period. This behavioural paradigm seems suitable since, in order to solve the task, rats use a specific form of memory what is now referred to as *recent-event working memory (RE-WM)*. RE-WM is a combination of short-term memory and decision making, exactly the kind of memory we want to investigate.

Chapter 3

Experimental Methods

3.1 Experimental overview

3.1.1 Animals

Four male Long Evans rats, all weighing between 360-400 g were put on food restriction until they reached 80-85% of their initial weight (pelleted food, $\sim$ 12 g a day). Three days before the training rats were given $\sim$ 0.3 g of reward (chocolate cornflakes) so that they were accustomed to the reward in a familiar environment. After 15 days of food restriction and daily handling (to familiarise with the experimenter) the rats were put on the maze. Throughout the whole experiment the rats maintained their 80-85% weight.
All experiments were carried out in accordance with protocols approved by KU Leuven animal ethics committee (P119/2015) and in accordance with the European Council Directive, 2010/63/EU.

3.1.2 8-arm radial maze with win-shift paradigm

The maze is located in a 3 x 3 m black room with distinctive visual cues on all four walls. It is elevated 40 cm above the ground and consists of a central platform (diameter 29 cm) connecting eight 90 cm long arms that each end on a square reward platform (side 20 cm). The arms are distributed either symmetrically or asymmetrically around the central platform depending on the phase of the experiment.
Rats had to learn the win-shift paradigm on a radial maze with 8-arms. At the beginning of a trial all arms are baited with one reward located in a food container on the reward platform (end of the arms). The rat has to find all the rewards with the most efficient strategy, that is by visiting each arm only once (= no re-entries). A trial starts once the animal is placed on the central platform facing a random direction, thereby allowed to freely explore the maze, and enters the first arm. A trials ends once the rat re-enters a previously visited arm, which is counted as an error or when it enters the eighth arm, reaching maximal performance. A third criterium for the end of a trial is when neither of the previous criteria are reached within two minutes (trial time-out = 2 min). When the trial ends the rat is taken out of the maze by the experimenter and placed on a separate platform (29 cm dimensions) in the right or left corner of the room. When the

rat makes an error or the trial time exceeds the trial time-out time the rat is removed as soon as possible, but after eight correct choices (maximal performance) the rat is taken out after it finishes the last reward. A new trial starts after $\sim$ 90 sec. The number of trials a day (daily session) was increased gradually from 4 to maximal 30 over the course of the experiment to avoid overtraining. The performance in each trial is quantified as the number of correct arm entries before the end of the trial. When the trial time-out exceeding trials are excluded the performance is named *entries until repeat (ETR)* with a minimum of ETR=1 (i.e. error on the second arm visit) and maximum of ETR=8 (i.e. no error).

3.1.3 Pre-training

At first, to familiarise with the new environment, the rats were allowed to explore the maze freely for 10 min. Initially, rewards were scattered all around the maze to promote exploration of the entire maze. The next days rewards were put only on the arms, later only on the end of the arms and finally strictly in the food container. After $\sim$ 7 days the rats were ready to learn the task as they felt comfortable in the testing environment (visits to all arms and reward consumption within 5 minutes) and with being picked up by the experimenter.

3.1.4 Behavioural procedure

This experiment was a pilot study to figure out the best protocol and parameters to study RE-WM on the 8-arm radial maze. For that reason the total experiment can be divided in 4 phases, each with a slightly different protocol. All four rats completed the two first phases and only two were selected (based on performance and ease of handling) to continue to phase 3 for electrophysiological recordings and one to phase 4 for the closed-loop experiment. Figure 3.4 provides an overview of the experiment by showing the performance evolution of the rat that completed all 4 phases.
During the first phase, the angles between the eight arms are unequal and their configuration changes after every trial. To allow the asymmetrical distribution of the arms there are 12 possible arms positions on the central platform of which only 8 contain an arm. This results in a minimal angle of 30° and a maximal angle of 150°.
Initially, to increase the learning speed the rats were not taken out after a re-entry (as previously described) but were allowed to re-enter arms until they found all the rewards or until the trial time exceeded the trial time-out (= 2 min). After 2-3 days the performance of all rats increased slightly and from that point they were taken out after re-entry each trial. Training occurred every day with the number of trials varying between 4-8.
The procedure followed in phase two was the same as at the end of phase one, except that the configuration of the arms was maintained the same during a daily session and only varied every session. Towards the end of this phase the number of trials gradually increased and after day 25 the best rats (based on performance and ease of handling) were selected and underwent surgery (see section 3.3).

After $\sim$ 5 days of post-surgical recovery and $\sim$ 1 week for placement of the tetrodes (see section 3.4.1) the animals were put back on the maze and for $\sim$ 3 days they could re-explore the maze freely to adapt to the implanted hyperdrive and recording setup. Once comfortable, training for the win-shift paradigm continued until they reached at least their pre-surgical performance (after $\sim$ 2 days). Electrophysiological recordings started from that time and the trial number per session gradually increased up to 20 to 30 trials depending on the motivation of the animal. Arm configuration was also held fixed during each session in this third phase. Because the trial number increased, training only occurred every other day to avoid overtraining.
Only one rat had a functional stimulation wire and started the fourth phase where now all eight arms were symmetrically distributed around the central platform. In this phase sessions with closed-loop disruption were recorded.

3.2 Hyperdrive assembly

The hyperdrive or micro-drive array used for the in-vivo recordings is a slightly modified version from the micro-drive array designed by Kloosterman et al. [61]. The fabrication procedure for the drive consists of three major parts: the assembly of the hyperdrive and micro-drives, the fabrication and loading of the tetrodes and final preparation of the hyperdrive and tetrodes for surgery.

3.2.1 Assembly of hyperdrive and micro-drives

The hyperdrive consists of two custom 3D printed plastic holders, a large top part, with space for 27 micro-drives (24 for tetrodes and 3 for stimulation electrodes) and a small bottom part with room for a small and large collector cannula. These last two hold the guiding tubes for the stimulation wires and the tetrodes respectively. Once placed in the cannula's of the bottom part, all guiding tubes were individually guided through small 0.8 mm holes in the top part whereafter the two plastic holders were fixed together with three screws, together forming the skeleton of the hyperdrive. Next, the 27 micro-drives were loaded on the hyperdrive. Each micro-drive contains two parts that are glued together with dental cement (SDI, Bayswater, Australia), see figure 3.1a. The first part is a screw which is used to fix the micro-drive in the correct position on the hyperdrive and allows control over the vertical position. The second part is a hollow support-tube for the tetrodes that slides smoothly over the guiding tubes. Finally an electrode interface board (EIB) was mounted on a support platform on the top part to establish the connection between the electrodes and the pre-amplifiers. The result when all pieces are assembled is shown in figure 3.1b.

3.2.2 Tetrodes

The tetrodes consist of four polyimide-insulated nickel-chrome wires (12 μm diameter, Sandvik, Kista, Sweden) twisted together and cut at a blunt angle. Two twisted

polyimide-insulated stainless steel wires (60 μm diameter, Sandvik, Kista, Sweden) also cut at a blunt angle make up the stimulation wires. The individual wires are fused together by heating the outer insulation layer along the whole length of the tetrode/stimulation wire. At one end the insulation is not fused thereby allowing access to the wires individually. Up to 24 tetrodes and 3 stimulation wires were loaded on the hyperdrive by inserting them in the guiding tubes and gluing them to the surrounding support tubes of the micro-drives. Next, all individual wires from each tetrode and stimulation wire, 4 and 2 respectively, were separately connected to the EIB and fixed with a gold pin (see figure 3.1c). A ground wire was also soldered to the EIB. This wire is connected to the skull of the animal to allow proper grounding.

3.2.3 Preparation for surgery

To prepare the tetrodes for surgery their tips were cleaned and thereafter gold-plated to increase the contact surface and as a result decrease the impedance. To do this the EIB of the micro-drive array was connected to the NanoZ device via the ADPT-NZ-EIB36 adapter (Neuralynx Inc.), a device capable of measuring impedances. Next tetrodes were either lowered in a 0.9% sodium chloride (Baxter International Inc., Deerfield, Illinois, USA) for cleaning or in a non-cyanide gold solution (Neuralynx Inc.) for gold plating and a positive current (0.100 μA) at 1004 Hz or negative current -0.05 μA at 1004 Hz respectively were passed through the wires for one second. One run was done for cleaning and multiple runs (maximum 10) for gold plating until a target impedance of 300 kOhm was reached.
Finally a plastic protective cone wrapped in aluminium foil was mounted around the hyperdrive to protect the electronics from the external environment and a plastic skull piece was added to the small bottom part to improve the stability of the hyperdrive on the animal's skull while implanted and allow reuse of the hyperdrive afterwards.

3.3 Surgical implantation

The hyperdrive described in the previous section was surgically implanted on the rat's skull using standard aseptic techniques. To induce anaesthesia the animal was placed in an induction chamber filled with oxygen (0.5-1 L/m) and 5% isoflurane. Next its head was securely mounted in a stereotaxic frame after shaving of the head and protection of the eyes with eye ointment and aluminium foil. During the surgery anaesthesia was maintained by administration of 0.5-2% isoflurane through a nose mask and adjusted if necessary based on vital signs; blood oxygen level, heart rate and breathing rate. The body temperature (measured with a rectal probe) was kept constant using a heating pad on the surgical table.
After disinfection of the skin with iodine and ethanol and administration of the anti-inflammatory drug metacam (0.3 ml) an incision with a scalpel along the midline exposed the skull and small scratches were carved in the bone plates to allow better adhesion of the dental cement used to fix the drive to the skull. Eight to ten anchoring bone screws were screwed in the skull (2-4 frontal, 2 left parietal, 2 occipital and 1 right parietal, see figure 3.3a), gaps between the screws and the skull were filled up with

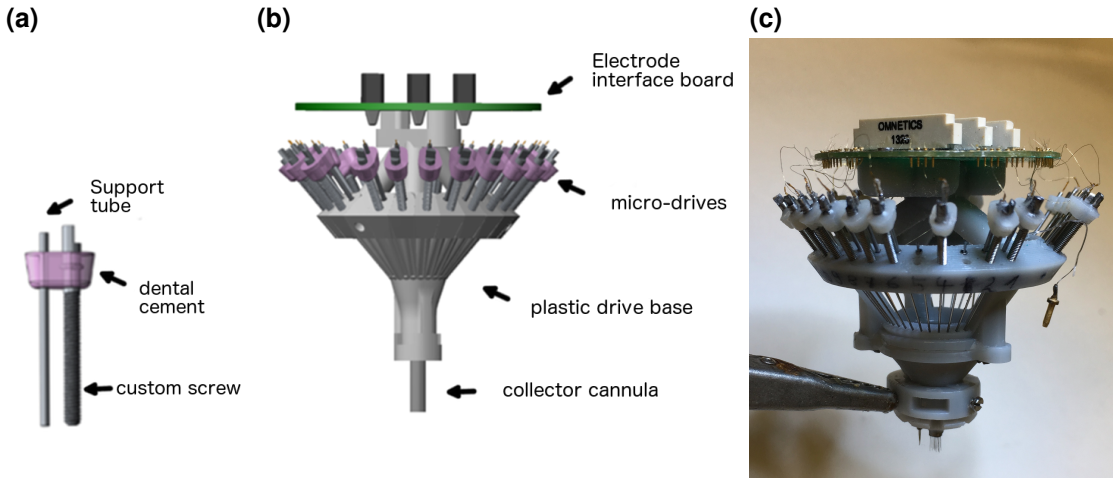

Figure 3.1: Hyperdrive for implantation a) Illustration of a micro-drive that allows the vertical movement of tetrodes. b) Illustration of the full hyperdrive with main constituents indicated. c) Photo of a hyperdrive with tetrodes loaded.

bio compatible glue (VetBond) and after extra disinfection (10 min baytril submersion) all screws were fused together with dental cement (see figure 3.3b). One of the bone screws was connected to the EIB to serve as a ground for electrophysiological recordings.

Next, two craniotomies were drilled and the dura was removed to allow access to the brain above the HC and ventral hippocampal commissure (VHC) (HC-craniotomy center coordinates: 4 mm posterior to Bregma, 2.5 mm right from the midline, VHC-craniotomy center coordinates: 1.3 mm posterior to Bregma, 0.9 mm right from the midline, see figure 3.3b). Before mounting of the drive the two cannulas were covered in silicon grease to seal the gaps between the edge of the hole in the skull and the cannula. Additionally mineral oil was applied to the tip of the cannula prior to implantation to fill the tetrode-carrying tubes which prevents back-filling (and possible clogging) with cerebrospinal fluid or blood. The drive was fixed to the skull with light-curable dental cement (SDI, Bayswater, Australia) and the grounding screw was connected to the EIB. Where necessary the skin was closed with surgical threads.

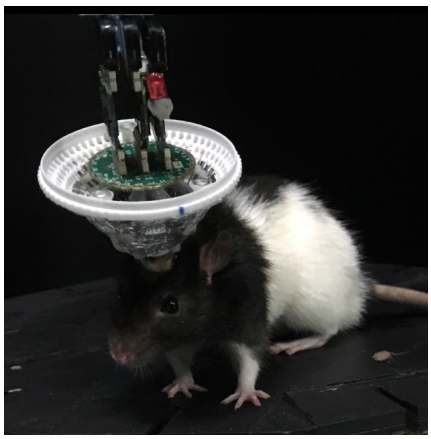

Figure 3.2: Implanted rat. Picture of a rat implanted with a hyperdrive for electrophysiological recordings from the hippocampus.

While the rat was still under light anaesthesia all tetrodes and stimulation wires were lowered 1 mm to the neocortex. Lastly, 0.7 ml of saline (anti-dehydration) and 0.3 ml metacam (anti-inflammatory) were administered subcutaneously. The metacam injection was repeated the next three days.

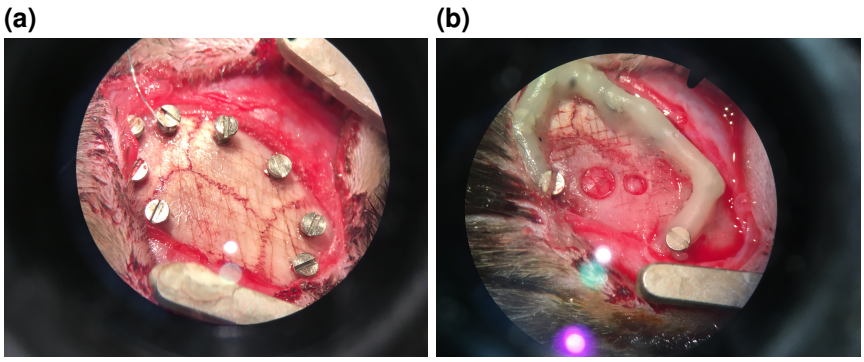

Figure 3.3: Major steps before implantation of a hyperdrive. a) 8 anchoring bone screws are screwed in the skull (2 frontal, 2 left parietal, 3 occipital and 1 right parietal). One of the occipital screws has a grounding wire attached to it and serves as the grounding screw. b) All screws are connected with dental cement to support the drive. Two craniotomies are performed to allow access to the brain for the tetrodes and stimulation wires. HC-craniotomy centre coordinates: 4 mm posterior to Bregma, 2.5 mm right from the midline, VHC-craniotomy centre coordinates: 1.3 mm posterior to Bregma, 0.9 mm right from the midline.

3.4 Electrophysiology protocol

3.4.1 Recording

After approximately one week of post-surgical recovery 10-15 tetrodes were slowly lowered in the CA1 pyramidal cell layer of the dorsal hippocampus over the course of one week to minimise tissue damage. Three tetrodes were lowered in the white-matter above the CA1 cell layer to serve as a reference and three tetrodes remained in the cortex to aid the online ripple detection (see section 3.4.2). Recording started when ripples were clearly observed and the rat reached at least its pre-surgical performance. Wide-band (0.1 - 6 kHz) signals were sampled at 32 kHz and digitised using a 128-channel data acquisition system (Digilynx SX acquisition system with HS-36 analog headstage and Cheetah software; Neuralynx, Bozeman, MO) and saved on an hard disk for offline analysis.
All sessions are recorded with an overhead video camera (25 Hz) to record the behaviour and track the position of the animal through two LED's mounted on one of the three headstages.

3.4.2 Stimulation

In phase 4 of the experiment, a live network stream of digitised multi-channel samples from the Digilynx acquisition system was fed into a quad-core workstation that runs the real-time detection software Falcon [24]. Falcon initiates TTL pulses via a microcontrollor board (Arduino UNO) that is connected to a constant-current stimulator (MultiChannel System, Reutlingen, Germany) which generates a biphasic current for electrical stimulation of the ventral hippocampal commissure.
Here, raw signals of 1-2 electrodes (with the clearest ripples) are first filtered in the ripple band (135-255 Hz) using a Chebyshev type-II IIR filter (order 20). Using the

neuralynx acquisition system the total round trip latency was below 1 ms [24]. After summing of the ripple power (RP) of the different electrodes, ripples were identified based on the following criterium.

$$RP - \mu(t) > f \cdot mad(t) \tag{3.1}$$

μ(t) and mad(t) are the running estimates of the mean and mean absolute deviation calculated on the ripple power, and f is a multiplier set to a value in the range [5,13]. The value of f was adjusted each daily session to maximise the ratio of positive over false ripple detections. The RP is the RMS of the filtered signal. Estimates of μ(t) and mad(t) were computed using an exponential moving average filter with span set to 15 seconds. Estimates were not updated during a 50 ms window after each detection.
To avoid false detections due to heavy head movements or chewing the same ripple detection procedure was applied to signals from 1-2 cortical electrodes. As ripples are not present in the cortex but artefacts like the ones mentioned above are, detections were marked as false if a cortical detection occurred within a fixed time window ([-40, 1.5] ms) around a HC detection. All not falsely marked detections triggered the generation of a TTL pulse by Arduino UNO of which the timing depends on the trial type (see next paragraph). This TTL-pulse was sent to the constant-current stimulator (MultiChannel System, Reutlingen, Germany) to electrically stimulate the VHC. Both the detection event and the time of stimulation (= stimulation event) were sent to the neuralynx acquisition system for logging.

The sessions where closed-loop stimulation was performed consist of two types of trials, that alternate randomly within the session: a disruption trial and a stimulated control trial. In a disruption trial, the stimulation event immediately follows the detection event, resulting in a disruption of the ripples. In a stimulated control trial, Falcon instructs Arduino to generate a stimulation event 100-250 ms after the detection. Due to this delay the detected ripple is not disrupted since ripples last on average $\pm$ 50 ms. This trial serves as a control for effect of the stimulation on the behaviour. Detections within the delay period are ignored. The amplitude of the biphasic electrical pulses (0.2 ms duration) varied from 100-200 μA and was set in each session to the lowest amplitude that resulted in consistent disruption of hippocampal ripple events. To avoid over-stimulation that could lead to damage of the surrounding tissue no detections (and stimulations) could occur within a 150 ms lockout period after a detection. Three sessions with no stimulation were also recorded during phase four to serve as an extra control (= unstimulated control).

3.5 Data analysis

Analysis of behavioural and neural data was performed using Python and its scientific extension modules, augmented with custom Python toolboxes. Analysis was only performed on the data from the implanted rat that completed all four experimental phases.

3.5.1 Behaviour analysis

Position and speed of the rat was recorded using LED lights mounted on one of the headstages and an overhead video camera (25 Hz).
For behavioural analysis the trial time-out exceeding trials are excluded since we are interested in the memory behaviour of the rat only. The performance in each trial is therefore quantified as the number of correct arm entries before a re-visit: *entries until repeat (ETR)* with a minimum of ETR=1 (i.e. error on the second arm visit) and a maximum of ETR=8 (i.e. no error). The rat is considered to make an arm entry once it travels at least 20 cm into the arm. Speed distributions are calculated by computing the kernel density estimate of the speed histograms with a symmetrical gaussian kernel (bandwidth: 3 cm/s).
Stereotyped behaviour is quantified using the sterotypy index (SI). The index is a measure of the uniformity of the egocentric arm-pick distribution across multiple trials. This distribution indicates the rat's preferred arm choice relative to its current position. The arm-pick distribution is calculated by plotting the arm the rat picks (for every arm choice in all the trials) relative to its present position in a histogram. The SI index is calculated as the difference between the highest and lowest arm-pick percentage. SI=0 indicates that all arms are visited equally and thus reflects no arm-pick preference whereas SI=1 indicates that only one arm is visited and thus reflects a very strong arm-pick preference. The error on the SI index is calculated by bootstrapping over all trials (500 times, sample size: 100%) and taking the 25-75 percentile interval.

3.5.2 Statistics

Linear regressions for two sets of measurements are preformed using a least-squares method. The corresponding p-value indicates the two-sided p-value for a hypothesis test with a null hypothesis that the slope (m) is zero, using a Wald test with t-distribution for the test statistic. A significance level of $p<0.05$ is used. The Wald-test test statistic is calculated as follows

$$W = \frac{m - \hat{m}}{sd}$$

where m and sd are the slope and standard deviation on the slope and $\hat{m}$ the slope of the null-hypothesis, in this case equal to zero.
To test the hypothesis that 2 or more samples represent similar distributions the Kruskal-Wallis (KW) H-test was used. The KW H-test tests the null hypothesis that the population medians of all of the groups are equal. It is a non-parametric version of ANOVA and does not assume that the distributions of the individual groups are normal. The test statistic is the KW H-statistic (corrected for ties) and the p-value indicates the probability for the calculated H-statistic to occur under the assumption that H has a chi-square distribution. The KW H-statistic is calculated by first ranking the data from all groups (ignoring group membership) starting from 1 for the smallest and N for the largest value. The tied values receive the average of the ranks they would have received if they had not been tied. After ranking H is calculated as follows:

$$H = (N-1)\frac{\sum_{i=1}^{g} n_i(\bar{r}_i - \bar{r})^2}{\sum_{i=1}^{g}\sum_{j=1}^{n_i}(r_{ij} - \bar{r})^2} \tag{3.2}$$

with n_i the number of observations in group i, r_{ij} the rank of observation j from group i, N the total number of observations (across groups), $\bar{r}_i$ the average rank of all observations in group i and $\bar{r}$ the average of all r_{ij}.

3.5.3 Offline ripple detection

The local field potential recorded from 1 tetrode was downsampled from 32kHz to 4kHz and filtered in the ripple frequency band (150-250 Hz). The ripple envelope was computed as the absolute value of the Hilbert-transformed ripple signal and smoothed with a Gaussian kernel (bandwidth 4 ms). Finally, start and end times of ripple events were detected when the ripple envelope exceeded a low threshold of $\mu + 0.5\sigma$ and when in between it exceeded a high threshold of $\mu + 3\sigma$ for at least 15 ms. Here, μ and σ represent the mean and standard deviation of the envelope.

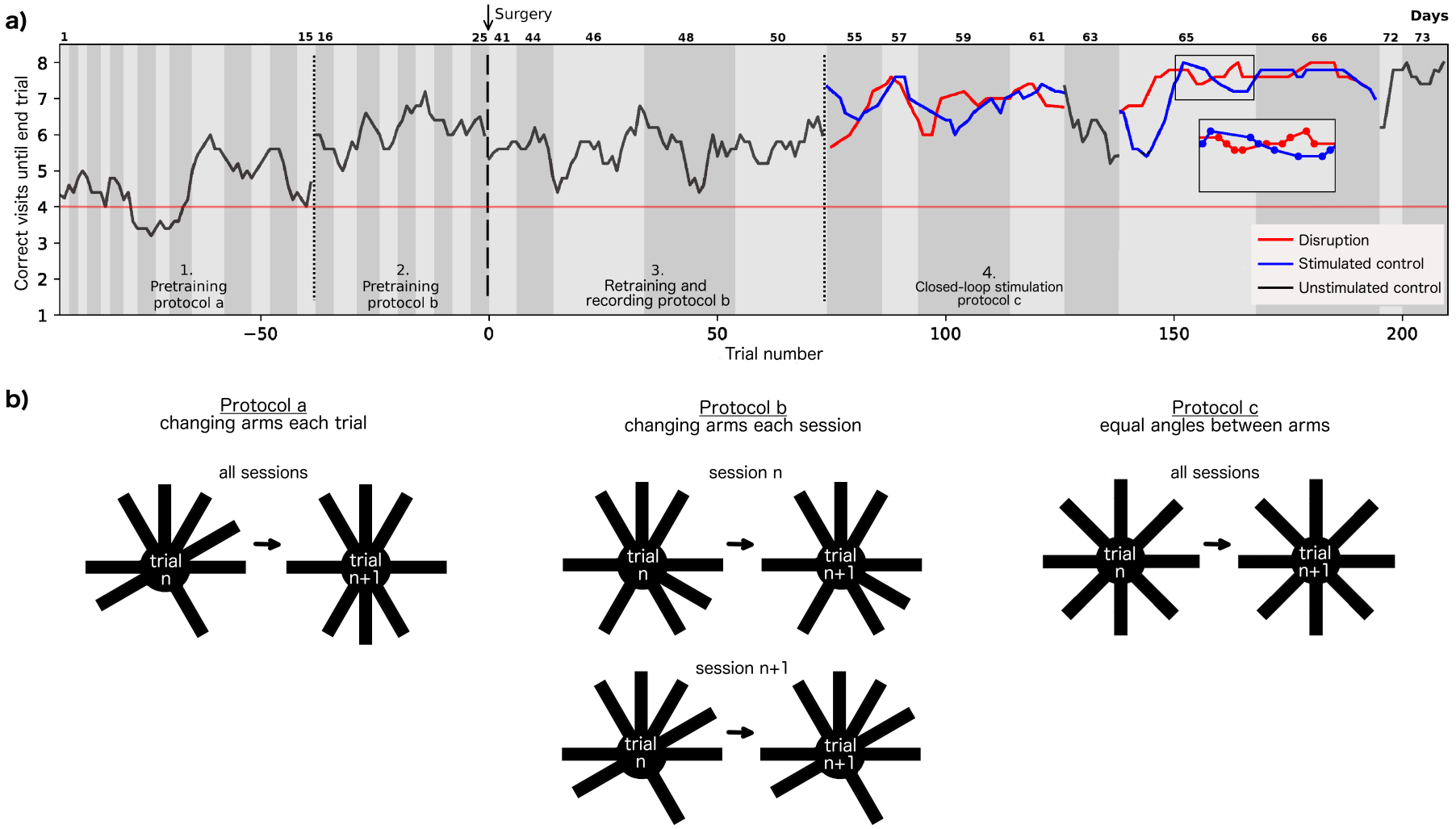

Figure 3.4: Experimental overview. Figure a) presents the number of correct entries of the rat in a trial during all four experimental phases (5-trial moving average). The red line indicates the average performance of a random rat (= chance level). Dotted lines indicate the end and start of a new experimental phase. The dashed line indicates the surgery moment. Trials are numbered relative to the surgery date. Days are indicated with grey bars. The inset shows that disruption and stimulated control trials are alternated in a random fashion. Figure b) shows schematically the 3 different protocols used.

Chapter 4

Results

This chapter presents the behavioural and electrophysiological data recorded from one rat that completed all four phases of the experiment (see section 3.1.4). Data from the other rat that completed phase 3 did not have a good signal to noise ratio. After pre-training (phase 1 and 2), the rat was implanted with a hyperdrive. Behavioural and electrophysiological recordings started in phase 3, when the rat was familiar with the task. In that way the recent-event working memory (RE-WM) component necessary to solve the win-shift paradigm in the 8-arm radial maze could be investigated separately from the task learning phase. In phase 4, closed-loop disruption of hippocampal sharp-wave ripples (SWRs) was performed to look for a causal relation with the RE-WM. Memory performance is quantified by the number of correct arm choices before the rat makes a mistake (entries until repeat (ETR)). Trials that ended because the total trial time exceeded the trial time-out (2 min) were excluded for analysis (remaining trials: 47 trials for phase 3, 131 trials for phase 4 of which 52 disruption, 55 stimulated control and 24 unstimulated control trials).
Figure 3.4 provides an overview of the total experiment by showing the evolution of the correct visits per trial (trial time-out trials included) during all four phases and their corresponding protocol.

4.1 Behavioural characterisation on 8-arm radial maze

This section reports the behavioural data recorded in phase 3. Position of the rat was tracked using an overhead camera and LED's mounted on the head of the rat.

4.1.1 Behavioural performance is not random

The average performance of the rat is 6 [5,6] (median [IQR] , 47 trials in total, taken from day 46, 48 and 50). During phase three the rat did not reach maximal performance, presumably due to the unequal angles between the arms which makes the task harder [47]. We also note that the rat never makes a 180° turn, consistent with the natural tendency to alternate and that the first choice is mostly the arm the rat is facing after being randomly placed on the central platform. The average performance of the rat over all trials is higher than the average performance of a simulated random-choice

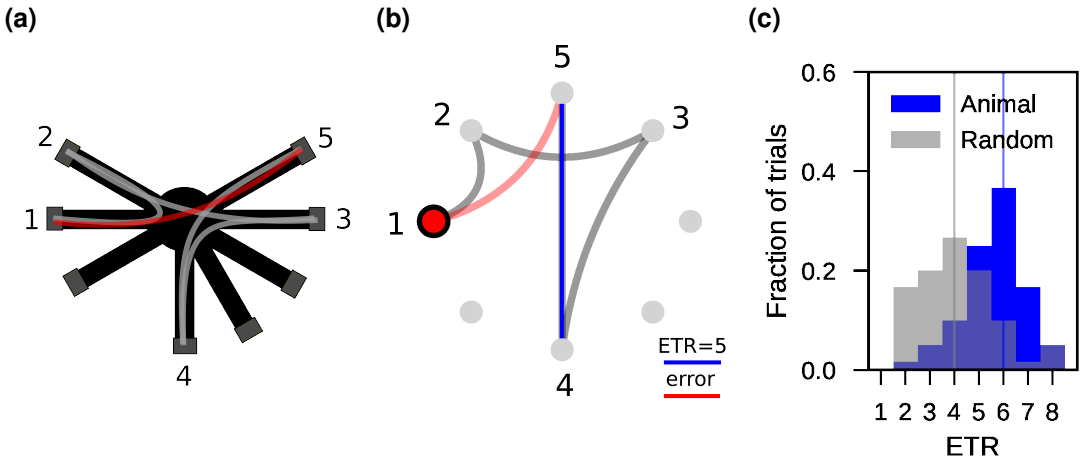

Figure 4.1: Arm choices of the rat are not random. Figure a) shows a schematic top view of the 8-arm radial maze with asymmetrically distributed arms. Lines on top indicate the trajectory of the rat in an example trial, grey lines for correct visit, (visit 1 to 5) and the red line for the incorrect visit (a re-entry on visit 1). Figure b) shows the trajectory of the same example trial more schematically, leaving out the unequal angles between the arms. The blue trajectory indicates the trajectory of the last correct visit, which quantifies the performance of the rat in a trial. The memory performance is quantified as the number of correct visits, in this example equal to five (Entries until repeat (ETR)= 5). Figure c) shows a histogram of the performance (ETR) of the rat vs. a simulated random-choice rat that picks arms randomly, excluding the arm it is currently in (no 180° turns). Vertical lines indicate the median. The difference is significant ($p<0.0001$, KW). (Data from phase 3 session day 46, 48 and 50, 47 trials in total)

rat performing an equal amount of trials, equal to 4 [3,5.25] (median [IQR]). The random rat picks arms (pseudo) randomly but is programmed in such way as to never pick the arm it is currently in, i.e. it never makes a 180° turn, consistent with the behaviour of the real rat. Figure 4.1c shows the performance distributions of the rat and simulated random-choice rat which are significantly different ($p<0.0001$, KW). The vertical lines indicate the medians of the distributions. The distribution of the real rat is skewed towards higher performance wheras the distribution of the random rat is skewed towards lower performance.

Figure 4.2a shows the speed of the rat on the maze during an example trial and all trials show this similar pattern; high speed almost exclusively on the centre of the arms (median [IQR]: 36.82 cm/s [23.99, 46.83]), intermediate speed on the platform (median [IQR]: 27.43 cm/s [18.05, 37.44]) and immobility at the reward site[1] (median[IQR]: 2.85 cm/s [1.22, 6.66]). The corresponding speed distributions for the three maze sites are presented in figure 4.2b.

Together these results show that the rat runs from reward to reward site in a non-random way which suggests that it learned the win-shift paradigm.

The non-random arm choices could be due to the rat picking arms based on his RE-WM (remember previous visits) or because it has a preference to turn a certain direction (not memory based). Analysis of the arm choices of the rat demonstrates a strong left-turn preference, visualised in figure 4.3. The 7 remaining arms that the rat

[1] Immobility is defined as speed $<$5cm/s.

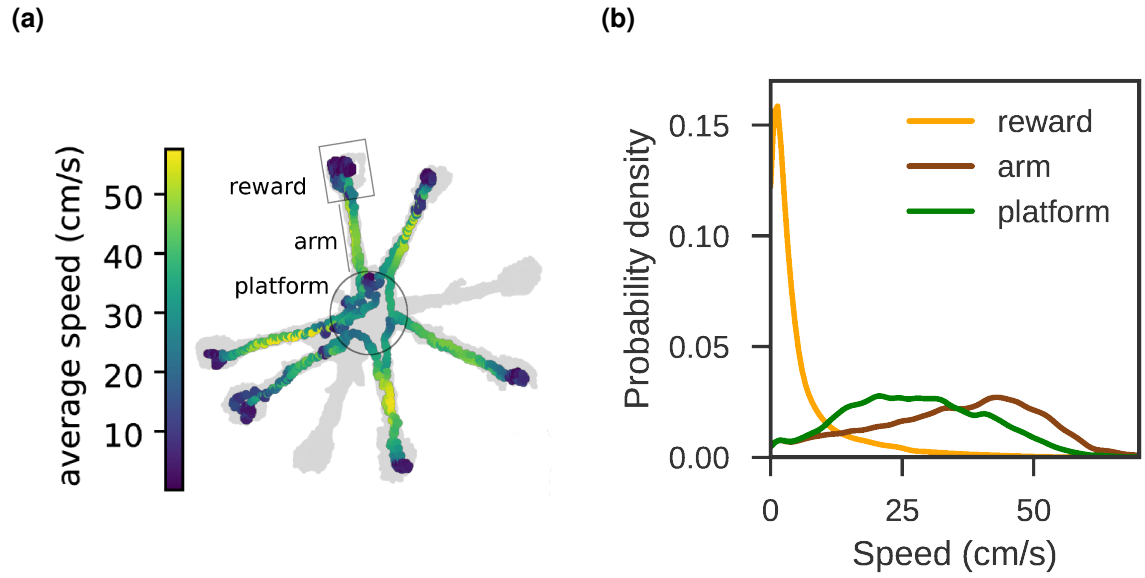

Figure 4.2: Rat spends most of its time at the reward site. Figure a) shows the average speed of the rat on the maze for one example trial (velocity data spatially binned and averaged within bin, number of bins x by y, 580 x 550). In figure b) the normalised speed distributions of all trials for three regions in the maze separately: reward site, arm and platform as indicated in a). Median velocity at the reward site, arm and platform is 2.85 cm/s [1.22, 6.66], 36.82cm/s [23.99, 46.83] and 27.43cm/s [18.05, 37.44] respectively (median [IQR]). (Data from phase 3 session day 46, 48 and 50, 47 trials in total)

can pick at each choice are named from a to g where a is the first arm on the left and g the first arm on the right (see figure 4.3a). The unequal angles between the arms are ignored. An egocentric arm choice is characterised by the name of the chosen arm. All egocentric arm choices (of all trials) are summarised in a radial histogram and normalised to the total number of arm choices. This normalised egocentric arm-pick distribution reveals the rats strong bias for arm a and b which are the first and second arm on his left (see figure 4.3b).

A stereotypy index (SI) quantifies the stereotyped behaviour. The index is a measure of the uniformity of the egocentric arm-pick distribution and is calculated by taking the difference between the highest and lowest arm-pick percentage (see figure 4.3). No egocentric arm-pick preference results in SI=0 and always the same egocentric arm-pick results in SI=1. The stereotyped behaviour of the rat in this phase of the experiment is quantified with SI=0.36 [0.36, 0.48], confirming the observed strong arm-choice bias (see figure 4.3c). The error was calculated using a bootstrapping method (see section 3.5.1). The arm-pick distribution of the simulated random-choice rat introduced in the previous paragraph is more uniform (SI=0.05 [0.04, 0.12], see figure S1a). A rat with no arm-pick bias but with perfect memory, hence that picks the non-visited arms randomly, would have a similar uniform distribution (not shown). This confirms that the non-random arm pick, deduced from the different performance distributions between the real and simulated random-choice random rat (see figure 4.1c), is not solely due to increased RE-WM usage but also due to stereotyped behaviour.

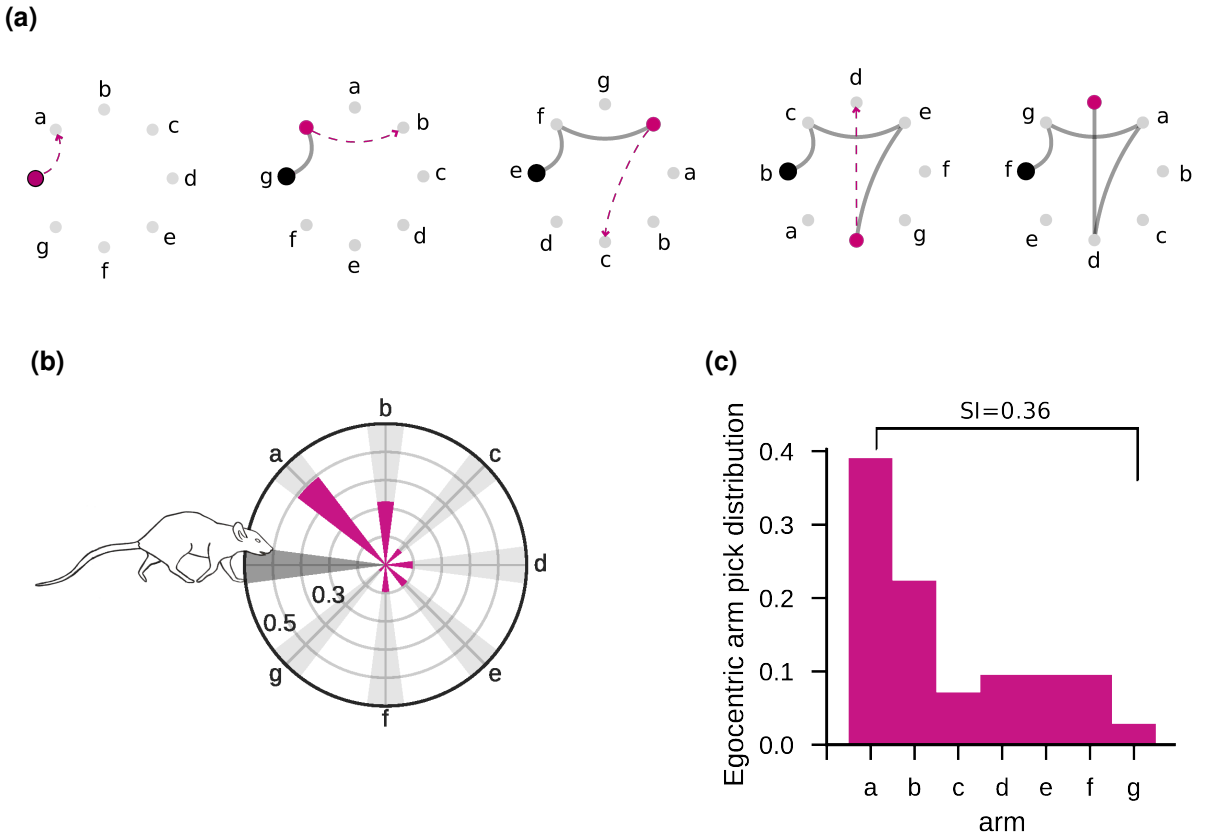

Figure 4.3: Rat prefers to turn left. Figure a) shows schematically the egocentric arm-picks of the rat for an example trial. The letters indicate the egocentric naming of the arms with a the first arm on its left and g the first arm on its right. In figure b) the normalised egocentric arm pick distribution for all trials. c) The same data as in b) shown linearly. Arm preference is quantified with the stereotypy index (SI) defined as the difference between the highest and lowest egocentric arm pick percentage (SI=0: all arms are visited equally, SI=1: only one arm is visited). The error is calculated by bootstrapping (500 times, sample size: 100%) over the contributing trials. (Data from phase 3 session day 46, 48 and 50, 47 trials in total)

In the above quantification, the unequal angles between the arms are ignored since the rat appears to have an arm preference rather than a turn angle preference. This is demonstrated by comparing the normalised egocentric arm-pick distribution with the normalised egocentric angle-pick distribution (see figure S2).

The movement of the rat on the maze can be summarised as follows. The rat moves from reward to reward site in a non-random fashion with a strong left-turn preference. This suggests that the rat learned the win-shift paradigm but that its arms choices are not purely made using RE-WM.

4.1.2 Intra-trial but no inter-trial variability is observed in the time spent at the reward site and platform

Within a trial the task difficulty changes. The first choice the rat makes is always correct, giving the rat an easy start. As the trial continues the rat has to remember what arms it visited previously by using its RE-WM. The more arm choices it makes, the more it has to remember which explains the intra-trial task difficulty change. The change in RE-WM demand within a trial could be reflected in the rat's behaviour. Additionally, if the rat's behaviour is linked to the RE-WM demand we could also expect a difference in behaviour across performance levels (inter-trial). That is, a higher or lower trial performance could be the consequence of a different behaviour on the maze.
To investigate a possible intra-trial or inter-trial behavioural change, trials were split up in visit and inter-visit periods, shown schematically in figure 4.4a. A visit is defined as the time that the rat is at the reward site and the inter-visit time is defined as the time between two visits, when the rat is on an arm or the platform. During visit periods the rat spends on average 12.40s [9.05, 14.16] at the reward site and during inter-visit periods 1.84s [1.70, 1.97] on an arm and 3.07s [2.32, 3.70] on the platform. Medians [IQR] are calculated for reward site, arm and platform visits of all trials.
Next, the average time spent at the reward site and platform was calculated for different visit and inter-visit periods separately, using all reward site and platform visit from trials where the rat reached that visit or inter-visit period. The result is presented in figure 4.4 and it shows a significant positive linear correlation between the time spent at the reward site or platform and the progression within a trial (visits: $r=0.23$ $p<0.0001$, inter-visits: $r=0.31$ and $p<0.0001$). This indicates that there is an intra-trial behavioural variability. That is, the rat spends more time at the reward site and platform towards the end of the trial. An inter-trial behaviour comparison is shown in figure 4.5. It presents the average times calculated over reward site and platform visits of trials were the rat reached the same performance. No significant linear correlation between trial performance and time spent is observed ($r=0.04$, $p=0.51$ and $r=0.07$, $p=0.25$ for the time spent at the reward site and platform respectively). Therefore, high or low trial performance is not reflected in the average time spent at the reward site or platform. Time spent at the arms was not analysed since the reward site and platform rather than the arms are thought to be possible choice points and reflect the use of RE-WM.

Next, to look for an intra-trial or inter-trial arm-pick preference variability the stereotypy index (SI) was computed over inter-visits and performance levels. Variation within the trial is analysed by assigning an SI to each inter-visit period. It indicates the uni-

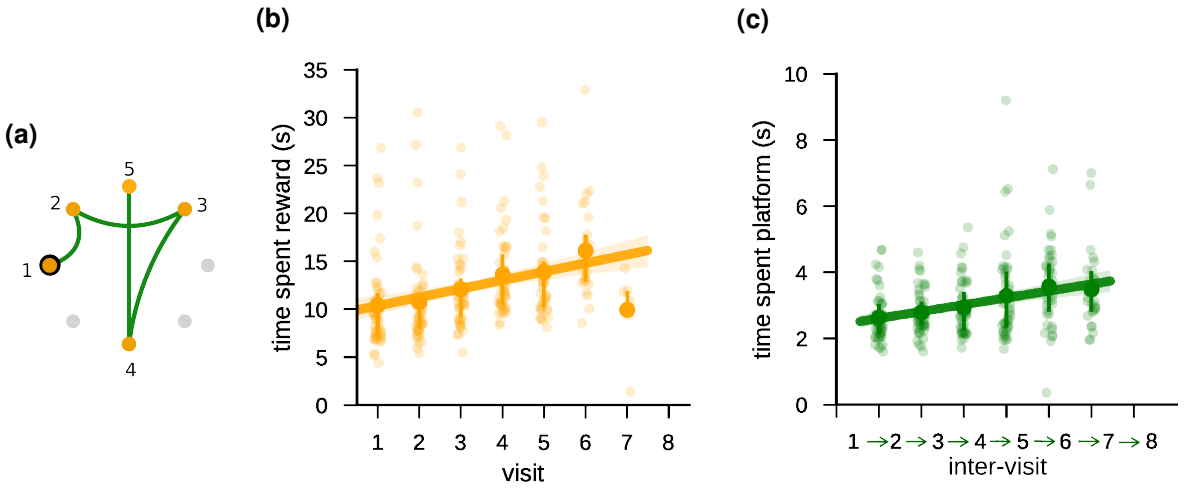

Figure 4.4: Intra-trial variability: Rat spends more time at the reward site and platform towards the end of a trial. Figure a) shows schematically a visit (orange) and corresponding inter-visit (green) period. The visit starts when the rat enters the reward site and the time in between is the inter-visit time. Figure b) and c) show the time spent at the reward site, during a visit, and platform, during an inter-visit, for all trials. Vertical lines indicate the 25-75 IQR and large dots indicate the average over the time spent at the reward sites and platform of all trials for a specific visit/inter-visit period. There is no 8^{th} visit or 7 to 8 transition since the rat did not reach ETR=8 in phase 3. Both for the time spent at the reward site and platform there is a significant linear regression showing a positive correlation with visit/inter-visit number (reward: r=0.23, platform: r=0.31, for both $p<0.0001$, KW). (Data from phase 3 session day 46, 48 and 50, 47 trials in total)

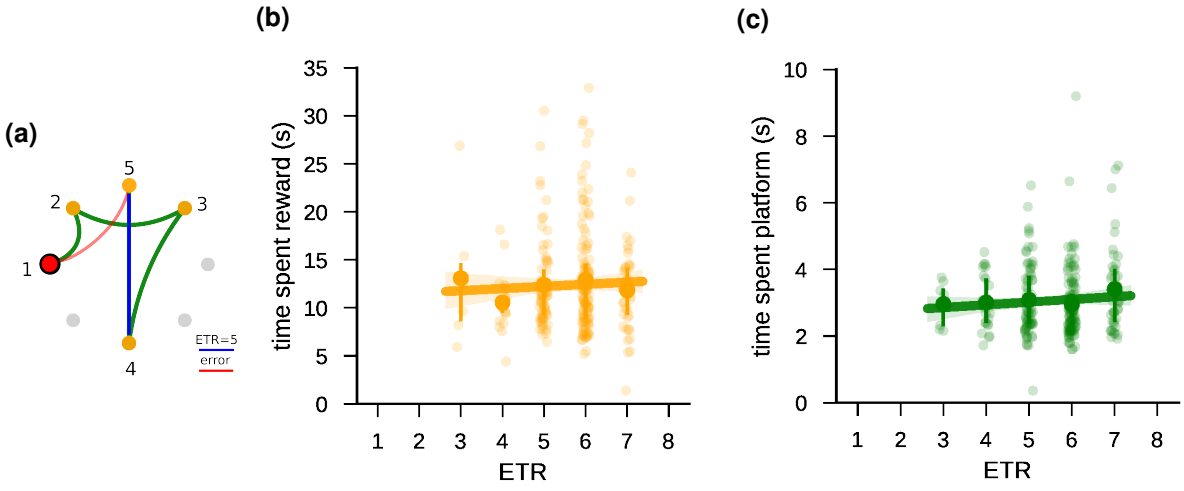

Figure 4.5: Inter-trial variability: Average time spent at the reward site and platform does not correlate with trial performance. Figure a) shows schematically a trial with performance equal to five (entries until repeat, ETR=5). Figure b) and c) show the average time spent on the reward site and platform across various performance levels. Vertical lines indicate the 25 - 75 IQR and the large dot indicates the average time over all reward site and platform visits during trials with a specific performance. There is no 8^{th} visit or 7 to 8 transition since the rat did not reach ETR=8 in phase 3. Both for the time spent at the reward site and platform there is no significant linear regression showing no correlation with the trial performance (r=0.04, p=0.51 and r=0.07, p=0.25 respectively, KW). (Data from phase 3 session day 46, 48 and 50, 47 trials in total)

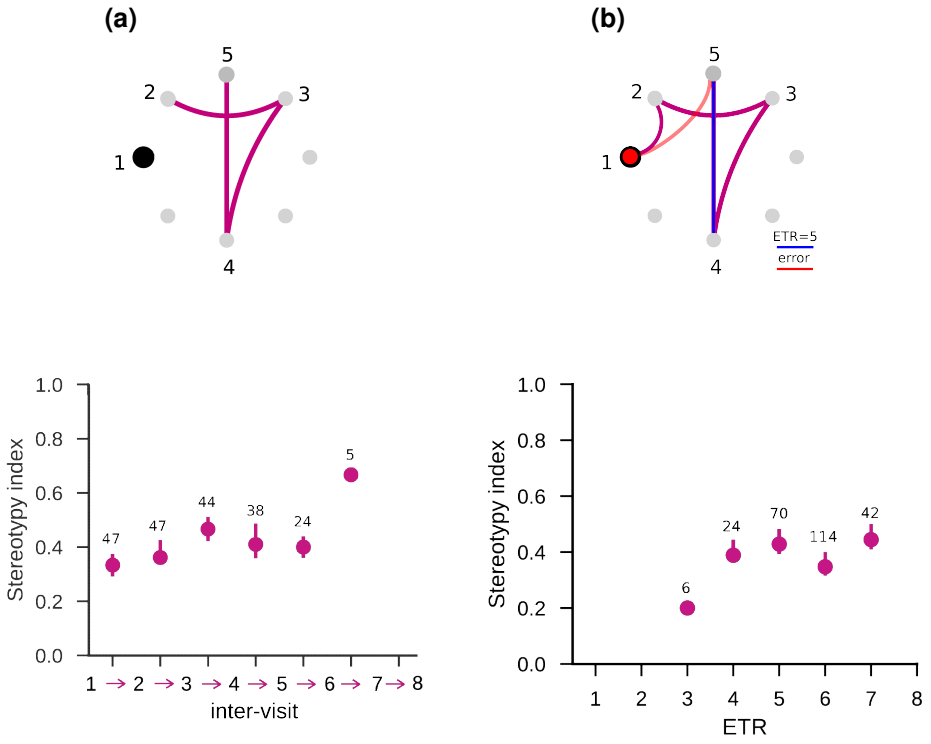

Figure 4.6: Stereotyped behaviour does not change significantly towards the end of a trial nor correlates with performance. Figure a) and b) show the stereotypy index (SI) characterising the arm pick distribution for inter-visit periods and trials with a specific performance respectively (SI=0: all arms are visited equally, SI=1: only one arm is visited). Number above data point indicates the number of choices in the corresponding arm pick distribution. The error is calculated by bootstrapping (500 times, sample size: 100%) over the contributing trials. Number of trials in a) is equal to the number of choices and in b) to the number of choices divided by the performance. (Data from phase 3 session day 46, 48 and 50, 47 trials in total)

formity of the egocentric arm-pick distribution for the choice from visit n to n+1. Figure 4.6a shows the result and there seems to be a slight increase in the SI towards the end of the trial. However this is difficult to interpret since not all SI are calculated using an equal number of choices, number indicated above the SI. Each SI is calculated with the choices from all trials where the rat performed/reached that choice. A possible way to analyse this data in more detail will be described in the discussion.
Exactly the same procedure was followed to look for an inter-trial variability based on performance except that now arm-pick distributions are calculated using arm choices from trials with the same performance. No immediate correlation between the SI and performance is observed (see figure 4.6b) but again, a more detailed analysis is necessary to make that statement.

4.2 Electrophysiology and behaviour

This section reports the electrophysiological data recorded in phase 3. After surgical implantation of a hyperdrive (see section 3.2 and 3.3) and approximately one week of

post-surgical recovery, tetrodes were lowered in the CA1 pyramidal cell layer over the course of one week. Recording in phase three started after the rat was accustomed with the recording setup ($\sim$ 3 days) and reached pre-surgical performance during pre-training ($\sim$ 2 days). Only data from two days (46 and 50) will be presented for the reason that the electrophysiological data from day 48 was improperly recorded.

4.2.1 Ripples occur mostly at the reward site

Hippocampal SWRs were detected offline using a double threshold [2] on the ripple envelope, the latter calculated as the absolute value of the Hilbert-transformed ripple band filtered (150-250 Hz) signal (see section 3.5.3). Figure 4.7a shows an overview of one trial by looking at the speed and recorded local field potential. In the example trial, the rat made five correct visits, clearly visible in the speed. The red dots indicate offline detected ripples and nearly all of them occur during periods of immobility. The figure also shows the trial spectrogram on a logarithmic scale (dB) for the range 0-20 Hz and 100-300 Hz. The last one includes the ripple band where high power is observed during the ripples. The 0-20 Hz range includes the theta band (6-10 Hz) which shows high power mostly during the run, alternating with the high power in the ripple band. This alternation confirms that the two main LFP states of the rat hippocampus are theta and LIA, the latter characterised by ripples (see section 2.2.2). Figure 4.7b zooms in on 10 s of the trial where the theta oscillations during run can be clearly observed in the LFP. A zoom on 100 ms during a visit shows a hippocampal SWR, its peak indicated with the dashed line and dot (figure 4.7c).
That ripples seem to occur almost exclusively during the reward site visits is confirmed when looking specifically at the rat's location during a ripple detection. Figure 4.8 shows the spatial distribution of the offline ripple detection for both session 1 and 3 (day 46 and 50). The full trajectory of the rat is shown in grey and its position during an offline ripple detection is shown with a red dot. The left figure presents the trajectories and detected ripples of all trials whereas the right three figures present single trial examples. The average number of ripples at the reward site is 13 [9, 17] (median [IQR]). The average ripple rate, defined as the number of ripples at the reward site during a visit divided by the duration of that visit, is 1.13 Hz [0.85, 1.38] (median [IQR]). These averages are calculated over all trials of all sessions.

4.2.2 Intra-trial variability is observed in the number of ripples but not in the ripple rate.

Within a trial, the memory demand changes (intra-trial variability). Furthermore trials with a higher ETR could reflect a better RE-WM performance of the rat (inter-trial variability). If hippocampal SWRs have an important role in RE-WM then the number or the rate of SWRs may be related to the increasing intra-trial memory demand or the trial performance. To test this, we looked first at the average number of ripples and average ripple rate across visits to check for any intra-trial change (see figure 4.9). Averages are calculated over visits of all trials where the rat reached that visit. The number of ripples per visit shows a significant positive linear correlation with visit number (r= 0.16,

[2] a low threshold for start and end of the ripple and a high threshold to check the duration of the ripple.

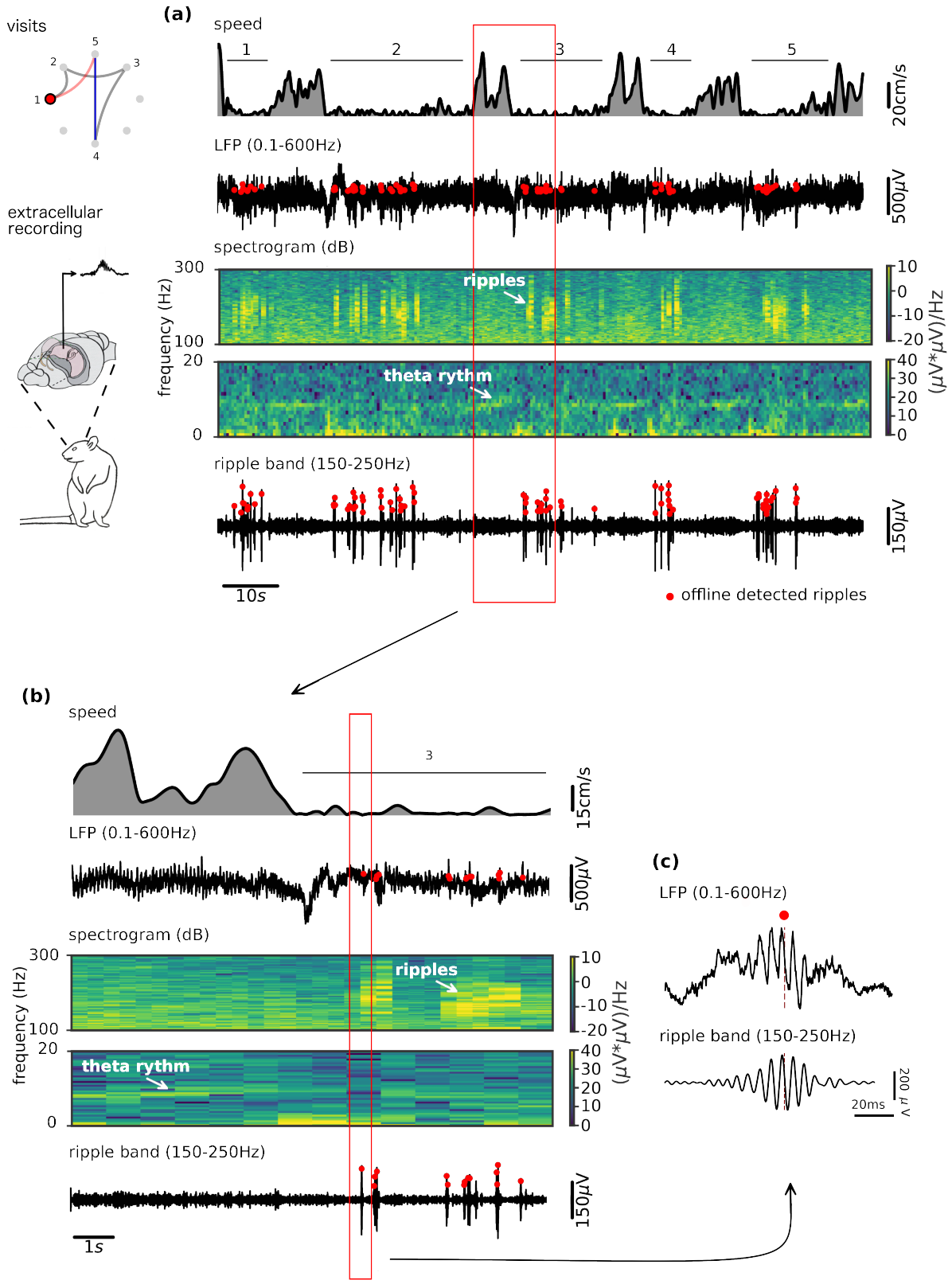

Figure 4.7: Ripples occur during visits and theta oscillations mostly during run. Figure a) shows for one example trial from top to bottom the visits (see schema in the top left corner), the running speed, LFP filtered for 0.1-600 Hz, logarithmic spectrogram for 100-300 Hz and 0-20 Hz and LFP filtered in the ripple band (150-250 Hz). Red dots indicate the offline detected ripples. The time window size and bandwidth for 0-20 Hz and 100-300 Hz spectrograms are 1 and 0.5 s and 0.5 and 2 Hz respectively. Both spectrograms have a window overlap of 0.5 s. Figure b) shows the same but zooms in on the red square of a). Figure c) zooms in on one ripple (red square in b)).

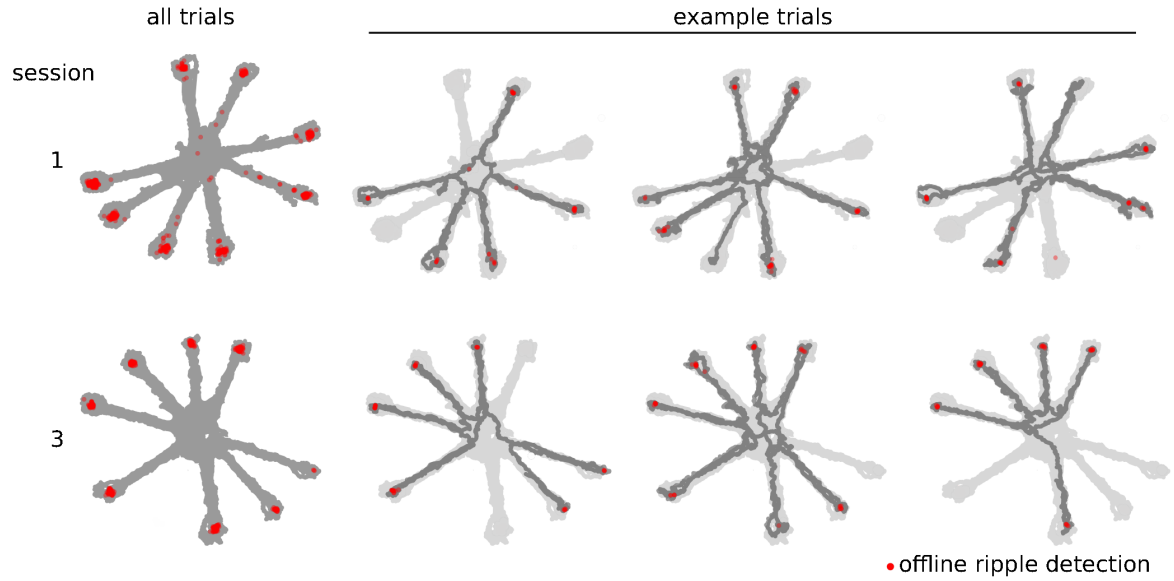

Figure 4.8: Ripples occur mostly at the reward site. On the left location of the rat during offline detected ripples of all trials in session 1 and 3 of phase 3 (day 46, 16 trials and day 50, 17 trials). On the right three example trials for each session.

p=0.034) but the ripple rate does not (r=-0.02, p=0.76). The increase in number of ripples per visit towards the end of a trial mirrors a similar increase in time spent at the reward site, see figure 4.4b. The inter-trial memory performance differences (based on ETR) are not reflected in the average number and rate of SWRs, as no significant linear correlation was observed (r=0.04, p=0.81 and r=0.07, p=0.78, see figure 4.10).

4.3 Closed-loop experiments

This section shows the data from phase 4 where closed-loop disruption of hippocampal SWRs was performed using electrical stimulation of the VHC in nearly all sessions. Those daily sessions contain ripple disruption trials and stimulated control trials that alternate randomly (see inset figure 3.4). In a disruption trial the VHC is stimulated immediately following a ripple detection, resulting in a disruption of the detected ripple. In a stimulated control trial the stimulation occurs 100-250 ms after the ripple detection, hence does not influence the detected ripple but still stimulates the brain at a comparable rate as in the disruption trials. This controls for the effect of electrical stimulation alone. An extra control is provided by 3 sessions (one in the middle and two at the end of phase 4) where no stimulation occurred. Short (300 ms) LFP traces from a disruption, stimulated control and unstimulated control trial are shown in figure 4.11. The dashed line indicates a ripple detection, the red line a stimulation.

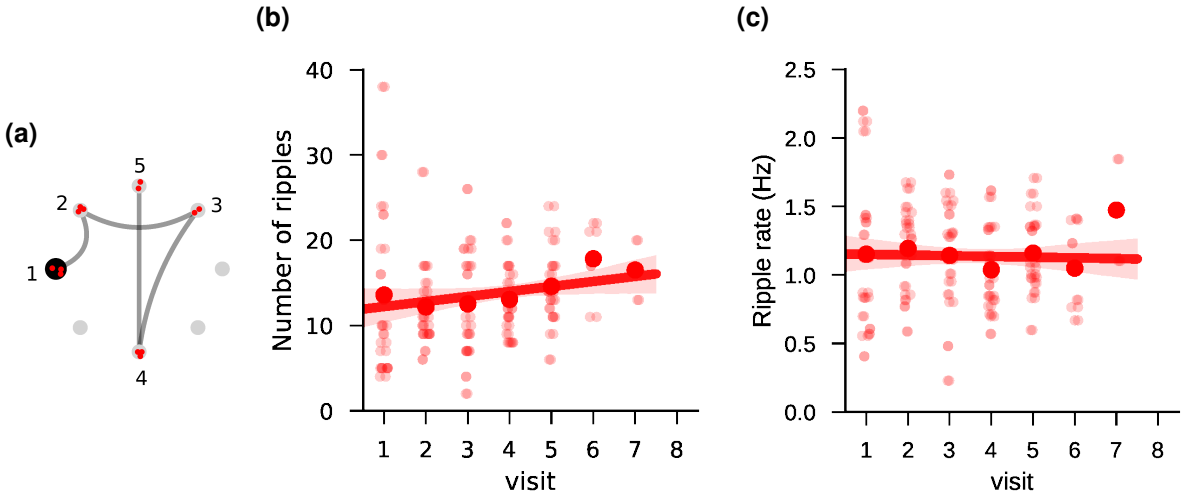

Figure 4.9: Intra-trial variability: Number of ripples but not the ripple rate changes throughout a trial. Figure a) shows schematically the visits with ripples (red). Figure b) and c) show the number of ripples and ripple rate across visits. Ripple rate is calculated as the number of ripples during a visit divided by the time spent at the reward for that visit. Vertical lines indicate the 25-75 IQR and large dots indicate the average. There is only a significant linear regression for the number of ripples indicating a positive correlation with visit number (r=0.16, p=0.034 for number of ripples, r=-0.02, p=0.76 for ripple rate, KW). (Data from phase 3 session day 46, and 50, 34 trials in total)

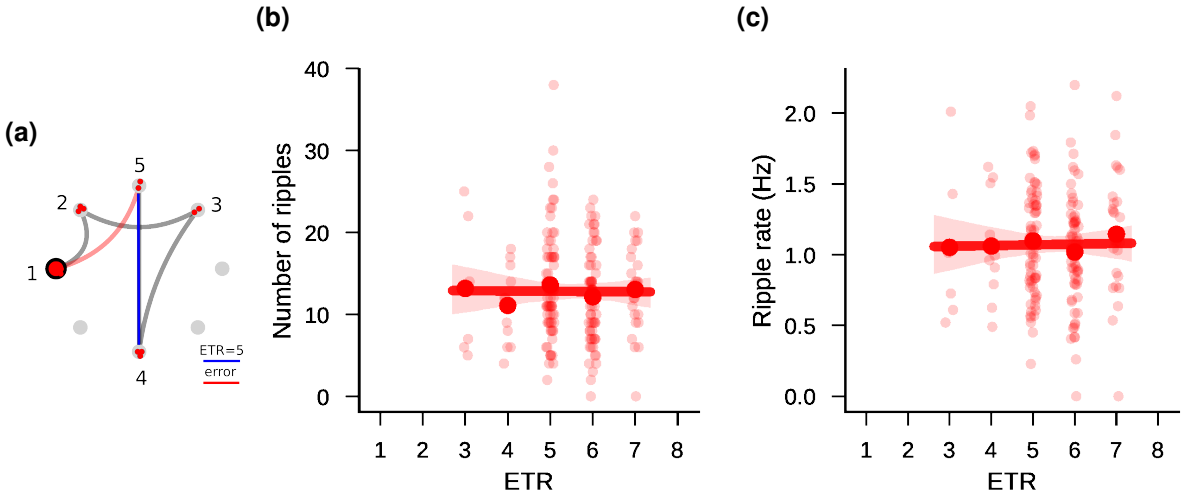

Figure 4.10: Inter-trial variability: Number of ripples and ripple rate at the reward site do not correlate with trial performance. Figure a) shows schematically a trial with performance equal to five (entries until repeat, ETR=5) . Figure b) and c) show the number of ripples and ripple rate during a visit across various performance levels. Ripple rate is calculated as the number of ripples during a visit divided by the time spent at the reward site for that visit. Vertical lines indicate the 25-75 IQR and the large dot indicates the average time over all number of ripples and ripple rate during a visit for trials with a specific performance. Both for the number of ripples and ripple rate during a visit there is no significant linear regression showing no correlation with the trial performance (r=0.04, p=0.81 and r=0.07, p=0.78 respectively, KW). (Data from phase 3 session day 46 and 50, 34 trials in total)

4.3.1 Run speed nor trial performance is influenced by ripple disruption

The closed-loop experiments for this paradigm are performed to investigate a causal relation between hippocampal SWRs and RE-WM. If hippocampal SWRs are causally involved in the expressioin of RE-WM in a trial, then it is expected that disruption of SWRs in a trial leads to decreased trial performance (i.e. lower ETR). In contrast, no significant difference was found between all three groups (median [IQR]: 8 [7, 8], 7 [7, 8] and 8 [6.5, 8] for the disruption, stimulated control and unstimulated control respectively, p=0.38 for disruption and stimulated control, p=0.67 for all three distributions, KW). Note that the averages are all higher than the average for the simulated random-choice rat (median [IQR]: 4 [3, 5.25]) showing that also in this phase of the experiment the rat makes its arms choices in a non random fashion (see section 4.1.1). Figure 4.11a, 4.11b and 4.11c show the performance distributions.

An effect of the ripple disruption on total RE-WM could also be observed in a change in general behaviour of the rat on the maze. Section 4.1.1 introduced two ways to look at this; speed distributions for different parts of the maze and the arm-pick distribution quantified with the stereotypy index (SI). The first one shows whether the rat moves from reward to reward site which is required to perform the win-shift paradigm. The second one shows whether the rat makes the non-random arms choices by using its RE-WM or because it has an egocentric arm-pick bias. Both are investigated for all three trial groups.
Consistent with the behaviour of phase 3 the rat is in all three trial types (disruption, stimulated control and unstimulated control) mostly immobile on the rewards sites (median [IQR]: 3.51 cm/s [1.69, 9.38], 3.47 cm/s [1.71, 9.20], 3.36 cm/s [1.66, 7.78]) and has an intermediate (median [IQR]: 39.87 cm/s [27.59, 50.66], 40.97 cm/s [29.08, 51.66], 40.15 cm/s [27.16, 51.41]) and high speed (median [IQR]: 53.65 cm/s [42.38, 62.18], 54.46 cm/s [43.50, 62.74], 54.76 cm/s [43.38, 64.19]) at the platform and arms respectively. No significant differences between mean trial run speed distributions for different maze regions were observed between the three groups of trials (reward: p=0.63, platform: p=0.72, arm: p=0.31, KW). When comparing only the disruption and stimulated control trials also no significant difference was observed (reward: p=0.64, platform: p=0.50, arm: p=0.28, KW). Thus, ripple disruption did not influence the running speed. Figure 4.11 shows the speed distributions for all three groups of trials.
Figure 4.12 presents the arm pick distributions for all three groups of trials. The SI for the disruption trials is slightly higher than those for the stimulated control trials (SI [IQR]: 0.43 [0.40, 0.46] and 0.41 [0.38, 0.44] respectively). In the unstimulated control trials the rat has a very strong arm-pick preference (SI [IQR]: 0.65 [0.625, 0.71]). A possible explanation for this result is that since most of the control trials come from sessions at the end of the experiment (day 72 and 73) the rat developed a higher stereotyped behaviour as a consequence of overtraining. For that reason the analyses of the unstimulated control trials will not be further discussed in the main text but are included in the supplementary. The observation that the SI is also higher than the one observed in phase 3 (SI [IQR]: 0.36 [0.36, 0.48]) is consistent with this. We also note that the rat now has a strong arm-pick preference to the (second) right whereas previously its preference was the first and second arm left. A different maze configuration and a

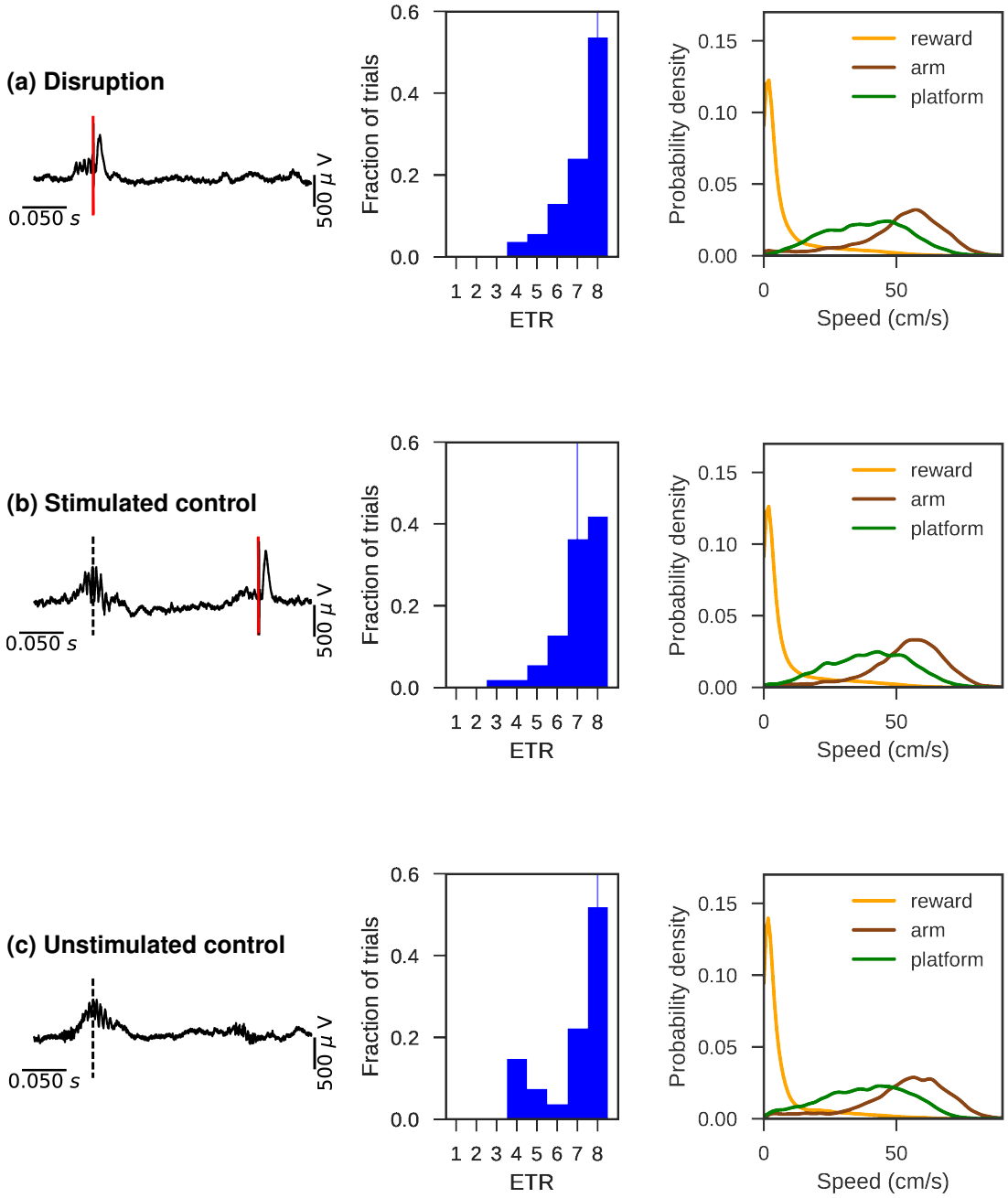

Figure 4.11: Trial performance histograms and speed distributions for disruption, stimulated control and unstimulated control trials. Figure a), b) and c) show data from phase 4 for the disruption trials (N=52), stimulated control trials (N=55) and unstimulated control trials (N=24). On the left an example of local field potential and corresponding detection/stimulation protocol for each type of trial. Detections are indicated with a dashed line and the red line indicates the stimulation. In the centre the performance histograms of the rat and on the right the speed distributions for different parts of the maze as indicated in figure 4.2a. The speed distributions are not significantly different when comparing the three groups of trials (reward: p=0.63, platform: p=0.72, arm: p=0.31, KW). When comparing only the disruption and stimulated control trials also no significant difference was observed (reward: p=0.64, platform: p=0.50, arm: p=0.28, KW).

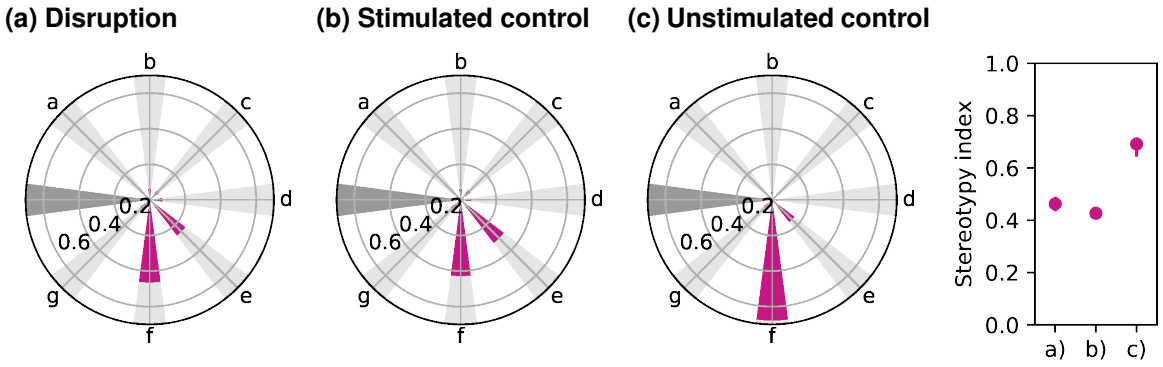

Figure 4.12: Rat prefers to turn to the (second) right. Figure a), b), c) show the normalized egocentric arm pick distribution for all disruption, stimulated control and unstimulated control trials. In d) the quantification of the stereotypy index (SI) for the distributions for the three types of trials (SI=0: all arms are visited equally, SI=1: only one arm is visited). The error is calculated by bootstrapping over the contributing trials (500 times, sample size: 100%). (Data from phase 4, all session, 52 disruption, 54 stimulated control and 24 unstimulated control trials)

week recess between phase 3 and 4 could be possible explanations for this switch.

4.3.2 Inter-trial variability in time spent at the reward site and platform is observed only when ripples are disrupted

To look for other effects of ripple disruption we analysed the time spent at the reward site and platform, during visits and inter-visits, throughout the trial and across performance levels. Average time spent (median [IQR]) at the reward site during visits and on the arms and platform during inter-visits are 7.12s [5.92, 8.59], 1.21s [1.10, 1.33] and 1,76s [1.56, 2.20] for disruption trials and 6.96s [5.92, 8.44], 1.19s [1.11, 1.30] and 1.76s [1.52, 2.20] for stimulated control trials The differences for the time spent at the reward site, arm and platform between disruption and stimulated control trials are not significant (p=0.68, p=0.95, p=0.84, KW). Thus, ripple disruption does not seem to interfere with the average time spent at the reward site, arms or platform.
Next the intra-trial and inter-trial behavioural variability was analysed by looking at average time spend across visits and across performance levels.
Ripple disruption did not have an effect on the intra-trial behaviour as shown by a similar increase towards the end of a trial in the time spent at the reward site and platform during visits and inter-visit periods for both groups of trials, see figure 4.13. The analysis is done in the same way as described in section 4.1.2 and all linear regressions have a p value <0.0001.
However, when averages of the times spent at different maze regions are calculated for trials with the same performance and compared, there is a negative trend towards higher performances only for the disruption trials (r=-0.18, p=0.0060 and r=-0.12, p=0.023 for time spent at the reward site and platform respectively). The result for the stimulated control trials is similar to the result for phase 3, that is no significant linear correlation.
Figure 4.15 shows the inter- and intra-trial analysis of the SI index for the two groups of trials (same analysis as described in section 4.1.2). The SI, characterising the choices

during inter-visit periods, for trials with the same performance does not show any clear trend with performance but when looking at the SI across visits, something interesting is observed. The SI increases slightly towards the end of the trial with a dip at the choice going from visit 4 to 5. This dip is even more profound in the unstimulated control trials (see figure S5). The dip can be understood by realising that the rat prefers the second arm on its right. When it takes that arm three times it cannot make that arm choice another time since that would be a re-entry into the first arm. The dip is stronger in the unstimulated control because stereotypical choice behaviour is stronger as indicated by a higher SI.

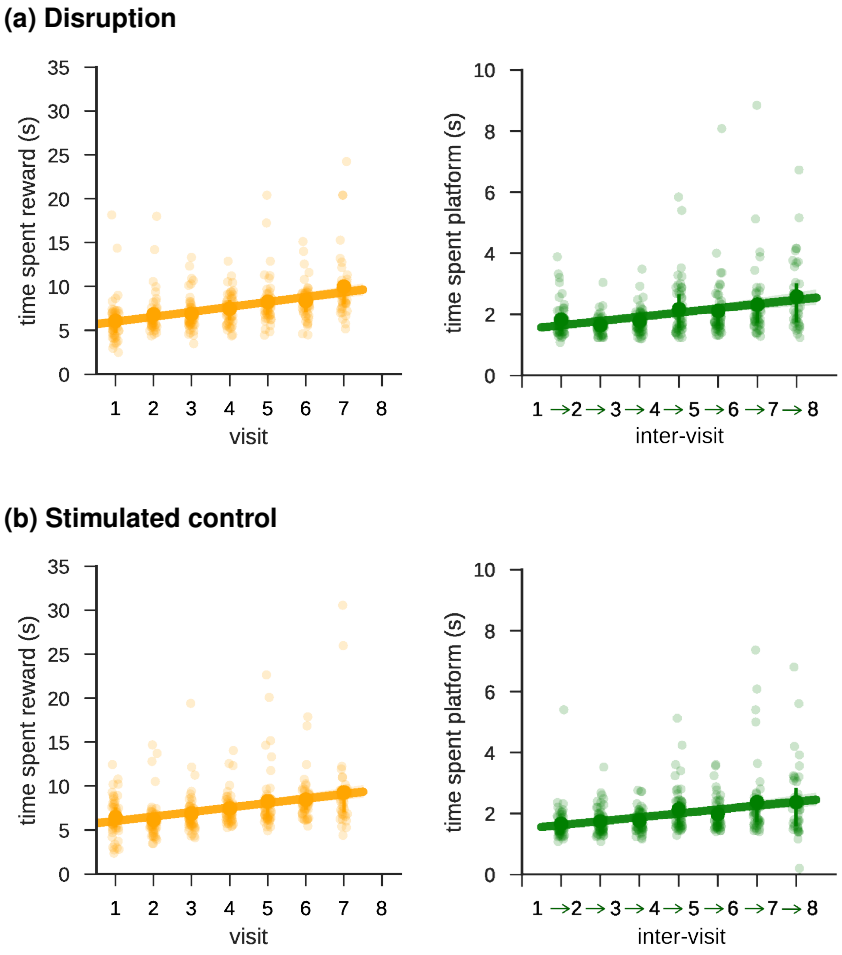

Figure 4.13: Intra-trial variability: Rat spends more time at the reward site and platform towards the end of a trial in both disruption and stimulated control trials. Figure a) and b) show the time spent at the reward site (left), during a visit, and on the platform (right), during an inter-visit, for disruption and stimulated control trials respectively. Vertical lines indicate the 25-75 IQR and large dots indicate the average time over reward site and platform visits of all trials for a specific visit/inter-visit period. The 8^{th} reward site visit is not considered since the rat was taken out after eating of the reward ($\sim$ 5s). For the two groups both the time spent on the reward site and platform show a significant positive linear regression with visit/inter-visit number (r=0.41 and r=0.30, r=0.35 and r=0.31 for reward site and platform, disruption and stimulated control respectively, for all $p < 0.0001$, KW). (Data from phase 4, all stimulation sessions, 52 disruption trials and 55 stimulated control trials)

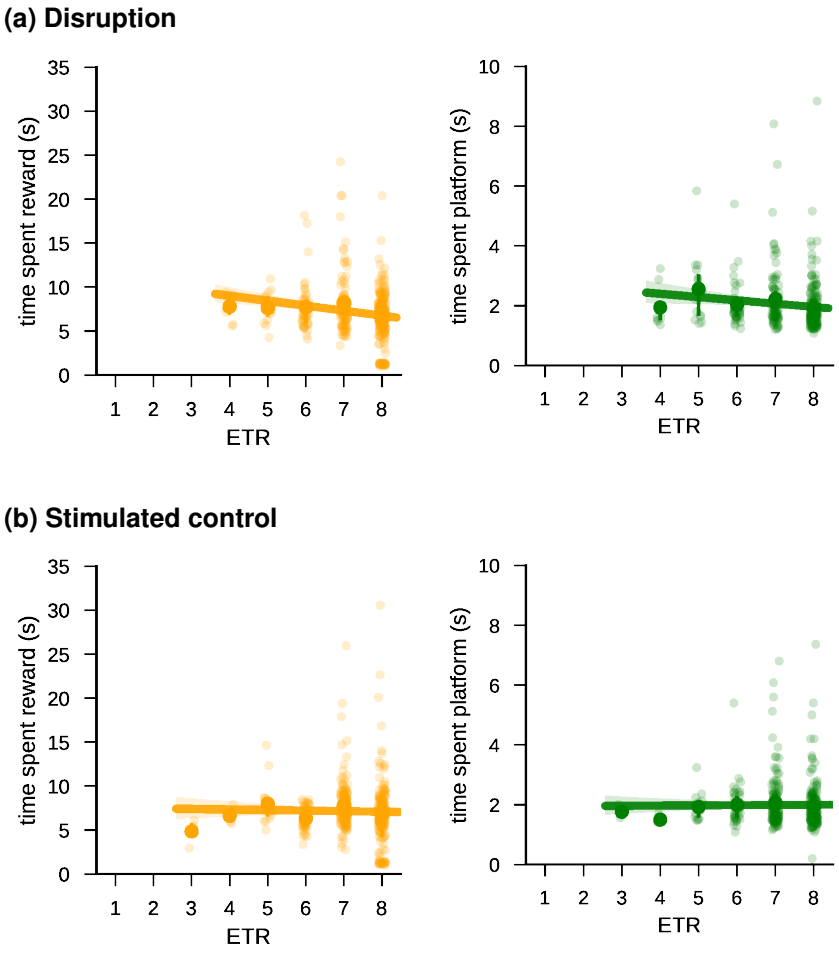

Figure 4.14: Inter-trial variability: Time spent at the reward site and platform shows a significant negative correlation with trial performance only in disruption trials. Figure a) and b) show the average time spent at the reward site (left) and on the platform (right) across various performance levels for all disruption and stimulated control trials respectively. Vertical lines indicate the 25-75 IQR and the large dot indicates the average over all reward site and platform time spendings during trials with a specific performance. The 8^{th} reward site visit is not considered since the rat was taken out after eating of the reward ($\sim$ 5s). Both for the time spent on the reward site and platform in the stimulated control there is no significant linear regression showing no correlation with the trial performance (r=-0.02, p=0.71 and r=0.01, p=0.87, KW). For the disruption trials on the other hand a significant negative correlation is observed for both reward site and platform (r=-0.18, p=0.00060 and r=-0.12, p=0.023, KW). (Data from phase 4, all stimulation sessions, 52 disruption trials and 55 stimulated control trials)

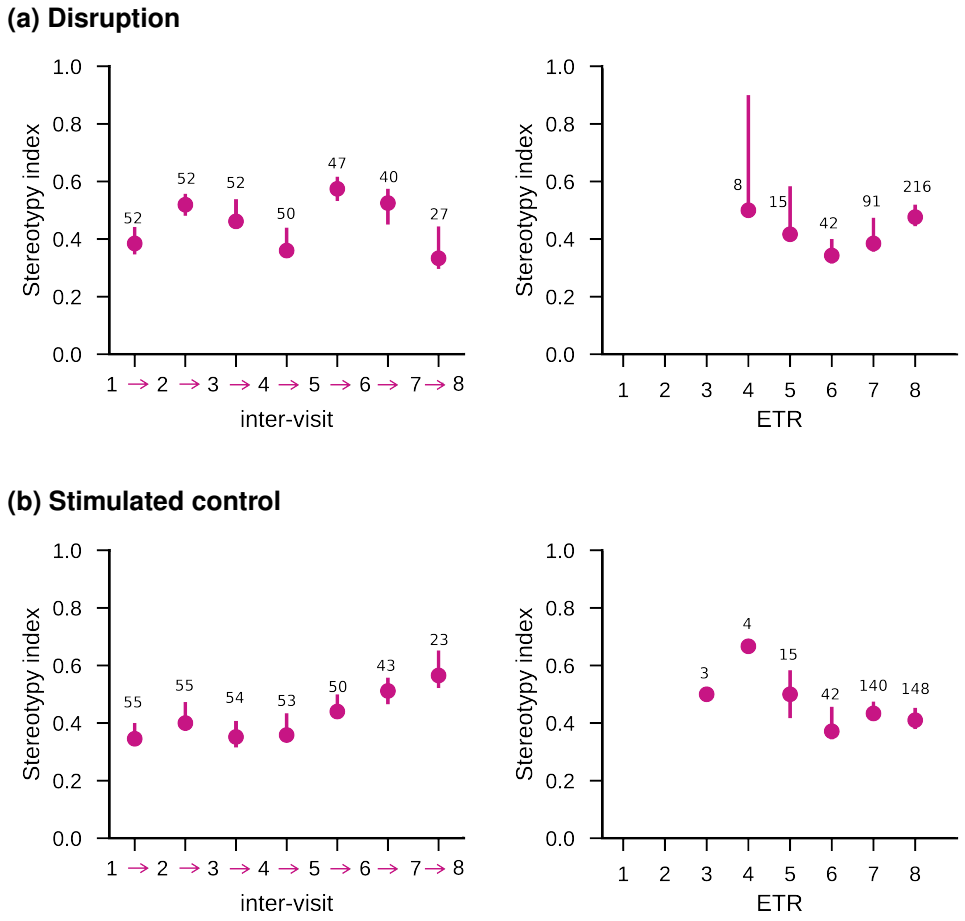

Figure 4.15: Stereotyped behaviour changes towards the 4^{th} visit in both disruption and stimulated control trials but does not correlate with performance. Figure a) and b) show the stereotypy index (SI) characterising the arm pick distribution for inter-visit periods (left) and across performance levels (right) for all disruption and stimulated control trials respectively (SI=0: all arms are visited equally, SI=1: only one arm is visited). Number above data point indicates the number of choices in the corresponding arm pick distribution. The error is calculated by bootstrapping over the contributing trials (500 times, sample size: 100%). Number of trials for the inter-visit arm pick distribution (left) is equal to the number of choices and for the performance arm pick distribution (right) equal to the number of choices divided by the performance. (Data from phase 4, all stimulation sessions, 52 disruption trials and 55 stimulated control trials)

Chapter 5

Discussion and conclusion

5.1 Main results and interpretation

Recent-event working memory (RE-WM) is defined in a recent review [25] as *that part of the mind that can be used to keep track of recent actions and their consequences in order to allow sequences of behaviours to remain effective over time*. As explained in section 2.3.3 this is the memory necessary for solving the win-shift paradigm on the 8-arm radial maze and represents a combination of short-term spatial memory and decision making. Awake hippocampal replay has been suggested to be important for short-term memory [60] [22] and decision making [30] [48] [91]. For that reason the 8-arm radial maze with win-shift paradigm was chosen as behavioural protocol to investigate the role of hippocampal SWRs for short-term memory and decision making or in short, RE-WM.
Trial performance is quantified by the number of arm visits prior to an erroneous revisit. The rat performed better than the simulated random-choice rat, indicating that arm choices are not made randomly. We also observed that both the time spent at the reward site and platform increased with visits in a trial but not across performance levels. The number of ripples at the reward site showed similar trends. However, the ripple rate, defined as the number of ripples at the reward site divided by the time spent at the reward site for that visit, showed no change across visits nor performance levels.

The working hypothesis for this experiment is that awake hippocampal SWRs are important for RE-WM. During ripples cell-firing sequences related to previous experiences are replayed which could be a possible mechanism by which recent memories are recalled [43] [30] to make future decisions [32] [91] [105] [30] or to construct novel paths [37] [81]. We observed that the time spent at the reward site and the number of ripples positively correlates with the increasing RE-WM load in a trial i.e. the more visits a rat makes, the more previously visited arms need to be kept in WM. In this scenario, replay events may serve to maintain and update RE-WM, in which case replay events would be expected to represent the current and previously visited arms, rather than the yet-to-be-visited arms. Future experiments with large scale cellular recordings could test this.
If the above model is true, time spent at reward site and number ripples at reward site should also positively correlate with trial performance. In trials with a higher performance more previous visits have to remembered to make a correct arm choice later in

the trial. This increases the RE-WM load and thus also the average time spent and the number of ripples at the reward site. However, we observe no such relation. To reconcile the two findings, a different model can be considered: the rat spends on average less time at the reward site and platform during the early visits (1-4) in a trial compared to the late visits (5-8) in a trial. No variation across performance levels indicates that on average the rat spends as much time at the reward site or platform for each visit when an error is made in an early visit (low performance and low ETR), as when an error is made in a late visit (high performance, high ETR). This indicates that for low performance trials, which are dominated by early visits, the rat spends more time at the reward site and platform from the beginning. Whereas for high performance trials, the rat spends less time in early visits and increasingly more time in later visits until an error is made. Time spent and the number of ripples still increase over visits in each trial, but the rate at which these changes occur varies across trials and inversely relates to the performance in a trial. Additional analyses can be performed in the future to address this issue more directly. If this model is true, the time spent at the reward site and number of ripples may reflect the level of uncertainty of the rat regarding its next choice, and replay events may represent the evaluation of possible arms to visit in the near future, rather than the most recently visited arms (although available data goes against this, because awake replay often represents the current arm; again future experiments could test this).

In either model, perturbing replay events by disruption of SWRs would be expected to negatively affect trial performance. Our experiments did not provide evidence for this, as the entries until repeat measure did not differ between disruption and control trials. What did change after SWR disruption, however, was that time spent at reward site and platform became negatively correlated with the trial performance. In light of model 2 above, this result could point to an increased level of uncertainty, but it is currently unclear why this does not result in a measurable reduction in task performance. Previous lesion experiments did show that learning the 8-arm radial maze win-shift paradigm is hippocampus dependent [72]. On top of that, hippocampal lesions also strongly influenced the overall behaviour of the rat [79].
It is possible that other hippocampal activity is necessary to properly solve the task and contributes to RE-WM. Theta sequences for example have been implied to reflect goals and be involved in future planning [118]. On the other hand, the 8-arm radial maze win-shift task as performed in this study can be solved using strategies that do not require RE-WM. For example, the rat could learn a fixed sequence of arm visits or use a (counter)clockwise serial searching strategy, resulting in a stereotypical set of choices. The next section (section 5.2.1) describes the measures taken throughout the experiment to reduce the stereotyped behaviour, but it was still there. Incidentally, finding a way to quantify stereotypy is hard (see section 5.2.2). Given that the rat developed a stereotypical choice pattern, the dependence on RE-WM to solve the task is greatly reduced.
The observation that the ripple rate did not change over visits in a trial nor across performance levels might be consistent with this. Previous studies suggests that the ripple rate (and not the number of ripples) corresponds to memory performance. A report from Papale et al showed a negative correlation between the ripple rate and vicarious trial and error (VTE) behaviour which suggests that an increased certainty at choice

points is caused by a higher ripple rate at previously visited reward sites [88]. Another study suggest that the ripple rate reflects the engagement of the rat in a task [41]. It is also possible that lower RE-WM load due to high stereotyped behaviour decreased strongly the engagement of the rat in the task which could account for the similar ripple rate throughout a trial and across performance. It is possible that the rat knew that it can restart multiple times in one session. It therefore didn't care too much about making an error and was less engaged in the task. Increasing the inter-trial time and performing less trials in one daily session could solve this problem.
The reduced RE-WM requirement may explain why SWR disruption did not have an effect.

In the future the task will be adapted so that the performance can not be influenced by stereotyped behaviour (see section 5.3).

5.2 Stereotyped behaviour

Performance on the 8-arm radial maze with win-shift paradigm is quantified in this experiment by counting the number of visits before a re-entry (ETR). Other possibilities are counting the number of re-entries or correct visits during a fixed number of visits [82] [79] [47] [65] [117]. Mostly the performance of the rat is thereafter compared to the performance of a simulated random-choice rat which was also done in this experiment. However, careful observation indicates that there exist many other strategies that do not require high memory performance but still lead to a high performance, for example the (counter)clockwise serial searching strategies. These stereotyped behavioural patterns rely on the animal's spontaneous motor preference and are not hippocampus dependent. To address the involvement of the hippocampal SWRs in solving the win-shift paradigm it is thus very important to reduce and quantify the stereotyped behaviour in the task [65]. Especially when trying to establish a causal link using closed-loop disruption we have to know to what extent the observed behaviour is memory driven.

5.2.1 Unequal angles between arms reduce but not prohibit stereotyped behaviour

Normally the 8-arm radial maze has doors at each entry that can be opened and closed together on command [117]. The rat is put on the platform with all doors initially closed. A trial starts with all doors opening together and the rat is allowed to make a free choice. Each time the rat returns to the platform this process is repeated. In this way a controllable delay is introduced between the arm-choices which discourages the development of stereotyped behaviour [38]. The maze used in this experiment has no automated doors and is referred to as the free-choice 8-arm radial maze. To discourage stereotyped behaviour other strategies were explored.
Previous behavioural research shows that a rat's behaviour strongly depends on the geometry of the maze. For example when two arms of the 8-arm radial maze are parallel but the others equally radially distributed, one of the parallel arms is significantly

less visited than the other arm [100]. In alternation studies where the rat has to return to a start arm before visiting another goal arm its performance is strongly influenced by the angle between the goal arms. Smaller angles reduce the chance of two subsequent goal visits [36] [100]. Thus a rat that does not use its memory to solve the task but purely relies on spontaneous motor behaviour will always make the same and preferably large sized turns i.e. stereotyped behaviour [65]. For that reason unequal angles between the arms were introduced in phase 1, 2 and 3 of the experiment.

As can be seen from the learning curve in figure 3.4 the performance in phase one was very low, around the average of a simulated random-choice rat. During this phase the arm configuration changed each subsequent trial. The performance did not increase over time possibly because the rat got too confused due to the arm changing and as a consequence was not able to learn the task. This was also observed for the other three rats (data not shown). For that reason the arms remained fixed during a daily session in the subsequent phases (phase 2 and 3). The performance immediately increased but maximal performance was rarely reached. This is consistent with previous research that showed that rats indeed perform worse on an 8-arm radial maze with unequal angles between the arms [47].
The eventual goal of this experiment was to look for a link between awake hippocampal SWRs and RE-WM by comparing memory behaviour between trials with and without ripple disruption. To make this comparison an overall consistent but not necessarily high performance is required which was achieved at the end of phase 3. Unfortunately after day 50 the rat was able to ignore the unequal angles and simply solved the task by always taking the first arm on its left, complete stereotyped behaviour (SI=1). Most probably the rat was overtrained on the maze, a danger known from the start. We tried to limit the number of trials per day during pre-training, but this resulted in a long learning process that again increased the chance for stereotyped behaviour. There was no point in continuing to the closed-loop experiments.
After one week of recess the rat was put back on the maze, this time with arms equally distributed (phase 4). The different configuration was recognised by the rat as a different environment and the very strong stereotyped behaviour (SI=1) was not observed anymore. Figure 3.4 also shows that the performance increased during phase 4 compared to phase 3 (medians [IQR]: 6 [5,6] (phase 3) and 7 [7,8] (phase 4, stimulated control)). The equal angles thus made the task more easy for the rat, consistent with previous observations, see [47]. As expected the rat also developed a stronger stereotyped behaviour (SI [IQR]: 0.39 [0.37, 0.41] in phase 3 compared to SI [IQR]: 0.42 [0.40, 0.45] in phase 4 (stimulated control)).

5.2.2 Quantification of stereotyped behaviour is challenging

To quantify the overall stereotyped behaviour we introduced a stereotypy index (SI). This is defined as the difference between the lowest and the highest arm-pick percentage and quantifies the normality of the arm-pick distribution. A random rat with no memory has a uniform distribution with an SI close to zero. The index rises when there is a clear preference for a certain arm, as was observed for the rat in this experiment. A rat with good memory but no arm pick preference would also have an SI close to zero but can be distinguished from the random rat by a higher average performance.

The SI index together with a performance measure (ETR) provide a good view of the behaviour of the rat on the maze. However, this SI index can only be defined for populations of trials.

Other methods to quantify the stereotyped behaviour have been introduced and assign a single index to individual trials. For example, instead of naming the arms from a to g as was done in this experiment, the arms can also be numbered. The egocentric arm pick choices are now characterized by a number, the unit of divergence, and the trial SI is defined as the sum of the units of divergence. A trial SI of 7 reports a complete clockwise strategy [38]. In another example they looked at the relative frequency of adjacent arm choices [28]. A complete clockwise strategy in this case is represented by a 100% relative frequency. The downside of these quantifications is that they primarily focus on one type of stereotyped behaviour; the clockwise strategy. Other arm-pick preferences are not easily distinguished from random arm-picking using these indices. Seeing that the rat in phase 4 preferred the second arm on its right the population SI was a better way to quantify the rat's stereotyped behaviour in this experiment. A study from Lanke et al. proposes another way to quantify the stereotyped behaviour for one trial and this one does allow to distinguish between stereotyped and memory-driven arms choices [65]. Unfortunately this quantification does not work with the win-shift paradigm where the rat is taken out after a re-entry as it compares the number of error-visits in a fixed number of visits of the rat with a random rat with the same stereotyped behaviour.

The population SI does allow to compare behaviour across various levels of performance and across subsequent visits. However, complete interpretation of the results requires a more sophisticated analysis. A simple linear fitting through the calculated SI does not take into account the different sampling sizes used to construct the arm-pick distribution. This is however important since it gives the SI another weight. A possible way to do the fit without arbitrarily assigning weights is by bootstrapping the arm-choice population and perform a linear correlation with trial performance and subsequent visits for each bootstrapping sample. The average over all bootstrap linear fits would then represent a correctly weighted linear fit of the original data.

To conclude, it is challenging but very important to quantify the stereotyped behaviour when analysing the memory-performance in the free-choice 8-arm radial maze with win-shift paradigm. The SI in this paradigm is a good way to quantify that behaviour for a population of trials but it would be very interesting to quantify the stereotyped behaviour of a single trial.

5.3 Future research

The results described above hint for a role for awake SWRs in RE-WM, which was our initial hypothesis. This hypothesis emerged from the results of Jadhav et al. who used a W-mase to show that awake SWRs are necessary to learn a short-term spatial working memory rule and hypothesised that SWRs are also necessary for the execution of that rule, i.e RE-WM. We picked the 8-arm radial maze with win-shift paradigm to increase

the RE-WM load hoping to increase the chance of seeing a performance deficit due to ripple disruption. However, this was not observed, most likely because the rat had a strong arm-pick bias. We hypothesise that when using a paradigm with similar RE-WM load but where performance can not be influenced by stereotyped behaviour, ripple disruption would induce a performance deficit. Such a paradigm has been used in a recent study investigating the role of the DG activity and spatial working memory [99]. The paradigm uses an 8-arm radial maze with arms equally distributed and consists of two phases: a forced phase and a choice phase, see figure 5.1a. There is a door at each entry that can be closed and opened on command. Initially all doors are closed and the rat is placed on the central platform. After all arms are baited, one door opens and the rat is allowed to enter the corresponding arm and consume the reward. This is repeated four times (forced phase). Immediately after the fourth choice all arms are made available and the rat has to remember what arms were not presented during the forced phase i.e. still contain a reward. The most optimal strategy is to visit each arm only once, a correct trial. When DG lesions were performed, the percentage of correct trials dropped dramatically 5.1b. This shows that the task is DG-dependent. Seeing that the DG provides a major input for the CA3 region it is likely that the task is also CA3-CA1 dependent.
The RE-WM in the above described paradigm is necessary to perform maximally in the choice phase. The rat can still solve the task using a clockwise/anti-clockwise strategy but will always have to remember what arms to enter and what arms were already presented in the forced phase. In this way the stereotypic arm choice does not eliminate the need for RE-WM. Using a SI=1 strategy will not lead to a correct trial. If SWRs are involved in RE-WM, ripple disruption in this paradigm should lead to a performance deficit.

5.4 Conclusion

This project investigated a causal link between awake replay and RE-WM, a combination of short-term spatial memory and decision making. For this we used extra-cellular recordings and closed-loop electrical disruption of the hippocampal SWRs in freely-moving rats. The rats performed a RE-WM task (win-shift paradigm) on the 8-arm radial maze. We observed that the time spent on the reward site and the number of ripples increased with increasing visits. More visits have to be remembered towards the end of a trial to make a correct choice which suggests that replays might reflect the consolidation and retrieval of previous visits. However, other observations suggest that the rate at which the time spent and the number of ripples at the reward site change depends on the trial performance. That is, time spent and the number of ripples are always very high before an erroneous choice. If this is true more SWRs might reflect an increased uncertainty concerning the rat's next arm choice in which case replays would represent the evaluation of possible future choices. Ripple disruption did not reduce trial performance but in light of the second model did increase the level of uncertainty. A large stereotypical arm-choice behaviour might have reduced the RE-WM load and corresponding need for replay to solve the task. In the future a version of the win-shift paradigm where performance is not influenced by stereotyped behaviour might provide more clarity on the role of hippocampal SWR in RE-WM.

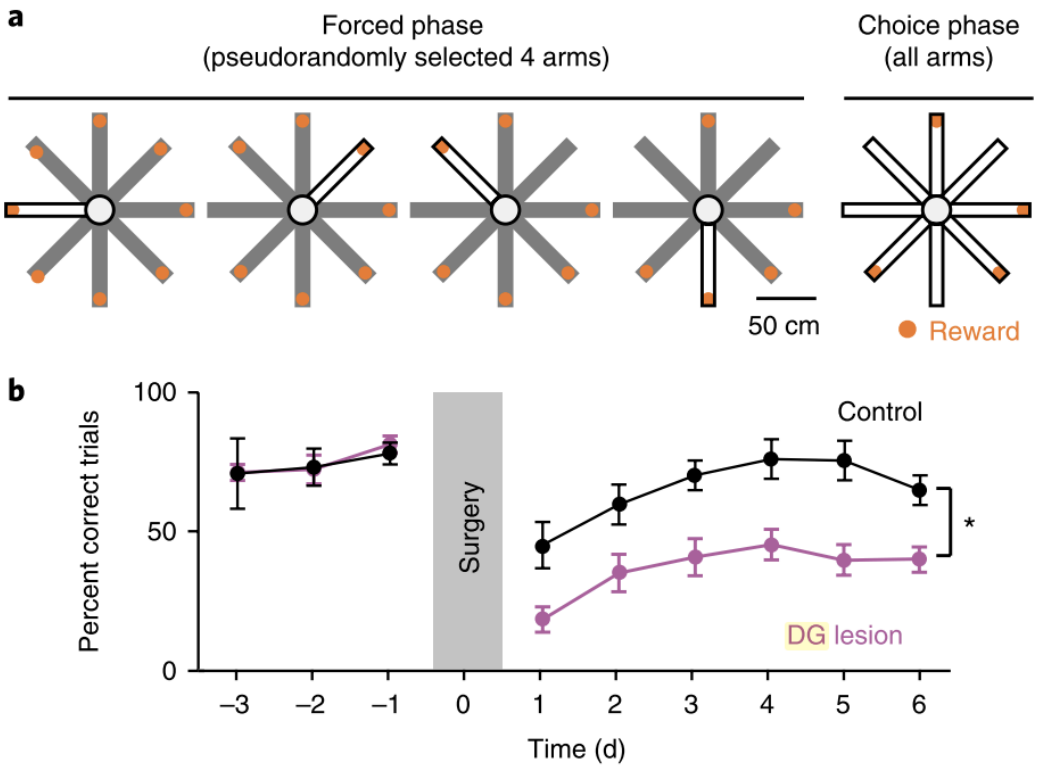

Figure 5.1: Alternative protocol for win-shift paradigm on 8-arm radial maze. a, An alternative RE-WM task on an eight-arm radial maze with reward locations (orange) at the end of each arm. Four arms were individually presented during the forced phase, after which all arms were made available in the choice phase. Open and closed arms in the schematic are shown in white and grey, respectively. b, Mean ($\pm$ s.e.m.) percent correct performance in the spatial WM task as a function of testing day. Selective pharmacological lesions of dentate granule neurons with colchicine resulted in significant memory impairment (n = 5 control rats, 11 lesioned rats; F1,70 = 16.07, P = 0.0013, repeated-measures ANOVA; $P < 0.05$, comparison between groups). (Figure from [99])

Supplementary figures

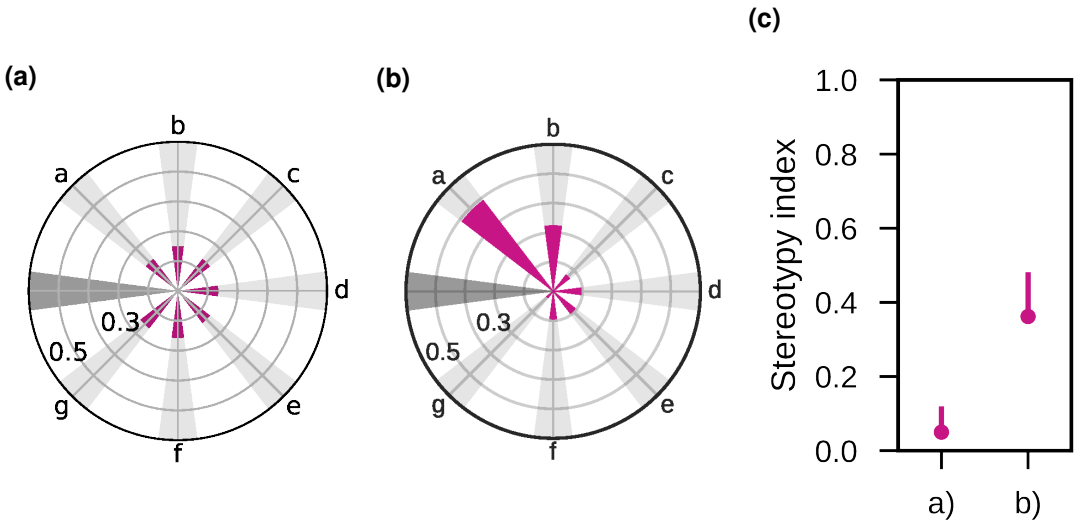

Figure S1: Rat spends most of its time at the reward site. Rat has an arm preference. The normalised egocentric arm pick distribution for a simulated random rat (a)) and the real rat (b)). The simulated rat picks arms randomly, excluding the arm it is currently in (no 180 degree turns). In c) the quantification of the stereotypy index for the distributions for the random rat and real rat. (SI=0: all arms are visited equally, SI=1: only one arm is visited). The error is calculated by bootstrapping (500 times, 100%) over the contributing trials.

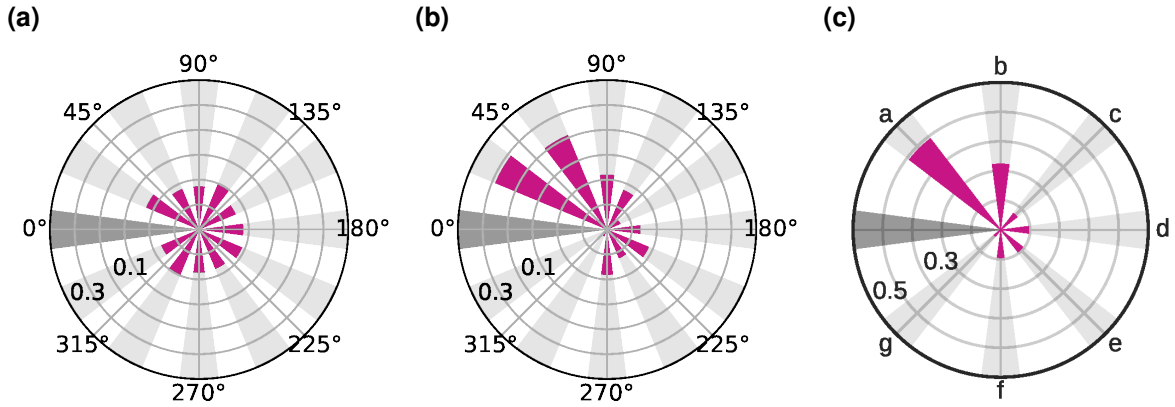

Figure S2: In phase 3, the animal has an arm preference rather than an angle preference. The angles between the arms in phase 3 are unequal with a minimal angle of 30° and a maximal angle 150° (protocol b, see figure 3.4). As a consequence there are 11 possible positions for the arms relative to the rat at each choice and thus labels start from 30° for the first position on its left to 330° for first position on its right. Figure a) presents the normalised egocentric angle presence distribution showing the chance an arm was present at a certain angle. Figure b) presents the normalised egocentric angle pick distribution showing the chance the rat picked an arm at a certain angle. Despite the fact that not every angle can be chosen at each choice (only 7 of the 11 positions contain an arm), normalisation is also performed by division with the total number of choices. This is reasonable since the arm presence distribution (figure a)) is almost uniform over all 47 trials. Figure c) presents the same data as in figure 4.3b, the normalised egocentric arm-pick distribution over all trials. (Data from part 3 session day 46, 48 and 50, 47 trials in total)

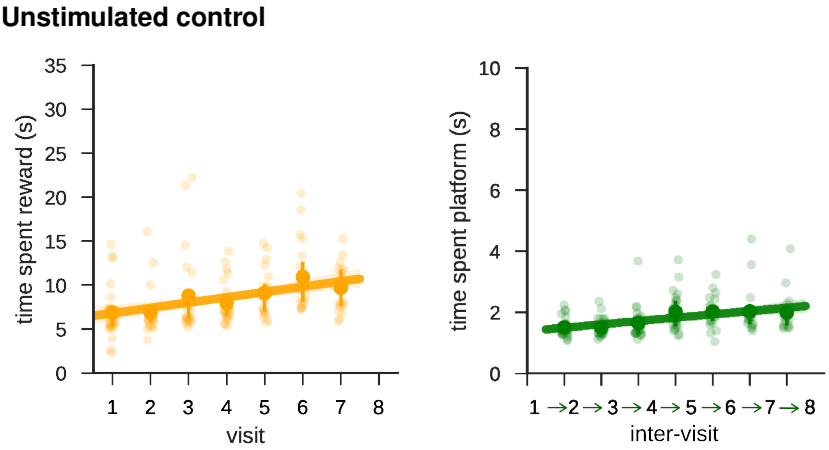

Figure S3: Rat spends more time at the reward site and platform towards the end of a trial in unstimulated control trials. This figure shows the time spent on the reward site (left), during a visit, and on the platform (right), during an inter-visit for unstimulated control trials. Vertical lines indicate the 25-75 IQR and large dots indicate the average over reward site and platform time spendings of all trials for a specific visit/inter-visit period. The 8^{th} reward site visit is not considered since the rat was taken out after eating of the reward ($\sim$ 5s). For both the time spent on the reward site and platform there is a significant linear regression showing a positive correlation with visit/inter-visit number (r=0.34 and r=0.37 for reward site and platform respectively, for all $p < 0.0001$, KW). (Data from part 4, all unstimulated control session, 24 trials)

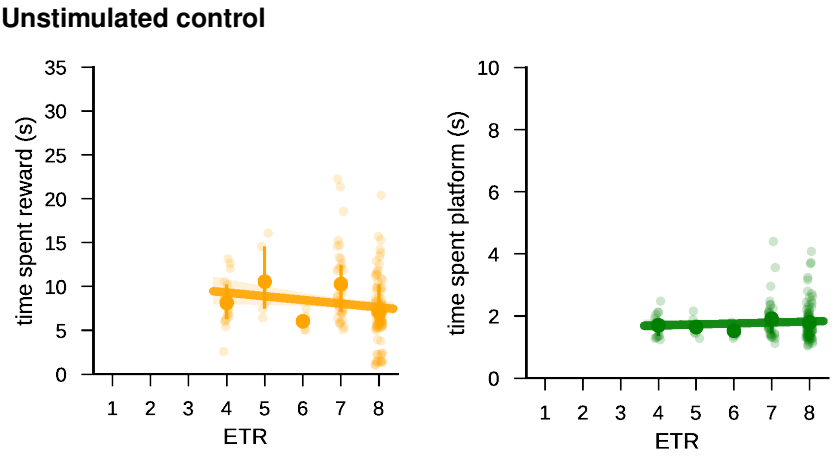

Figure S4: Time spent at the reward site and platform across performance levels for unstimulated control trials. This figure shows the time spent on the reward site (left), during a visit, and on the platform (right) across performance levels for unstimulated control trials. Vertical lines indicate the 25-75 IQR and large dots indicate the average over reward site and platform time spendings of all trials with a specific performance. The 8^{th} reward site visit is not considered since the rat was taken out after eating of the reward site ($\pm$ 5s). There is a negative linear correlation for the time spend at the reward site (r= -0.14,p=0.071, KW) and no linear correlation for the time spend at the platform (r=0.07, p= 0.35, KW). Data from part 4, all unstimulated control session, 24 trials.

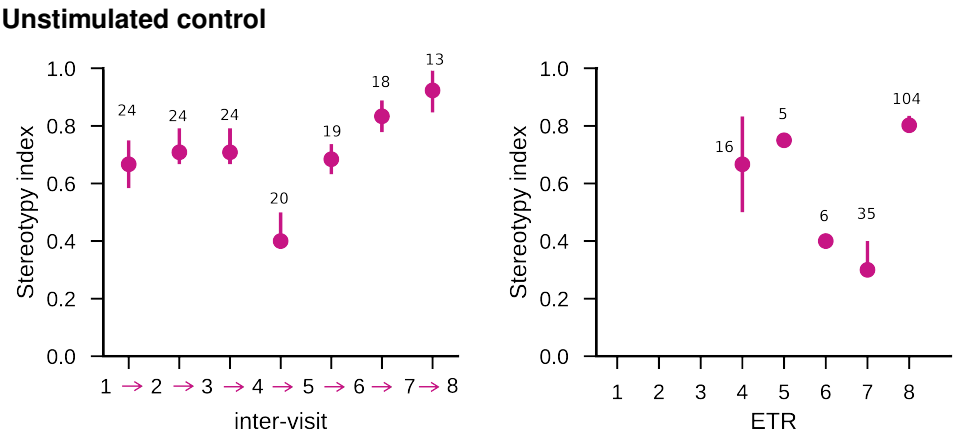

Figure S5: Stereotyped behaviour changes towards the 4^{th} visit but does not correlate with performance in the unstimulated control trials. This figure shows the stereotypy index (SI), characterising the arm pick distribution for inter-visit periods, throughout a trial (left) and across performance levels (right) for unstimulated control trials (SI=0: all arms are visited equally, SI=1: only one arm is visited). Number above data point indicates the number of choices in the corresponding arm pick distribution. The error is calculated by bootstrapping over the contributing trials (500 times, sample size: 100%). Number of trials for the inter-visit arm pick distribution (left) is equal to the number of choices and for the performance arm pick distribution (right) equal to number of choices divided by the performance. Data from part 4, all unstimulated control session, 24 trials.

Bibliography

[1] GK Aghajanian, FE Bloom Brain Research, and undefined 1967. The formation of synaptic junctions in developing rat brain: a quantitative electron microscopic study. *Elsevier*.

[2] Per. Andersen. *The hippocampus book*. Oxford University Press, 2007.

[3] N. Axmacher, C. E. Elger, and J. Fell. Ripples in the medial temporal lobe are relevant for human memory consolidation. *Brain*, 131(7):1806–1817, jul 2008.

[4] Frederico A.C. Azevedo, Ludmila R.B. Carvalho, Lea T. Grinberg, José Marcelo Farfel, Renata E.L. Ferretti, Renata E.P. Leite, Wilson Jacob Filho, Roberto Lent, and Suzana Herculano-Houzel. Equal numbers of neuronal and nonneuronal cells make the human brain an isometrically scaled-up primate brain. *The Journal of Comparative Neurology*, 513(5):532–541, apr 2009.

[5] T L Babb, J K Pretorius, W R Kupfer, and P H Crandall. Glutamate decarboxylase-immunoreactive neurons are preserved in human epileptic hippocampus. *The Journal of neuroscience : the official journal of the Society for Neuroscience*, 9(7):2562–74, jul 1989.

[6] Riccardo Barbieri, Loren M. Frank, David P. Nguyen, Michael C. Quirk, Victor Solo, Matthew A. Wilson, and Emery N. Brown. Dynamic Analyses of Information Encoding in Neural Ensembles. *Neural Computation*, 16(2):277–307, feb 2004.

[7] Delwyn J Bartlett, Caroline Rae, Campbell H Thompson, Karen Byth, David A Joffe, Tony Enright, and Ron R Grunstein. Hippocampal area metabolites relate to severity and cognitive function in obstructive sleep apnea. *Sleep medicine*, 5(6):593–6, nov 2004.

[8] Mark F. Bear, Barry W. Connors, and Michael A. Paradiso. *Neuroscience : exploring the brain*. Lippincott Williams & Wilkins, 2007.

[9] Mark F. Bear, Barry W. Connors, and Michael A. Paradiso. *Neuroscience : exploring the brain*. Lippincott Williams & Wilkins, 2007.

[10] István Biró and Michele Giugliano. A reconfigurable visual-programming library for real-time closed-loop cellular electrophysiology. *Frontiers in Neuroinformatics*, 9:17, jun 2015.

[11] A Bragin, G Jandó, Z Nádasdy, M van Landeghem, and G Buzsáki. Dentate EEG spikes and associated interneuronal population bursts in the hippocampal hilar region of the rat. *Journal of neurophysiology*, 73(4):1691–705, apr 1995.

[12] E N Brown, L M Frank, D Tang, M C Quirk, and M A Wilson. A statistical paradigm for neural spike train decoding applied to position prediction from ensemble firing patterns of rat hippocampal place cells. *The Journal of neuroscience : the official journal of the Society for Neuroscience*, 18(18):7411–25, sep 1998.

[13] György Buzsáki. Hippocampal sharp waves: Their origin and significance. *Brain Research*, 398(2):242–252, nov 1986.

[14] György Buzsáki. Two-stage model of memory trace formation: A role for "noisy" brain states. *Neuroscience*, 31(3):551–570, jan 1989.

[15] György Buzsáki. Hippocampal sharp wave-ripple: A cognitive biomarker for episodic memory and planning. *Hippocampus*, 25(10):1073–1188, 2015.

[16] György Buzsáki and G. Czéh. Commissural and perforant path interactions in the rat hippocampus - Field potentials and unitary activity. *Experimental Brain Research*, 43(3-4):429–438, aug 1981.

[17] György Buzsáki and Andreas Draguhn. Neuronal oscillations in cortical networks. *Science (New York, N.Y.)*, 304(5679):1926–9, jun 2004.

[18] György Buzsáki, Leung Lai-Wo S., and Cornelius H. Vanderwolf. Cellular bases of hippocampal EEG in the behaving rat. *Brain Research Reviews*, 6(2):139–171, oct 1983.

[19] György Buzsáki, Nikos Logothetis, and Wolf Singer. Scaling Brain Size, Keeping Timing: Evolutionary Preservation of Brain Rhythms. *Neuron*, 80(3):751–764, oct 2013.

[20] Christian Cajavilca, Joseph Varon, and George L. Sternbach. Luigi Galvani and the foundations of electrophysiology. *Resuscitation*, 80(2):159–162, feb 2009.

[21] Natalia Caporale and Yang Dan. Spike TimingDependent Plasticity: A Hebbian Learning Rule. *Annual Review of Neuroscience*, 31(1):25–46, jul 2008.

[22] Margaret F Carr, Shantanu P Jadhav, and Loren M Frank. Hippocampal replay in the awake state: a potential substrate for memory consolidation and retrieval. *Nature Neuroscience*, 14(2):147–153, feb 2011.

[23] J J Chrobak and G Buzsáki. Selective activation of deep layer (V-VI) retrohippocampal cortical neurons during hippocampal sharp waves in the behaving rat. *The Journal of neuroscience : the official journal of the Society for Neuroscience*, 14(10):6160–70, oct 1994.

[24] Davide Ciliberti and Fabian Kloosterman. Falcon: a highly flexible open-source software for closed-loop neuroscience. *Journal of Neural Engineering*, 14(4):045004, aug 2017.

[25] Nelson Cowan. The many faces of working memory and short-term storage. *Psychonomic Bulletin & Review*, 24(4):1158–1170, aug 2017.

[26] J Csicsvari, H Hirase, A Czurkó, A Mamiya, and G Buzsáki. Fast network oscillations in the hippocampal CA1 region of the behaving rat. *The Journal of neuroscience : the official journal of the Society for Neuroscience*, 19(16):RC20, aug 1999.

[27] Jozsef Csicsvari, Hajime Hirase, Akira Mamiya, and György Buzsáki. Ensemble Patterns of Hippocampal CA3-CA1 Neurons during Sharp WaveAssociated Population Events. *Neuron*, 28(2):585–594, nov 2000.

[28] Robert H I Dale and Nancy K Innis. Interactions betzeen response stereotypy and memory strategies on the eight-arm radial maze. *Behavioural Brain Research*, 19:17–25, 1986.

[29] Thomas J. Davidson, Fabian Kloosterman, and Matthew A. Wilson. Hippocampal Replay of Extended Experience. *Neuron*, 63(4):497–507, aug 2009.

[30] Thomas J. Davidson, Fabian Kloosterman, and Matthew A. Wilson. Hippocampal Replay of Extended Experience. *Neuron*, 63(4):497–507, aug 2009.

[31] Alan D Degenhart, John W Kelly, Robin C Ashmore, Jennifer L Collinger, Elizabeth C Tyler-Kabara, Douglas J Weber, and Wei Wang. Craniux: a LabVIEW-based modular software framework for brain-machine interface research. *Computational intelligence and neuroscience*, 2011:363565, apr 2011.

[32] Kamran Diba and György Buzsáki. Forward and reverse hippocampal place-cell sequences during ripples. *Nature neuroscience*, 10(10):1241–2, oct 2007.

[33] Kamran Diba and György Buzsáki. Hippocampal network dynamics constrain the time lag between pyramidal cells across modified environments. *The Journal of neuroscience : the official journal of the Society for Neuroscience*, 28(50):13448–13456, dec 2008.

[34] Susanne Diekelmann and Jan Born. The memory function of sleep. *Nature Reviews Neuroscience*, 11(2):114, oct 2010.

[35] R. M. Douglas, B. L. McNaughton, and G. V. Goddard. Commissural inhibition and facilitation of granule cell discharge in fascia dentata. *The Journal of Comparative Neurology*, 219(3):285–294, sep 1983.

[36] Robert J. Douglas, Denis Mitchell, and Robert Del Valle. Angle between choice alleys as a critical factor in spontaneous alternation. *Animal Learning & Behavior*, 2(3):218–220, sep 1974.

[37] George Dragoi and Susumu Tonegawa. Preplay of future place cell sequences by hippocampal cellular assemblies. *Nature*, 469(7330):397–401, jan 2011.

[38] Diane Dubreuil, Céline Tixier, Gérard Dutrieux, and Jean Marc Edeline. Does the radial arm maze necessarily test spatial memory? *Neurobiology of Learning and Memory*, 79(1):109–117, 2003.

[39] Paul A. Dudchenko. An overview of the tasks used to test working memory in rodents. *Neuroscience & Biobehavioral Reviews*, 28(7):699–709, jan 2004.

[40] David Dupret, Joseph O'Neill, Barty Pleydell-Bouverie, and Jozsef Csicsvari. The reorganization and reactivation of hippocampal maps predict spatial memory performance. *Nature Neuroscience*, 13(8):995–1002, aug 2010.

[41] Valérie Ego-Stengel and Matthew A. Wilson. Disruption of ripple-associated hippocampal activity during rest impairs spatial learning in the rat. *Hippocampus*, 20(1):1–10, jan 2010.

[42] Arne D. Ekstrom, Michael J. Kahana, Jeremy B. Caplan, Tony A. Fields, Eve A. Isham, Ehren L. Newman, and Itzhak Fried. Cellular networks underlying human spatial navigation. *Nature*, 425(6954):184–188, sep 2003.

[43] David J Foster and Matthew A Wilson. Reverse replay of behavioural sequences in hippocampal place cells during the awake state. *Nature*, 440(7084):680–683, 2006.

[44] Tamas Freund and Szabolcs Kali. Interneurons. *Scholarpedia*, 3(9):4720, 2008.

[45] Gabrielle Girardeau, Karim Benchenane, Sidney I Wiener, György Buzsáki, and Michaël B Zugaro. Selective suppression of hippocampal ripples impairs spatial memory. *Nature Neuroscience*, 12(10):1222–1223, oct 2009.

[46] JD Green. A simple microelectrode for recording from the central nervous system. *nature.com*, 1958.

[47] M. C. Grobéty and F. Schenk. The influence of spatial irregularity upon radial-maze performance in the rat. *Animal Learning & Behavior*, 20(4):393–400, dec 1992.

[48] Anoopum S. Gupta, Matthijs A.A. van der Meer, David S. Touretzky, and A. David Redish. Hippocampal Replay Is Not a Simple Function of Experience. *Neuron*, 65(5):695–705, mar 2010.

[49] F Hammersen, A Gidlöf, J Larsson, and D H Lewis. The occurrence of paracrystalline mitochondrial inclusions in normal human skeletal muscle. *Acta neuropathologica*, 49(1):35–41, 1980.

[50] Anupam Hazra, Feng Gu, Ahmad Aulakh, Casey Berridge, Jason L. Eriksen, and Jokbas Žiburkus. Inhibitory Neuron and Hippocampal Circuit Dysfunction in an Aged Mouse Model of Alzheimer's Disease. *PLoS ONE*, 8(5):e64318, may 2013.

[51] DO Hebb. The organization of behavior: A neuropsychological theory. 1949.

[52] Darrell A. Henze, Zsolt Borhegyi, Jozsef Csicsvari, Akira Mamiya, Kenneth D. Harris, and György Buzsáki. Intracellular Features Predicted by Extracellular Recordings in the Hippocampus In Vivo. *Journal of Neurophysiology*, 84(1):390–400, jul 2000.

[53] LR Hochberg, MD Serruya, GM Friehs, JA Mukand Nature, and undefined 2006. Neuronal ensemble control of prosthetic devices by a human with tetraplegia. *nature.com*.

[54] A L Hodgkin and A F Huxley. Propagation of electrical signals along giant nerve fibers. *Proceedings of the Royal Society of London. Series B, Biological sciences*, 140(899):177–83, oct 1952.

[55] Gregory L Holmes and Yehezkiel Ben-Ari. The Neurobiology and Consequences of Epilepsy in the Developing Brain. *Pediatric Research*, 49(3):320–325, mar 2001.

[56] David H Hubel. Eye, Brain, and Vision: Scientific American Library Series. *Freeman, New York*, 1988.

[57] DH Hubel. Tungsten microelectrode for recording from single units. *Science*, 1957.

[58] S. P. Jadhav, C. Kemere, P. W. German, and L. M. Frank. Awake Hippocampal Sharp-Wave Ripples Support Spatial Memory. *Science*, 336(6087):1454–1458, jun 2012.

[59] Beata Jarosiewicz, Bruce L McNaughton, and William E Skaggs. Hippocampal population activity during the small-amplitude irregular activity state in the rat. *The Journal of neuroscience : the official journal of the Society for Neuroscience*, 22(4):1373–84, feb 2002.

[60] Mattias P Karlsson and Loren M Frank. Awake replay of remote experiences in the hippocampus. *Nature Neuroscience*, 12(7):913–918, jul 2009.

[61] Fabian Kloosterman, Thomas J. Davidson, Stephen N. Gomperts, Stuart P. Layton, Gregory Hale, David P. Nguyen, and Matthew A. Wilson. Micro-drive array for chronic in vivo recording: drive fabrication. *Journal of Visualized Experiments*, (0), apr 2009.

[62] Bryan Kolb and Robbin Gibb. Principles of neuroplasticity and behavior. In Donald T. Stuss, Gordon Winocur, and Ian H. Robertson, editors, *Cognitive Neurorehabilitation*, pages 6–21. Cambridge University Press, Cambridge.

[63] Krisztián A. Kovács, Joseph O'Neill, Philipp Schoenenberger, Markku Penttonen, Damaris K.Ranguel Guerrero, and Jozsef Csicsvari. Optogenetically blocking sharp wave ripple events in sleep does not interfere with the formation of stable spatial representation in the CA1 area of the hippocampus. *PLoS ONE*, 11(10):e0164675, oct 2016.

[64] Dimitri M Kullmann. Interneuron networks in the hippocampus. *Current Opinion in Neurobiology*, 21(5):709–716, oct 2011.

[65] Jan Lanke, Lennart Månsson, Margareta Bjerkemo, and Per Kjellstrand. Spatial memory and stereotypic behaviour of animals in radial arm mazes. *Brain Research*, 605(2):221–228, 1993.

[66] Albert K. Lee, Ian D. Manns, Bert Sakmann, and Michael Brecht. Whole-Cell Recordings in Freely Moving Rats. *Neuron*, 51(4):399–407, aug 2006.

[67] Albert K. Lee and Matthew A. Wilson. Memory of sequential experience in the hippocampus during slow wave sleep. *Neuron*, 36(6):1183–1194, dec 2002.

[68] Timothy K. Leonard and Kari L. Hoffman. Sharp-Wave Ripples in Primates Are Enhanced near Remembered Visual Objects. *Current Biology*, 27(2):257–262, jan 2017.

[69] C R C Press Llc. Methods of behavior analysis in neuroscience. *New York*, 3:329, 2001.

[70] Lisa Marshall, Halla Helgadóttir, Matthias Mölle, and Jan Born. Boosting slow oscillations during sleep potentiates memory. *Nature*, 444(7119):610–613, nov 2006.

[71] Paolo Mazzarello. A unifying concept: the history of cell theory. *Nature Cell Biology*, 1(1):E13–E15, may 1999.

[72] Robert J Mcdonald and Norman M White. A Triple Dissociation of Memory Systems: Hippocampus, Amygdala, and Dorsal Striatum. 1981.

[73] Bruce L. McNaughton, John O'Keefe, and Carol A. Barnes. The stereotrode: A new technique for simultaneous isolation of several single units in the central nervous system from multiple unit records. *Journal of Neuroscience Methods*, 8(4):391–397, aug 1983.

[74] Kenji Mizuseki, Kamran Diba, Eva Pastalkova, and György Buzsáki. Hippocampal CA1 pyramidal cells form functionally distinct sublayers. *Nature Neuroscience*, 14(9):1174–1181, sep 2011.

[75] Morris Moscovitch, Lynn Nadel, Gordon Winocur, Asaf Gilboa, and R Shayna Rosenbaum. The cognitive neuroscience of remote episodic, semantic and spatial memory. *Current Opinion in Neurobiology*, 16(2):179–190, apr 2006.

[76] Jonathan P. Newman, Riley Zeller-Townson, Ming-Fai Fong, Sharanya Arcot Desai, Robert E. Gross, and Steve M. Potter. Closed-Loop, Multichannel Experimentation Using the Open-Source NeuroRighter Electrophysiology Platform. *Frontiers in Neural Circuits*, 6:98, jan 2013.

[77] T K T Nguyen, Z Navratilova, H Cabral, L Wang, G Gielen, F P Battaglia, and C Bartic. Closed-loop optical neural stimulation based on a 32-channel low-noise recording system with online spike sorting. *Journal of Neural Engineering*, 11(4):046005, aug 2014.

[78] Miriam S Nokia, Jarno E Mikkonen, Markku Penttonen, and Jan Wikgren. Disrupting neural activity related to awake-state sharp wave-ripple complexes prevents hippocampal learning. *Frontiers in Behavioral Neuroscience*, 6:84, 2012.

[79] Hiroshige Okaichi and Yuko Oshima. Choice behavior of hippocampectomized rats in the radial arm maze. *Psychobiology*, 18(4):416–421, 1990.

[80] J. O'Keefe and J. Dostrovsky. The hippocampus as a spatial map. Preliminary evidence from unit activity in the freely-moving rat. *Brain Research*, 34(1):171–175, nov 1971.

[81] H Freyja Ólafsdóttir, Caswell Barry, Aman B Saleem, Demis Hassabis, and Hugo J Spiers. Hippocampal place cells construct reward related sequences through unexplored space. *eLife*, 4:e06063, jun 2015.

[82] David S. Olton, Christine Collison, and Mary Ann Werz. Spatial memory and radial arm maze performance of rats. *Learning and Motivation*, 8(3):289–314, aug 1977.

[83] David S. Olton and Robert J. Samuelson. Remembrance of places passed: Spatial memory in rats. *Journal of Experimental Psychology: Animal Behavior Processes*, 2(2):97–116, 1976.

[84] Joseph O'Neill, Timothy Senior, and Jozsef Csicsvari. Place-Selective Firing of CA1 Pyramidal Cells during Sharp Wave/Ripple Network Patterns in Exploratory Behavior. *Neuron*, 49(1):143–155, jan 2006.

[85] T Ono, K Nakamura, H Nishijo, and S Eifuku. Monkey hippocampal neurons related to spatial and nonspatial functions. *Journal of neurophysiology*, 70(4):1516–29, oct 1993.

[86] Francis A. Ortega, Robert J. Butera, David J. Christini, John A. White, and Alan D. Dorval. Dynamic Clamp in Cardiac and Neuronal Systems Using RTXI. pages 327–354. Humana Press, New York, NY, 2014.

[87] Jorge J Palop and Lennart Mucke. Amyloid-βinduced neuronal dysfunction in Alzheimer's disease: from synapses toward neural networks. *Nature Neuroscience*, 13(7):812–818, jul 2010.

[88] Andrew E. Papale, Mark C. Zielinski, Loren M. Frank, Shantanu P. Jadhav, and A. David Redish. Interplay between Hippocampal Sharp-Wave-Ripple Events and Vicarious Trial and Error Behaviors in Decision Making. *Neuron*, 92(5):975–982, dec 2016.

[89] Carrillo Mora Paul, Giordano Magda, and Santamar Abel. Spatial memory: Theoretical basis and comparative review on experimental methods in rodents. *Behavioural Brain Research*, 203(2):151–164, nov 2009.

[90] C Pavlides and J Winson. Influences of hippocampal place cell firing in the awake state on the activity of these cells during subsequent sleep episodes. *The Journal of neuroscience*, 9(8):2907–2918, aug 1989.

[91] Brad E Pfeiffer and David J Foster. Hippocampal place-cell sequences depict future paths to remembered goals. 2013.

[92] Tine Pooters, Ann Van Der Jeugd, Zsuzsanna Callaerts-Vegh, and Rudi D'Hooge. Telencephalic neurocircuitry and synaptic plasticity in rodent spatial learning and memory. *Brain Research*, 1621:294–308, 2015.

[93] Dimiter Prodanov and Jean Delbeke. Mechanical and Biological Interactions of Implants with the Brain and Their Impact on Implant Design. *Frontiers in Neuroscience*, 10(FEB), feb 2016.

[94] M Reece and J O'Keefe. The tetrode : a new technique for multi-unit extracellular recording. *Soc. Neurosci. Abstr.*, 15:1250, 1989.

[95] Yann Renard, Fabien Lotte, Guillaume Gibert, Marco Congedo, Emmanuel Maby, Vincent Delannoy, Olivier Bertrand, and Anatole Lécuyer. OpenViBE: An Open-Source Software Platform to Design, Test, and Use BrainComputer Interfaces in Real and Virtual Environments. *Presence: Teleoperators and Virtual Environments*, 19(1):35–53, feb 2010.

[96] Vincent Robert, Sadiyah Cassim, Vivien Chevaleyre, and Rebecca A. Piskorowski. Hippocampal area CA2: properties and contribution to hippocampal function. *Cell and Tissue Research*, pages 1–16, jan 2018.

[97] E T Rolls. Spatial view cells and the representation of place in the primate hippocampus. *Hippocampus*, 9(4):467–80, 1999.

[98] Lisa Roux, Bo Hu, Ronny Eichler, Eran Stark, and György Buzsáki. Sharp wave ripples during learning stabilize the hippocampal spatial map. *Nature Neuroscience*, 20(6):845–853, 2017.

[99] Takuya Sasaki, Verónica C Piatti, Ernie Hwaun, Siavash Ahmadi, John E Lisman, Stefan Leutgeb, and Jill K Leutgeb. Dentate network activity is necessary for spatial working memory by supporting CA3 sharp-wave ripple generation and prospective firing of CA3 neurons. *Nature Neuroscience*, 21(2):258–269, feb 2018.

[100] F Schenk, B Contant, and M.-C Grobety. Angle and directionality affect rat's organization of visit sequences and spatial learning in modular mazes. *Learning and Motivation*, 21(2):164–189, may 1990.

[101] Philipp Schoenenberger, Joseph O'Neill, and Jozsef Csicsvari. Activity-dependent plasticity of hippocampal place maps. *Nature Communications*, 7:11824, jun 2016.

[102] Christof J Schwiening. A brief historical perspective: Hodgkin and Huxley. *The Journal of physiology*, 590(11):2571–5, jun 2012.

[103] W B Scoville and B Milner. Loss of recent memory after bilateral hippocampal lesions. *Journal of neurology, neurosurgery, and psychiatry*, 20(1):11–21, feb 1957.

[104] Joshua H Siegle, Aarón Cuevas López, Yogi A Patel, Kirill Abramov, Shay Ohayon, and Jakob Voigts. Open Ephys: an open-source, plugin-based platform for multichannel electrophysiology. *Journal of Neural Engineering*, 14(4):045003, aug 2017.

[105] Annabelle C. Singer, Margaret F Carr, Mattias P. Karlsson, and Loren M. Frank. Hippocampal SWR Activity Predicts Correct Decisions during the Initial Learning of an Alternation Task. *Neuron*, 77(6):1163–1173, mar 2013.

[106] W E Skaggs and B L McNaughton. Replay of Neuronal Firing Sequences in Rat Hippocampus During Sleep Following Spatial Experience. *Science*, 271(5257):1870–1873, mar 1996.

[107] Felix Strumwasser. Long-Term Recording from Single Neurons in Brain of Unrestrained Mammals. *Science, New Series*, 127(3296):469–470, 1958.

[108] David Sullivan, Jozsef Csicsvari, Kenji Mizuseki, Sean Montgomery, Kamran Diba, and György Buzsáki. Relationships between Hippocampal Sharp Waves, Ripples, and Fast Gamma Oscillation: Influence of Dentate and Entorhinal Cortical Activity. *Journal of Neuroscience*, 31(23):8605–8616, 2011.

[109] RJ Sutherland and H Lehmann. Alternative conceptions of memory consolidation and the role of the hippocampus at the systems level in rodents. *Current Opinion in Neurobiology*, 21(3):446–451, jun 2011.

[110] Jaime L. Tartar, Christopher P. Ward, James T. McKenna, Mahesh Thakkar, Elda Arrigoni, Robert W. McCarley, Ritchie E. Brown, and Robert E. Strecker. Hippocampal synaptic plasticity and spatial learning are impaired in a rat model of sleep fragmentation. *European Journal of Neuroscience*, 23(10):2739–2748, may 2006.

[111] Masami Tatsuno. *Analysis and Modeling of Coordinated Multi-neuronal Activity*, volume 12 of *Springer Series in Computational Neuroscience*. Springer New York, New York, NY, 2015.

[112] Edward C. Tolman. Cognitive maps in rats and men. *Psychological Review*, 55(4):189–208, 1948.

[113] Endel Tulving. How Many Memory Systems Are There? *American Psychologist*, 40(4):385–398, apr 1985.

[114] Boston University. Animal Model Brains vs. Human Brain Laboratory of Addiction Genetics.

[115] Gido M. van de Ven, Stéphanie Trouche, Colin G. McNamara, Kevin Allen, and David Dupret. Hippocampal Offline Reactivation Consolidates Recently Formed Cell Assembly Patterns during Sharp Wave-Ripples. *Neuron*, 2016.

[116] DA Wells. The Science of Common Things; a Familiar Explanation of the First Principles of Physical Science, Etc. 1857.

[117] Gary L Wenk. Assessment of spatial memory using the radial arm maze and Morris water maze. *Current protocols in neuroscience / editorial board, Jacqueline N. Crawley ... [et al.]*, Chapter 8(January 2013):Unit 8.5A, 2004.

[118] Andrew M. Wikenheiser and A. David Redish. Hippocampal theta sequences reflect current goals. *Nature Neuroscience*, 2015.

[119] M. Wilson and B. McNaughton. Dynamics of the hippocampal ensemble code for space. *Science*, 261(5124):1055–1058, aug 1993.

[120] Lucia Wittner, Darrell A. Henze, László Záborszky, and György Buzsáki. Three-dimensional reconstruction of the axon arbor of a CA3 pyramidal cell recorded and filled in vivo. *Brain Structure and Function*, 212(1):75–83, jul 2007.

[121] Jonathan Witton, Lydia E. Staniaszek, Ullrich Bartsch, Andrew D. Randall, Matthew W. Jones, and Jonathan T. Brown. Disrupted hippocampal sharp-wave ripple-associated spike dynamics in a transgenic mouse model of dementia. *The Journal of Physiology*, 594(16):4615–4630, aug 2016.

[122] Xiaojing Wu and David J Foster. Hippocampal Replay Captures the Unique Topological Structure of a Novel Environment. *Journal of Neuroscience*, 34(19):6459–6469, may 2014.

[123] A Ylinen, A Bragin, Z Nádasdy, G Jandó, I Szabó, A Sik, and György Buzsáki. Sharp wave-associated high-frequency oscillation (200 Hz) in the intact hippocampus: network and intracellular mechanisms. *The Journal of neuroscience : the official journal of the Society for Neuroscience*, 15(1 Pt 1):30–46, jan 1995.

[124] Kechen Zhang, Iris Ginzburg, Bruce L. McNaughton, and Terrence J. Sejnowski. Interpreting Neuronal Population Activity by Reconstruction: Unified Framework With Application to Hippocampal Place Cells. *Journal of Neurophysiology*, 79(2):1017–1044, feb 1998.

[125] Michaël B Zugaro, Lénaïc Monconduit, and György Buzsáki. Spike phase precession persists after transient intrahippocampal perturbation. *Nature Neuroscience*, 8(1):67–71, jan 2005.

Department of physics and astronomy
Celestijnenlaan 200d - bus 2412
3001 Heverlee
Belgium
Tel: +32 16 327124
www.kuleuven.be